

Mineral equilibria at high PT-parameters

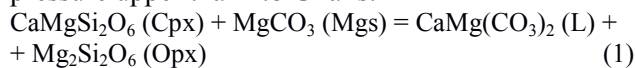
Arefiev A.V.^{1,2}, Podborodnikov I.V.^{1,2}, Shatskiy A.F.^{1,2}, Litasov K.D.^{1,2} Effect of potassium on the reaction controlling solidus of carbonated peridotite at 6 GPa UDC 551.14:544.015.4

¹V.S. Sobolev Institute of Geology and Mineralogy SB RAS, Novosibirsk,
²Novosibirsk State University, Novosibirsk (arefievanton@igm.nsc.ru)

Abstract. The reaction between clinopyroxene and Mg-carbonate is supposed to define the solidus of carbonated peridotite at pressure exceeding 5 GPa. To investigate the effect of alkalis (particularly potassium) on this reaction, subsolidus and melting phase relations in the following systems have been examined at 6 GPa: CaMgSi₂O₆ + 2MgCO₃ (Di + 2Mgs) and CaMgSi₂O₆ + K₂Mg(CO₃)₂ (Di + K₂Mg). The Di + 2Mgs system begins to melt at 1400 °C via the approximate reaction CaMgSi₂O₆ (clinopyroxene) + 2MgCO₃ (magnesite) = CaMg(CO₃)₂ (L) + Mg₂Si₂O₆ (orthopyroxene), whereas the system Di + K₂Mg starts to melt at 1050 °C via reaction CaMgSi₂O₆ (clinopyroxene) + 2K₂Mg(CO₃)₂ (solid) = Mg₂Si₂O₆ (orthopyroxene) + K₄CaMg(CO₃)₄ (liquid). We suggest that the clinopyroxene–Mg-carbonate reaction is very sensitive to the carbonate composition and shifts from 1400 °C to 1050 °C at 6 GPa, which yields K-rich carbonate melt if the subsolidus assemblage contains the K₂Mg(CO₃)₂ compound.

Keywords: double carbonate, alkalis, melting reactions, carbonated peridotite, mantle solidus, high-pressure research

High-pressure experimental studies (Dalton and Presnall 1998) reveal that dominant melting reaction across the solidus of magnesite-bearing lherzolite at pressure upper than 4.8 GPa is:



Dalton, Presnall (1998) experimentally determined the phase relationships in the CaO–MgO–Al₂O₃–SiO₂–CO₂ system (CMAS–CO₂) at 6 GPa. They found the solidus of magnesite-bearing lherzolite at 1380 °C. Further studies in more complex systems revealed that presence of K₂O may decrease the solidus temperature of carbonated peridotite, down to 1100 °C (Brey et al., 2011). The solidus temperature of anhydrous carbonated mantle rocks, and their resulting near-solidus melt composition, are largely determined by the composition of carbonate component. Therefore, the effect of alkalis on melting of carbonated peridotite depends on the host phase, which may be clinopyroxene or carbonate. According to experimental results (Brey et al., 2011, Litasov et al., 2013, Shatskiy et al., 2013, Shatskiy et al., 2016), K₂Mg(CO₃)₂ could be the potential host phase of K in oxidized domains of the upper mantle under anhydrous conditions. The formation of this carbonate, just above the solidus of magnesite-

bearing lherzolite, was confirmed in experiments at 8 GPa and 1200 °C (Brey et al., 2011). Recently, the K₂Mg(CO₃)₂ compound was found in microinclusions trapped in peridotitic diamonds together with inclusions of orthopyroxene and carbonate-bearing high-density fluid (Jablon, Navon, 2016). Assuming typical mantle C and K abundances of 100 and 260 ppm, respectively (Palme, O'Neill, 2003), and assuming all K and C form carbonates, the average contents of K₂Mg(CO₃)₂ and MgCO₃ in the oxidized mantle domains are estimated to be 740 and 141 ppm, respectively. In addition to the work by (Kushiro et al., 1975, Brey et al., 1983), a dearth of studies on the clinopyroxene–magnesite reaction have been made; yet, the direct impact of potassium on this reaction has not yet been studied, although indirect data from complex systems exist (Brey et al., 2011). Furthermore, there are very few data that indicate how carbonate melt compositions change as temperature increases above the carbonated lherzolite solidus at pressures of at least 6 GPa (Dalton, Presnall, 1998, Brey et al., 2011). To ameliorate this situation, and disclose the role of alkali elements on phase relations in carbonate–silicate systems, we have conducted experiments on phase relations in CaMgSi₂O₆–MgCO₃ and CaMgSi₂O₆–K₂Mg(CO₃)₂ systems at a pressure of 6 GPa and over a range of temperatures from 900 to 1800 °C.

High-pressure experiments have been conducted using a uniaxial 1500-ton press, ‘Discoverer’, equipped with DIA-type guide bock installed at the V.S. Sobolev Institute of Geology and Mineralogy SB RAS in Novosibirsk, Russia. ‘Fujillo TN-05’ 26-mm tungsten carbide dices with truncation edge length of 12 mm were employed as Kawai-cell anvils. We used ZrO₂ semi-sintered ceramics (OZ-8C, MinoYogyo Co., Ltd) as a pressure medium shaped as a 20.5 mm octahedron with ground edges and corners. Unfired pyrophyllite gaskets, 4.0 mm in both width and thickness were used to seal the compressed volume and support the anvil flanks. The cell contains several samples, 1 mm in diameter and length, loaded into graphite holders (cassettes), 3.5 mm in outer diameter, surrounded by an electrically insulating sleeves made of talk dehydrated at 1000 °C for 1 h and ZrO₂ plugs inserted at both heater ends. High temperature was generated using graphite heater, 4.5/4.0 mm in outer/inner diameter and 11 mm in length. The sample temperature was monitored via a W–Re_{3%/25%} thermocouple, 0.1 mm in diameter, inserted through the heater walls and electrically insulated by Al₂O₃ tubes. Thicker (0.3 mm) thermocouple extensions were inserted from outside through gasket holes into the pressure medium to the point where the Al₂O₃ tubes begin. No

correction for the effect of pressure on thermocouple electromotive force was applied. The temperature was maintained within 2.0 °C of the desired value using temperature control mode. After experiments, recovered graphite cassettes were cut using a low-speed diamond saw to get vertical cross-sections of samples. The obtained specimens were mounted into epoxy and polished in low-viscosity oil using 400-, 1000-, and 1500-mesh sandpapers. The sample surface was cleaned using an oil spray between each step of polishing. The final polishing was done on satin cloth with 3 µm diamond paste. We used petroleum benzene to remove oil after polishing. The cleaned samples were stored in petroleum benzene prior to coating and loading into a scanning electron microscope. Samples were studied using a MIRA 3 LMU scanning electron microscope (Tescan Orsay Holding) coupled with an INCA energy-dispersive X-ray microanalysis system 450 equipped with the liquid nitrogen-free Large area EDS X-Max-80 Silicon Drift Detector (Oxford Instruments Nanoanalysis Ltd) at V.S. Sobolev IGM SB RAS (Novosibirsk, Russia). The energy-dispersive X-ray spectra (EDS) were collected by electron beam-

rastering in which the stage is stationary while the electron beam moves over a surface area with linear dimensions 5-10 µm (for mineral phases) and 50-500 µm (for quenched melt) at 20 kV accelerating voltage and 1.5 nA beam current. Live counting time for X-ray spectra was 30 s.

The system Di + 2Mgs have been studied in the range of temperature 1350–1800 °C (Fig. 1a). First melt appears at 1400 °C. According to mass balance calculation the melting reaction can be presented as follows: $\text{CaMgSi}_2\text{O}_6$ (Cpx)+2MgCO₃ (Mgs) = Mg₂Si₂O₆ (Opx)+CaMg(CO₃)₂ (L). At 1400 °C, the melt has essentially Ca-dolomitic composition Ca_{0.56}Mg_{0.44}CO₃ and contains 3.5 mol% SiO₂. This melt is similar in composition to peritectic melt established in the CaCO₃–MgCO₃ system at 1400 °C and Ca# = 57 (Shatskiy et al. 2018). With increasing of temperature, concentration of SiO₂ in the melt increases gradually to 8.5 mol%, whereas Ca# decreases to 39 mol% at 1600 °C (Fig.2a,d). Consequently, concentration of SiO₂ does not increase drastically in the melt with increasing temperature to 1500 °C and 1600 °C, as previously reported for the CMAS–CO₂ system.

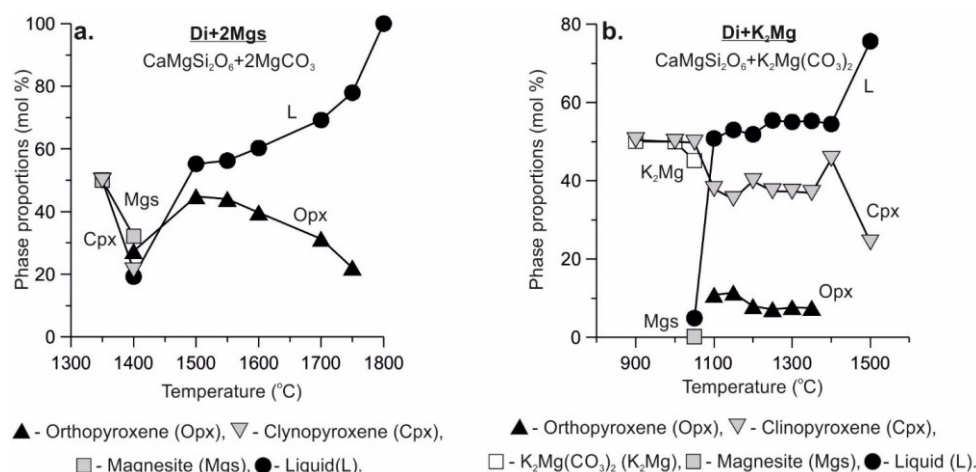
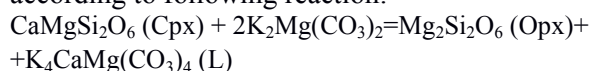


Fig 1. Modal abundances of phases in the system CaMgSi₂O₆ + 2MgCO₃ (Di + Mgs) (a) and CaMgSi₂O₆ + K₂Mg(CO₃)₂ (Di + K₂Mg) (b) at 6 GPa. Modes in mol% were determined from the bulk compositions of starting mixtures and compositions of phases measured by electron microprobe.

The system Di + K₂Mg have been studied in the range of temperature 900–1500 °C (Fig.1b). Initial melt in the system is established at 1050 °C according to following reaction:



which leads to formation of ultrapotassic dolomitic liquid with the composition 43K₂CO₃·57Ca_{0.4}Mg_{0.6}CO₃ + 0.6 mol% SiO₂. Melt compositions changes insignificantly between 1050 and 1400 °C, varying within 42–45K₂CO₃·55–58Ca_{0.3–0.4}Mg_{0.6–0.7}CO₃ + 0.4–4.3 mol% SiO₂. With increasing temperature to 1500 °C, the concentration of SiO₂ in the melt increases to 17 mol% whereas

concentration of K₂O decreases to 16 mol% (Fig.2a,c).

We suggest that the clinopyroxene–Mg-carbonate reaction controlling the solidus of carbonated lherzolite is very sensitive to the carbonate composition and shifts from 1400 °C to 1050 °C at 6 GPa yielding K-rich carbonate melt [43K₂CO₃·57Ca_{0.4}Mg_{0.6}CO₃ + 0.6 mol% SiO₂] if subsolidus assemblage contains K₂Mg(CO₃)₂ compound. Such a decrease in solidus temperature has been observed previously in the K-rich carbonated lherzolite system (Brey et al., 2011). We also found that the partial melt does not undergo significant changes as temperature increases to 1400

Mineral equilibria at high PT-parameters

°C retaining its Ca#, high K₂O and low SiO₂. These observations suggest that ultrapotassic Mg-rich carbonatite melts from microinclusions in fibrous (Zedgenizov et al., 2007) and single crystal diamonds (Jablon, Navon, 2016) worldwide could be derived by low degree partial melting of K₂Mg(CO₃)₂-bearing lherzolite at temperature of ≥ 1050 °C and pressures near 6 GPa, i.e. at the *P-T* conditions of

diamond formation in the lithospheric mantle (Boyd et al., 1985). This idea is consistent with recent finding of the K₂(Mg,Ca)(CO₃)₂ compound as microinclusions in peridotitic diamonds along with inclusions of orthopyroxene and ultrapotassic carbonate-bearing high-density fluid (Jablon, Navon, 2016).

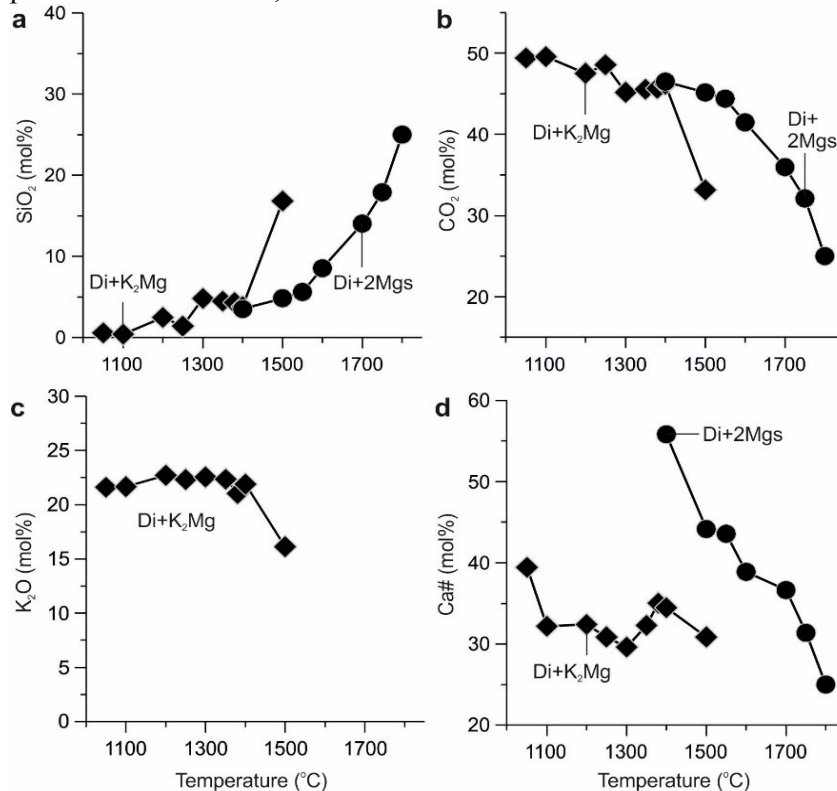


Fig. 2. Run temperature plotted against selected oxide concentrations (a-c) and Ca# (d) in liquid phase obtained in the systems CaMgSi₂O₆ + 2MgCO₃ (Di + 2Mgs) and CaMgSi₂O₆ + K₂Mg(CO₃)₂ (Di + K₂Mg) at pressure of 6.0 GPa.

This work was supported by RF the state assignment project No. 0330-2016-0012.

References:

Boyd F., Gurney J. and Richardson S. Evidence for a 150–200-km thick Archaean lithosphere from diamond inclusion thermobarometry // *Nature*. - 1985. - V. 315. - № 6018. - P. 387-389.

Brey G., Brice W.R., Ellis D.J., Green D.H., Harris K.L. and Ryabchikov I.D. Pyroxene-carbonate reactions in the upper mantle // *Earth and Planetary Science Letters*. - 1983. - V. 62. - № 1. - P. 63-74.

Brey G.P., Bulatov V.K. and Girmis A.V. Melting of K-rich carbonated peridotite at 6-10 GPa and the stability of K-phases in the upper mantle // *Chemical Geology*. - 2011. - V. 281. - № 3-4. - P. 333-342.

Dalton J.A. and Presnall D.C. The continuum of primary carbonatitic-kimberlitic melt compositions in equilibrium with lherzolite: Data from the system CaO-MgO-Al₂O₃-SiO₂-CO₂ at 6 GPa // *Journal of Petrology*. - 1998. - V. 39. - № 11-12. - P. 1953-1964.

Jablon B.M. and Navon O. Most diamonds were created equal // *Earth and Planetary Science Letters*. - 2016. - V. 443. - № 1. - P. 41-47.

Kushiro I., Satake H. and Akimoto S. Carbonate-silicate reactions at high pressures and possible presence of dolomite and magnesite in the upper mantle // *Earth and Planetary Science Letters*. - 1975. - V. 28. - № 2. - P. 116-120.

Litasov K.D., Shatskiy A., Ohtani E. and Yaxley G.M. The solidus of alkaline carbonatite in the deep mantle // *Geology*. - 2013. - V. 41. - № 1. - P. 79-82.

Palme H. and O'Neill H.S.C. Cosmochemical estimates of mantle composition // *Treatise on geochemistry* / Davis A.M., Holland H.D. and Turekian K.K. - New York: Elsevier, 2003. - V. 2. - pp. 1-38.

Shatskiy A., Sharygin I.S., Gavryushkin P.N., Litasov K.D., Borzdov Y.M., Shcherbakova A.V., Higo Y., Funakoshi K., Palyanov Y.N. and Ohtani E. The system K₂CO₃-MgCO₃ at 6 GPa and 900-1450 °C // *American Mineralogist*. - 2013. - V. 98. - № 8-9. - P. 1593-1603.

Shatskiy A., Litasov K.D., Palyanov Y.N. and Ohtani E. Phase relations on the K₂CO₃-CaCO₃-MgCO₃ join at 6 GPa and 900-1400 °C: implication for incipient melting in carbonated mantle domains // *American Mineralogist*. - 2016. - V. 101. - № 2. - P. 437-447.

Zedgenizov D.A., Rege S., Griffin W.L., Kagi H. and Shatsky V.S. Composition of trapped fluids in cuboid fibrous diamonds from the Udachnaya kimberlite: LAM-ICPMS analysis // *Chemical Geology*. - 2007. - V. 240. - № 1-2. - P. 151-162.

Butvina V.G.¹, Limanov E.V.¹, Safonov O.G.¹, Varlamov D.A.¹ Experimental study of the phlogopite-forming reactions in the system

pyrope-grossular-enstatite in the presence of the H₂O-KCl fluid at 5 GPa.

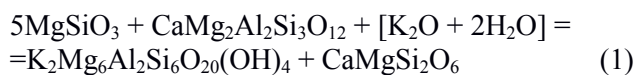
¹Korzhinskii Institute of Experimental Mineralogy (IEM) RAS, Chernogolovka, butvina@iem.ac.ru

Abstract. The paper presents results on the experimental study of the reaction $5\text{MgSiO}_3 + \text{CaMg}_2\text{Al}_2\text{Si}_3\text{O}_{12} + [\text{K}_2\text{O} + 2\text{H}_2\text{O}] = \text{K}_2\text{Mg}_6\text{Al}_2\text{Si}_6\text{O}_{20}(\text{OH})_4 + \text{CaMgSi}_2\text{O}_6$ (enstatite + garnet + fluid = phlogopite + diopside) in the presence of a H₂O-KCl fluid with starting $X_{\text{KCl}} = 0.05\text{-}0.4$ at 5 GPa and temperatures of 900-1250°C. An increase in the concentration of KCl in a starting fluid results in a decrease in the amount of garnet and orthopyroxene and formation of phlogopite (\pm diopside), so at $X_{\text{KCl}} = 0.4$, phlogopite becomes a dominant phase. The increase in the salt concentration stabilizes phlogopite to higher temperatures. Experiments have demonstrated that joint variation of the Al content in orthopyroxene and Cl in phlogopite serves as a reliable indicator of the KCl activity in the fluid and can be used to quantify it and, hence, the KCl concentration in aqueous-salt fluids in the processes of the modal mantle metasomatism.

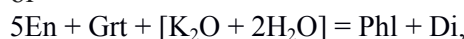
Keywords: *metasomatism, mantle, phlogopite, aqueous-salt fluid, alkali chlorides, HP-HT experiment*

Introduction. Mantle metasomatism is the process of transformation of mantle rocks due to their interaction with various deep-seated fluids. The concept of mantle metasomatism has been developed in the 1970 - 1980s on the basis of studies of upper mantle xenoliths in kimberlites and alkali basalts [1-4]. According to this concept, modifications of the mantle rocks via their interaction with external fluids and melts (regardless of their composition and origin), which leads to the formation of minerals atypical for mantle peridotites (amphiboles, phlogopite, apatite, carbonates, sulfides, titanite, ilmenite etc.), was collectively classified as the modal mantle metasomatism [3]. Modal mantle metasomatism is usually accompanied by partial melting resulting in formation of a wide spectrum of magmas, such as alkali basalts, ultrapotassic magmas, lamproites, kimberlites, carbonatites etc. The H₂O and/or CO₂ activities are considered to be the most important agents of the modal mantle metasomatism ([3] and references therein). However, mineralogical and geochemical data also indicate an active role of K and Na in this process. These components are dissolved in the mantle fluids as various salts. Among them, chlorides are of special interest, since they are abundant in fluid/melt inclusions in diamonds, kimberlite minerals, in minerals of spinel peridotite xenoliths in basalts from various geodynamic environments (see references in [5-6]).

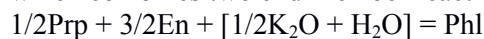
A characteristic mineral indicator of the modal mantle metasomatism is phlogopite [1-4]. Appearance of this mineral in the mantle rocks as a result of their interaction with potassium-bearing aqueous fluids is explained by the reaction (e.g. [7]):



or



which combines two end-member reactions [5-6]:



In mantle peridotites, these reaction result in gradual transformations of original upper-mantle garnet lherzolites and harzburgites through garnet-free phlogopite-bearing peridotites to phlogopite wherlites. Series of xenolith with these assemblages are well known in kimberlites [8-13].

In the above reactions, the alkaline component is taken as K₂O for clarity. However, in real fluids, K is present as chlorides, carbonates, etc. Present study shows results of the experiments at 5 GPa and 900-1250°C on the reaction (2) and 1000°C on the reaction (3) in presence of the H₂O-KCl fluid.

Starting materials, experimental and analytical procedures. To reproduce the reaction (2), a mixture of pyrope gel, brucite and quartz was used as a starting material. For the study of the reaction (3), a gel of the grossular composition was added to the mixture. KCl was added to produce the required starting $X_{\text{KCl}} = \text{KCl} / (\text{KCl} + \text{H}_2\text{O})$ from 0.05 to 0.4 (these concentrations are out of saturation of the aqueous fluid in salt). The H₂O content was ~ 8 wt. % in both systems.

The experiments were performed using a toroidal “anvil-with-hole” high-pressure apparatus [14] in the Korzhinskii Institute of Experimental Mineralogy RAS (IEM RAS) at a pressure of 5 GPa and temperatures of 900, 1000 and 1250°C. Platinum capsules of 0.2mm-wall thickness were used for the experiments. Run duration varied from 24 to 48 hours (depending on run temperature). After experiments, samples were sealed into epoxy mounts and polished.

Run products were analyzed using CamScan MV2300 (VEGA TS 5130MM) electron microscope equipped with EDS INCA Energy 350 and Tescan VEGA-II XMU microscope equipped with EDS INCA Energy 450 and WDS Oxford INCA Wave 700.

Results of the experiments. The conditions and results of individual experiments are presented in Table 1. The products of the KCl-free experiments contain pyrope and Al-bearing enstatite. In the presence of KCl in the starting fluid, phlogopite appears in the products of the experiments at 1000 and 900°C, but is absent at 1250°C. All run samples contain fine-grained aggregates interpreted as quench products of a melt (Fig. 1a, b). An increase in KCl is accompanied by a decrease of the amount of pyrope and enstatite in the products of the experiments, so that in experiments with fluids with $X_{\text{KCl}} = 0.4$ they are rare or absent, and phlogopite is the dominant phase (Fig. 1a).

Mineral equilibria at high PT-parameters

Table 1. Run conditions and products of experiments on the reaction $5\text{En} + \text{Grt} + [\text{K}_2\text{O} + 2\text{H}_2\text{O}] = \text{Phl} + \text{Di}$ at 5 GPa.

| Run no. | T, °C | duration, hours | X _{KCl} | Run products |
|----------|-------|-----------------|------------------|------------------------|
| PEH-1 | 1250 | 24 | 0 | Opx+Grt+Q ¹ |
| PEH-2 | 1250 | 24 | 0.05 | Ol+Grt+Q |
| PEH-3 | 1250 | 24 | 0.1 | Opx+Ky+Q |
| PEH-4 | 1250 | 24 | 0.2 | Opx+Grt+Ky+Q |
| PEH-6 | 1000 | 48 | 0 | Opx+Grt+Q |
| PEH-8 | 1000 | 48 | 0.05 | Opx+Grt+Phl+Q* |
| PEH-7.14 | 1000 | 48 | 0.1 | Opx+Phl+Q* |
| PEH-9 | 1000 | 48 | 0.2 | Opx+Phl+Ky+Q* |
| PEH-11 | 1000 | 48 | 0.4 | Phl+Q* |
| PEH-12 | 900 | 48 | 0.05 | Opx+Grt+Phl |
| PEH-16 | 900 | 48 | 0.1 | Opx+Grt+Phl |
| PEH-13 | 900 | 48 | 0.2 | Opx+Grt+Ky+Phl |
| PEH-15 | 900 | 48 | 0.4 | Opx+Grt+Phl |
| PGEH-1 | 1000 | 48 | 0.05 | Grt+Opx+Q |
| PGEH-2 | 1000 | 48 | 0.1 | Grt+Phl+Opx+Cpx |
| PGEH-3 | 1000 | 54 | 0 | Cpx+Opx+Q+Q* |
| PGEH-4 | 1000 | 48 | 0.4 | Phl+Q |
| PGEH-5 | 1000 | 48 | 0.2 | Phl+Cpx+Q |

Note. ¹ Q-products of melt quenching. Q* - phlogopite-like quenching phases.

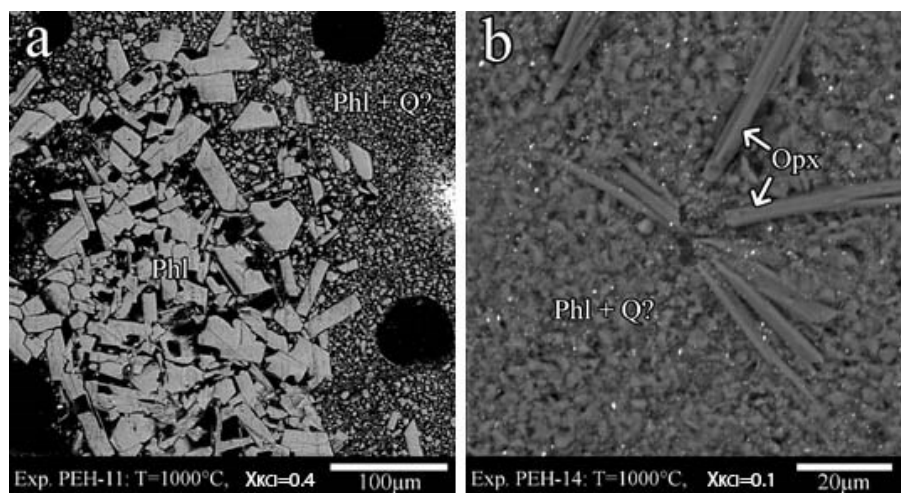
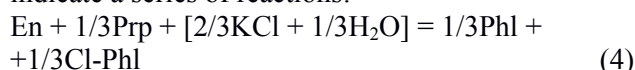


Fig. 1. Phases relations in the run products on the reactions (2) and (3): (a) Abundant phlogopite coexisting with quench products in the run PEH-11 (Table 1) at T=1000°C. X_{KCl} = 0.4; (b) Orthopyroxene coexisting with quench products in the run PEH-14 (Table 1) at T=1000°C. X_{KCl} = 0.1; no garnet is present, only orthopyroxene (Opx) and

Experiments at 1000°C show that pyrope is the first phase to disappear as the concentration of KCl in the starting fluid increases (Fig. 1b). Subsequently Al-bearing enstatite gives up. These relations indicate a series of reactions:



where MgTs is the Mg-Tschermack molecule ($\text{MgAl}_2\text{SiO}_6$) and Cl-Phl – is the $\text{KMg}_3\text{AlSi}_3\text{O}_{10}\text{Cl}_2$ end-member in the phlogopite solid solution. These reactions express a regular disappearance of the garnet accompanied by a decrease in Al content in orthopyroxene and an increase in Cl content in the

newly formed phlogopite with an increase in the KCl content in the starting fluid.

In the Ca-bearing system, an increase in the concentration of KCl also destabilizes of the pyrope-grossular garnet with the formation of clinopyroxene and phlogopite (Fig. 2) according to the reaction (3). Such relationships are well known in upper mantle xenoliths in kimberlites and alkali basalts. For example, [13] described a series of garnet harzburgite to phlogopite wehrlite xenoliths from the Lethlakane kimberlite pipe in Botswana, which showed gradual garnet replacement by the assemblage $\text{Cpx} + \text{Phl} \pm \text{Cr-Spl}$ and a simultaneous decrease in the modal orthopyroxene. The newly formed clinopyroxene developed together with phlogopite in harzburgites that had not contained primary clinopyroxene.

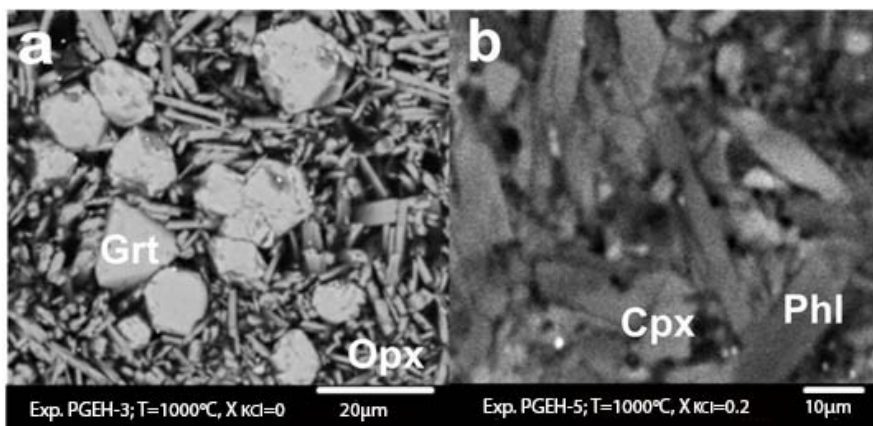


Fig. 2. Phases relations in the run products on the reaction (1): (a) Garnet (Grt) coexisting with orthopyroxene (Opx) in the run PGEH-1 (Table 1) at $T=1000^{\circ}\text{C}$ in absence of KCl; (b) Clinopyroxene (Cpx) coexisting with phlogopite (Phl) in the run PGEH-5 (Table 1) at $T=1000^{\circ}\text{C}$ and $X_{\text{KCl}} = 0.1$.

Fig. 3. Dependence of the Al-content (a.p.f.u.) in orthopyroxene on the KCl content in the starting fluid at 900°C and 1000°C .

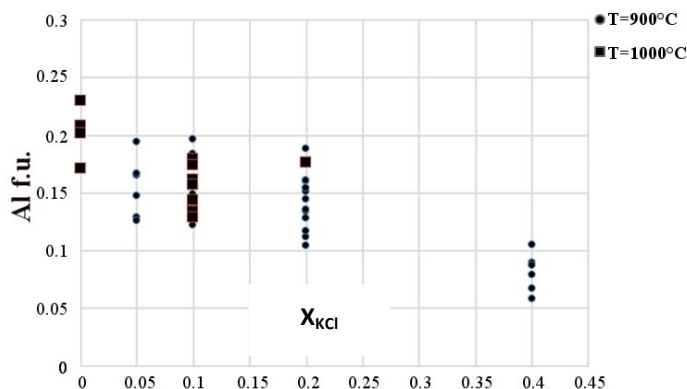
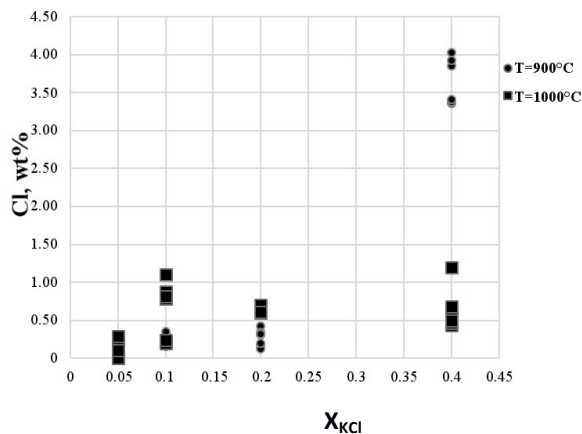


Fig. 4. Dependence of the Cl-content (wt. %) in phlogopite on the KCl content in the starting fluid at 900°C and 1000°C .

Reaction (5) is manifested in a decrease of the Al content in orthopyroxene with the increase in X_{KCl} in the starting fluid (Fig. 3). With the increase of X_{KCl} in the starting fluid, the Cl content in mica increases as well, reaching 0.6 - 0.8 wt. % at $X_{\text{KCl}} = 0.2 - 0.4$ (Fig. 4). Such Cl content in the synthetic phlogopite is consistent with the Cl content in phlogopites of metasomatized peridotites and inclusions in diamonds (see Figure 3 in [5]).

In the products of some experiments at $X_{\text{KCl}} > 0.1$, kyanite (Ky) appears. Its formation is also related to the decomposition of pyrope in the presence of the H_2O -KCl fluid by a reaction

$$\text{Prp} + [\text{KCl} + 1/2\text{H}_2\text{O} + 1/2\text{SiO}_2] = 1/2\text{Phl} + 1/2\text{Cl-Phl} + 1/2\text{Ky} \quad (6)$$

The presence of SiO_2 in the fluid can be due to either the initial slight excess of this component in the starting mixtures or the sufficiently high solubility of SiO_2 in the fluid in equilibrium with the Phl + En assemblage (e.g. [15]). High activity of SiO_2 in the saline fluid is indirectly indicated by the absence of forsterite in the run products (it was

observed only in the experiment PEH-2 experiment, Table 1), which is a typical product of phlogopite dissolution in aqueous fluids (e.g. [15]).

Discussion and conclusion. The experiments reproduce the major reaction occurring during transformation of upper-mantle garnet peridotites in the course of mantle metasomatism under the influence of the H_2O -KCl fluids, leading to the formation of phlogopite-bearing assemblages. Al-bearing orthopyroxene and garnet are not stable in the presence of H_2O -KCl fluid even at $X_{\text{KCl}} = 0.05$. This result is comparable with the results of previous experimental studies, which used other potassic fluid components. Thibault and Edgar [16] have experimentally studied reactions of phlogopite formation in the model pyrolite interacting with H_2O - K_2CO_3 solutions at 2–3 GPa and 850 – 950°C . Content of phlogopite systematically increased relative to those of orthopyroxene, olivine, and clinopyroxene, as well as the Opx/Cpx and Opx/Ol ratios decreased, with increasing K_2CO_3 concentration in the solutions. The dominant phase

whose decomposition results in phlogopite is garnet according to reaction (1). However, authors did not reported variations of mineral compositions with the fluid composition. Our results show that the Al content of orthopyroxene and Cl in phlogopite according to reaction (5) are direct indicators of the KCl activity in the fluid. This effect can be used to quantify this activity, and hence the concentration of KCl in saline fluids acting in the processes of the modal mantle metasomatism.

The study was supported by the Russian Foundation for Basic Research (project 16-05-00266).

References:

- Dawson JB. (1980) Kimberlites and their xenoliths. Berlin: Springer.
- Harte B. Mantle peridotites and processes—the kimberlite sample. (1983) In: Hawkesworth CJ and Norry MJ. editors. Continental Basalts and Mantle Xenoliths. Cheshire: Shiva. p. 46–91.
- O'Reilly SY, Griffin WL. (2013) Mantle metasomatism. In: Harlov DE and Austerheim H. editors. Metasomatism and the chemical transformation of rock. Berlin. Heidelberg: Springer. p. 471–533.
- Sobolev NV. (1977) The Deep-Seated Inclusions in Kimberlites and the Problem of the Composition of the Upper Mantle. Washington: American Geophysical Union.
- Safonov OG, Butvina VG. (2013) Interaction of the model peridotite with the H₂O-KCl fluid: an experiment at a pressure of 1.9 GPa and its application to the processes of upper mantle metasomatism. *Petrology*. V. 21(6), p.599–615. <https://doi.org/10.1134/s0869591113060076>
- Safonov OG, Butvina VG. (2016) Indicator reactions of K and Na activities in the upper mantle: natural mineral assemblages, experimental data, and thermodynamic modeling. *Geochemistry*. V.54(10), p. 858–872. <https://doi.org/10.1134/S0016702916100098>
- Aoki K. (1975) Origin of phlogopite and potassic richterite bearing peridotite xenoliths from South Africa. *Contrib. Mineral. Petrol.* V.53, p.145-156. <https://doi.org/10.1007/bf00372601>
- Jones AP, Smith JV, Dawson JB. (1982) Mantle metasomatism in 14 veined peridotites from Bultfontein Mine, South Africa. *J. Geol.* p. 435–453.
- Erlank AJ, Waters FG, Hawkesworth CJ, Haggerty SE, Allsopp HL, Rickard RS, Menzies MA. (1987) Evidence for mantle metasomatism in peridotite nodules from the Kimberley pipes, South Africa. In *Mantle Metasomatism* (Academic Press, London). p. 221–311.
- Waters FG, Erlank AJ. (1988) Assessment of the vertical extent and distribution of mantle metasomatism below Kimberley, South Africa. *J. Petrol. Spec. Lithosphere*, p. 185–204.
- Lloyd FE, Bailey DK. (1975) Light element metasomatism of the continental mantle: the evidence and the consequences. *Phys. Chem. Earth*. V. 9. p. 389–416.
- Konzett J, Armstrong RA, Gunther D. (2000) Modal metasomatism in the Kaapvaal craton lithosphere: constraints on timing and genesis from U–Pb zircon dating of metasomatized peridotites and MARID-type xenoliths. *Contrib. Mineral. Petrol.* V. 139, p.704–719.
- van Achterbergh E, Griffin WL, Stiefenhofer J. (2001) Metasomatism in mantle xenoliths from the Letlhakane kimberlites: estimation of element fluxes. *Contrib. Mineral. Petrol.* V. 141, p. 397–414. <https://doi.org/10.1007/s004100000236>
- Litvin YuA. Physicochemical studies of the melting of the deep matter of the Earth. Moscow: Nauka; 1991.
- Schneider ME, Eggler DH. (1986) Fluids in equilibrium with peridotite minerals: implications for mantle metasomatism. *Geochimica et Cosmochimica Acta*. V. 50, № 5, p. 711–724. [https://doi.org/10.1016/0016-7037\(86\)90347-9](https://doi.org/10.1016/0016-7037(86)90347-9)
- Thibault Y, Edgar A. D. (1990) Patent mantle–metasomatism: inferences based on experimental studies. *Proc.Ind. Acad. Sci.–Earth and Planetary Sci.* V. 99, № 1, p. 21–37.

Chanyshv A.D.¹, Litasov K.D.¹, Goncharov A.F.² Raman spectroscopic study of n-docosane (C₂₂H₄₆) at high pressures UDC 552.1:549.08

¹Sobolev Institute of Geology and Mineralogy SB RAS, Novosibirsk, Russia, chanyshv_90@mail.ru
klitasov@igm.nsc.ru

²Geophysical Laboratory, Carnegie Institution of Washington, Washington DC, USA
agoncharov@carnegiescience.edu

Abstract. This work is devoted to the experimental study of n-docosane C₂₂H₄₆ at high pressure up to 29 GPa and 298 K using *in situ* Raman spectroscopy in a diamond anvil cell. We observed shift of Raman bands to higher frequencies and detected phase transitions at 1.6–3.8 and 10.8–11.0 GPa.

Keywords: High pressure, Raman spectroscopy, diamond anvil cell, n-docosane, phase transition.

Introduction. N-Docosane (C₂₂H₄₆) is an acyclic saturated n-alkane. It is solid at standard conditions with melting temperature of 317.7 K (Makarenko et al., 2004). The study of heavy n-alkanes becomes extremely important due to their importance in practical applications, especially in terms of understanding of their role with respect to the cold flow behavior of fuels. n-Alkanes form the basis of lipids, some liquid crystals and polymers, and take part in the vital functions of plants and animals. n-Docosane is an important component in petroleum systems. Heavy alkanes are predicted to be stable in planetary mantle fluids at depths of 300–600 km and deeper (Spanu et al., 2011; Zubkov, 2009). High-pressure study of n-docosane is critical for experimental petrology and chemistry: solid hydrocarbon can be used as the source of carbon and hydrogen in model systems using multianvil and toroid apparatuses or diamond anvil cell (DAC) (e.g., Sokol et al., 2017). Numerous high-pressure studies of linear n-alkanes have been conducted over the past decades, including methane (Hirai et al., 2008; Sun et al., 2009), ethane (Shimizu et al., 1989), propane (Kudryavtsev et al., 2017), pentane (Qiao and Zheng, 2005), hexane (Kavitha and Narayana, 2007) and heptane (Kavitha and Narayana, 2006). At ambient pressure and room temperature n-docosane possesses a triclinic structure *P*1 with one molecule per unit

cell (Broadhurst, 1962). Increasing temperature leads to rotational phase transition at 311.3-312.1 K (Makarenko et al., 2004). In this paper we performed in situ Raman spectroscopic measurements of n-docosane to 29 GPa at room temperature.

Experimental details. Symmetric-type diamond anvil cell with a culet size of 300 μm was used for present experiments. A pre-indented stainless steel gasket was drilled to have 80 μm hole at the center to load the n-docosane along with a small ruby chip. The n-docosane itself acted as the quasihydrostatic pressure medium. The ruby fluorescence technique was used to calibrate the pressure applied on the sample (Mao et al., 1986).

We used custom Raman spectrometer with the 514.5 nm line of an Ar-ion laser (Goncharov and Crowhurst, 2005). The spectra were collected with the 460-mm focal length f/5.3 imaging spectrograph equipped with two 1500 and 300 grooves per mm

gratings on the same turret. The spectra were collected at room temperature with resolution of approximately 2 cm^{-1} . Acquisition time was 300–600 s. Spectra calibration was carried out using the 520.6 cm^{-1} line of a silicon wafer. We have determined the frequency and intensity of the Raman spectra using Lorentzian function with appropriate background.

Results and Discussion. The Raman spectra of n-docosane at ambient condition and high pressures are shown at Figure 1. n-Docosane possesses a great number of Raman modes, which could be classified into the following groups: (1) C-C-C angle bending mode, (2) methyl rocking mode, (3) C-C skeletal stretching modes, (4) methylene and methyl bending modes and (5) polymethylene and methyl stretching modes. Some of these Raman modes are weak due to the presence of the predominant first-order diamond peak from the experimental cell.

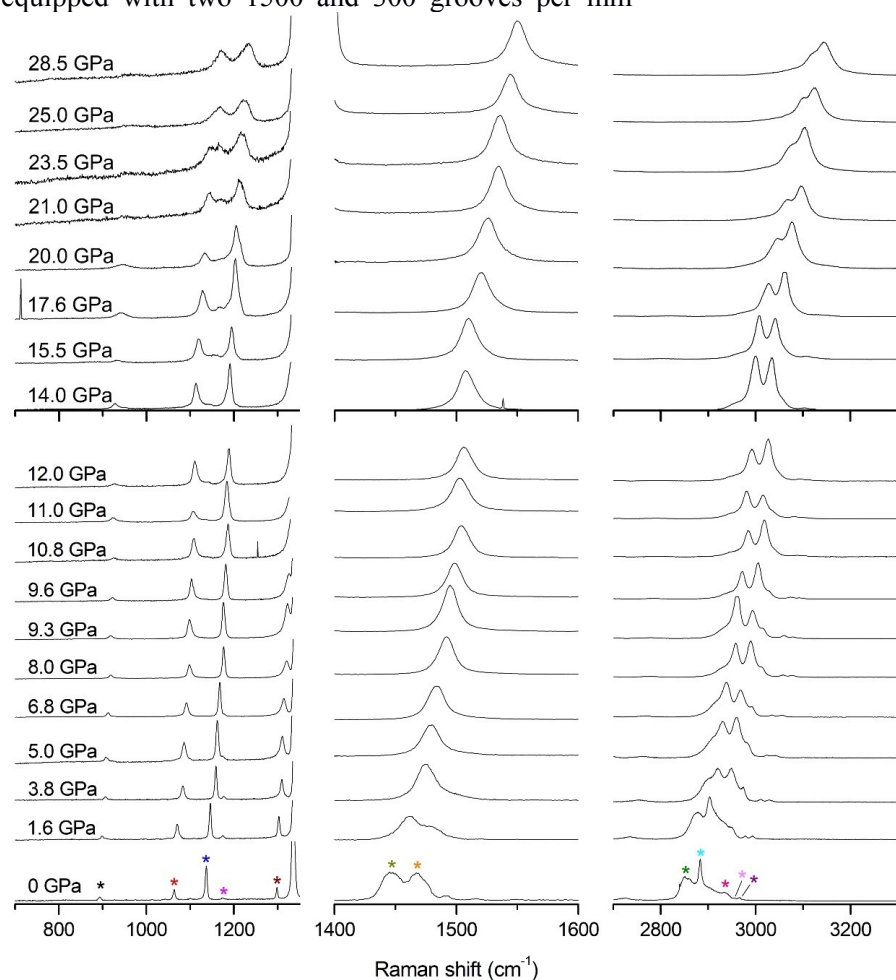


Fig. 1. Raman spectra of n-docosane obtained at ambient temperatures and high pressures upon compression to 28.5 GPa. For clarity, the spectra have been divided into three regions: 700–1350, 1400–1600 and 2700–3300 cm^{-1} . The 1350–1400 cm^{-1} region is dominated by the diamond first-order peak and is not shown. The colored stars represent various Raman modes.

The drastic changes in the Raman mode behavior with pressure is an indicator of a phase transition. The pressure dependency of various Raman modes are shown at Figure 2. The mode assignment was based on the results by Mayo et al. (2003). It was found that all these Raman bands shifted to higher wavenumbers almost linearly with increasing pressure, and at about 1.6–3.8 and 10.8–11.0 GPa sudden changes occurred.

C-C skeletal stretching region and CH_2/CH_3 rocking region (700–1300 cm^{-1}) The modes in the 700–1300 cm^{-1} region are associated with the symmetric and asymmetric skeletal stretching of the C-C bonds and the CH_3 and CH_2 rocking modes. Figure 2 shows the pressure dependence of these modes. Mode at 893 cm^{-1} is associated with the $-\text{CH}_3$ end group (methyl rocking mode). This mode has a positive $d\omega/dP$. The disappearance of this mode was observed at 20 GPa.

Mineral equilibria at high PT-parameters

The mode at 1063 cm^{-1} has contribution from skeletal C-C stretching. This mode has a positive $d\omega/dP$ to 28.5 GPa (Table 1). Band at 1136 cm^{-1} has contribution from methyl rocking and C-C stretching modes. The band has a positive value of $d\omega/dP$ to 28.5 GPa (Table 1). At 11 GPa, a new mode at 1136 cm^{-1} appears on the spectra. The mode is characterized by a positive value of $d\omega/dP$ up to 23.5 GPa (Table 1). The band at 1173 cm^{-1} corresponds to

symmetric CH_3 rocking mode. The mode has a positive value of $d\omega/dP$ up to 28.5 GPa (Table 1). The mode at 1299 cm^{-1} corresponds to methylene in-phase twisting. The mode has a positive $d\omega/dP$. The disappearance of this mode was observed at 9.6 GPa.

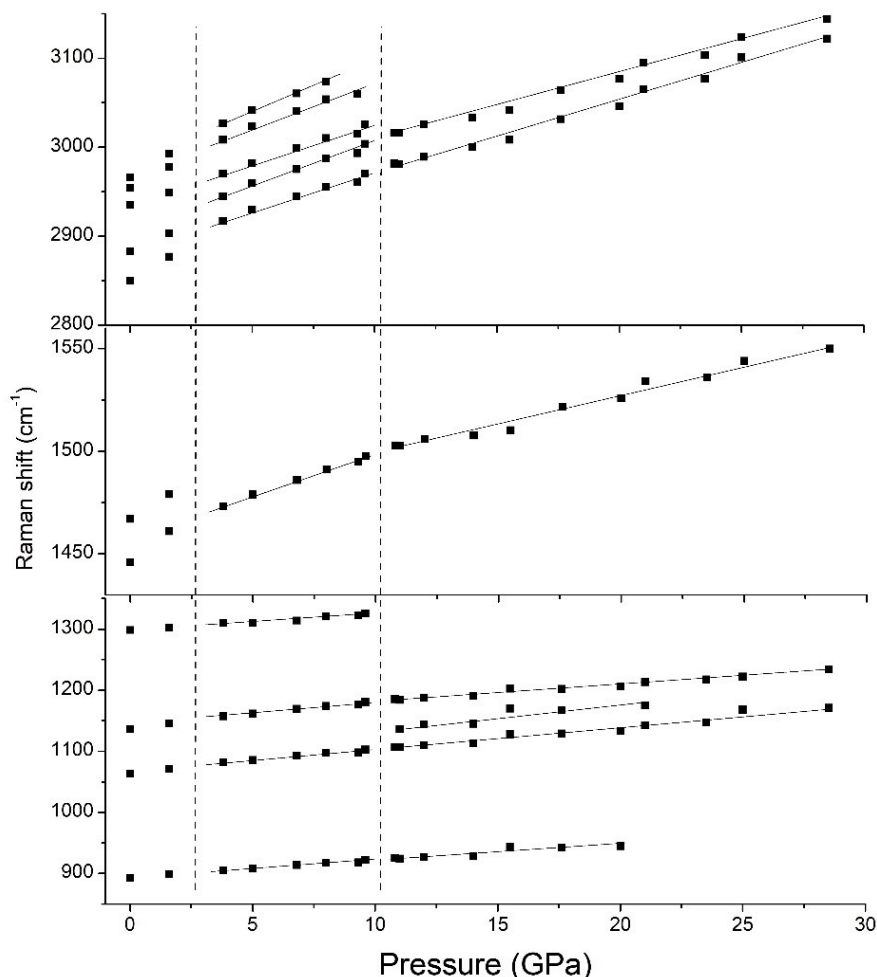


Fig. 2. Raman modes of n-docosane as a function of pressure. The solid lines are the linear fit to the data. Vertical dashed lines indicate the phase transition boundaries for n-docosane.

Table 1. Frequency (ω) of the Raman modes of n-docosane and its pressure derivative ($d\omega/dP$) observed in different phases.

| Phase I (1 atm) | | Phase II (> 3,8 GPa) | | Phase III (> 11,0 GPa) | | mode assignment |
|-------------------------------|--------------|-------------------------------|--------------|-------------------------------|--------------|--|
| ω (cm^{-1}) | $d\omega/dP$ | ω (cm^{-1}) | $d\omega/dP$ | ω (cm^{-1}) | $d\omega/dP$ | |
| 893 | 3.8 | 905 | 2.8 | 924 | 2.5 | methyl rocking mode |
| 1063 | 5.0 | 1082 | 3.5 | 1107 | 3.8 | skeletal C-C stretching |
| 1136 | 6.3 | 1157 | 3.9 | 1136 | 4.0 | CH_3 rocking + C-C stretching |
| 1173 | 1.3 | 1177 | 0.0 | 1184 | 2.7 | symmetric CH_3 rocking |
| 1299 | 2.5 | 1310 | 2.8 | | | $(\text{CH}_2)_n$ in-phase twisting |
| 1446 | 9.4 | 1473 | 4.1 | 1503 | 2.9 | asymmetric CH_2 , CH_3 bending |
| 1467 | 7.5 | | | | | CH_3 deformation |
| 2850 | 16.9 | 2917 | 8.8 | 2981 | 8.3 | symmetric CH_3 stretching |
| 2883 | 12.5 | 2945 | 9.7 | 3016 | 7.5 | symmetric CH_2 stretching |
| 2935 | 8.8 | 2970 | 8.9 | | | asymmetric CH_2 stretching |
| 2954 | 15.0 | 3008 | 9.5 | | | asymmetric CH_3 stretching |
| 2966 | 16.9 | 3027 | 11.1 | | | asymmetric CH_3 stretching |

CH₃ and CH₂ stretching region (2800-3200 cm⁻¹)

The C-H stretching region is influenced by large intramolecular interaction and interaction between symmetric C-H stretching fundamental and the overtone of the >CH₂ scissor mode (Kavitha and Narayana, 2007). The modes at 2850 и 2883 cm⁻¹ are associated with symmetric CH₂ and CH₃ stretching, respectively. The modes have a positive d ω /dP up to 28.5 GPa (Table 1). The mode at 2935 cm⁻¹ has contribution from asymmetric CH₂ stretching, the modes at 2954 and 1966 cm⁻¹ are associated with asymmetric CH₃ stretching. These modes have a positive value of d ω /dP up to 8.0-9.6 GPa (Table 1). At higher pressures we observed the disappearance of these modes.

Conclusions We have defined the shift of all modes of n-docosane to the higher wavelengths region. We have also determined the disappearance of the Raman bands and the appearance of new modes in the pressure intervals of 1.6-3.8 and 10.8-11.0 GPa, which indicates phase transitions of the n-docosane. It is important to note that the phase transitions affect the behavior of the vibrational mode in the same way as in lighter alkanes, such as ethane (Shimizu et al., 1989), propane (Kudryavtsev et al., 2017), pentane (Qiao and Zheng, 2005), hexane (Kavitha and Narayana, 2007) and heptane (Kavitha and Narayana, 2006).

This work was supported by the RF state assignment project No. 0330-2016-0012. AC thanks for partial support from the BP grant 2018 for young scientists.

References:

Broadhurst M.G. An analysis of the solid phase behavior of the normal paraffins // Journal of Research of the National Bureau of Standards A. – 1962. – V.66 – P.241–249.
Goncharov A.F., Crowhurst J.C. Raman spectroscopy under extreme conditions // Journal of Low Temperature Physics – 2005. – V.139 – P.727–737.
Hirai, H., Konagai, K., Kawamura, T., Yamamoto, Y., Yagi, T. Phase changes of solid methane under high pressure up to 86 GPa at room temperature // Chemical Physics Letters. – 2008. – V.454 – P. 212-217.
Kavitha G., Narayana C. Raman scattering studies on n-heptane under high pressure // The Journal of Physical Chemistry B. – 2006. – V.110 – P.8777–8781.
Kavitha G., Narayana C. Raman spectroscopic investigations of pressure-induced phase transitions in n-hexane // The Journal of Physical Chemistry B. – 2007. – V.111 – P.14130–14135.
Kudryavtsev D., Serovaikii A., Mukhina E. et al. Raman and IR spectroscopy studies on propane at pressures of up to 40 GPa // The Journal of Physical Chemistry A. – 2017. – V.121. – P.6004-6011.
Makarenko S., Puchkovska G., Kotelnikova E., Filatov S. Spectroscopic study of rotation-crystalline modifications of mixtures of n-paraffins C₂₂–C₂₄ // Journal of Molecular Structure. – 2004. – V.704 – P.25–30.

Mao H., Xu J.-A., Bell P. Calibration of the ruby pressure gauge to 800 kbar under quasi-hydrostatic conditions // Journal of Geophysical Research: Solid Earth. – 1986. – V.91 – P. 4673–4676.
Mayo D. W., Miller F. A., Hannah R. W. Course notes on the interpretation of infrared and Raman spectra. – Wiley. – 2004.
Qiao E., Zheng H. Raman scattering spectroscopic study of n-pentane under high pressure // Applied spectroscopy. – 2005. – V.59 – P.650–653.
Shimizu H., Shimazaki I., Sasaki S. High-pressure Raman study of liquid and molecular crystal ethane up to 8 GPa // Japanese Journal of Applied Physics. – 1989. – V. 28 – P. 1632–1635.
Sokol, A.G., Tomilenko, A.A., Bul'bak, T.A. et al. Carbon and nitrogen speciation in N-poor C-O-H-N fluids at 6.3 GPa and 1100–1400° C // Scientific Reports. – 2017. – V.7 – P.706.
Spanu L., Donadio D., Hohl D., Schwegler E., Galli G. Stability of hydrocarbons at deep Earth pressures and temperatures // Proceedings of the National Academy of Sciences. – 2011. – V.108 – P.6843-6846.
Sun L., Yi W., Wang L., et al. X-ray diffraction studies and equation of state of methane at 202 GPa // Chemical Physics Letters. – 2009. – V.473 – P.72-74.
Zubkov, V. On the probable lifting of deep hydrocarbons into the crustal waveguide // Doklady Earth Sciences. – 2009. – V.427 – P. 1017-1019.

Fedkin V.V. Geochemical features of eclogites from the Maksyutov complex (South Urals)

UDC 549.6+552.16:552.48

D.S.Korzhinsky Institute of Experimental Mineralogy RAS, Chernogolovka (vfedkin@iem.ac.ru)

Keywords: Maksyutov complex, Ural Mountains, UHP metamorphism, protolith, eclogite, subduction, XRF bulk-rock chemistry

The Maksyutov eclogite-glaucophane schist complex in the South Urals is one of the perfect examples of plate-tectonic formations (terranes) within collision zone between large structural-tectonics elements of the Earth's crust. Usually, such complexes trace convergent suture zones and normally bear high (HP) or ultrahigh pressure (UHP) features. Characteristic UHP phases (quartz pseudomorphs after coesite, graphite cuboids pseudomorphs after diamond, and diamond microinclusions in garnet) are also found in Maksyutov mafic and quartz-feldspar rocks (Chesnokov and Popov, 1965; Dobretsov and Dobretsova, 1988; Leech, Ernst, 1998, 2000; Bostick et al., 2003). These data suggest that, during the Late Devonian, parts of the Maksyutov complex were subjected to UHP conditions (~600° C, >2.8 GPa for coesite and >3.0 GPa for diamond). The peak of UHP eclogite-facies metamorphism occurred at ~385 Ma, and the complex was later exhumed through

retrograde blueschist-facies and greenschist facies conditions by ~360-335 Ma.

Despite the long history of the study of the complex, the issues of the relationship between both P-T-t conditions of formation of UHP rocks, the geochemistry of their protoliths, the evolution of metamorphic processes and geodynamic development of the region remain unclear. In this paper, an attempt is made to generalize available data and to perform a comprehensive study of UHP rocks of the complex: to determine the nature and sources of protolith of UHP rocks based on bulk-rock chemistry, to calculate P-T parameters of mineral formation using the microprobe data, and to decipher the periodicity and stages of the of metamorphic and geodynamic evolution of the region. To this end, 18 representative samples of UHP rock were collected in the southern part of the Maksyutov complex, high-quality XRF and ICP MS bulk-rock analyzes were made, detailed microprobe studies of the composition and zonality of rock-forming minerals were performed and the parameters of their formation were calculated.

The Maksyutov complex is located in the zone of the Main Ural fault at the boundary of the Riphean rocks of the Suvanyak complex of the East European platform in the west and the Kempirsai hyperbasite belt, as a part of the Magnitogorsk island arc, in the east. Three structural-material (lithologic-tectonic) units are distinguished within the complex (Lennykh et al., 1995, Beane, Leech, 2007):

(1) the lower "subcontinental" eclogite-glaucophane schist unit: glaucophane and feldspar-micaceous schists, quartzites with lenses, boudins and interlayers of eclogites, garnet-pyroxene and less often olivine-enstatite rocks;

(2) upper metaophiolitic unit, consisting of rocks of the oceanic crust, associated graphite crystalline schists and metagreywacks, sometimes including bodies and lenses of serpentinites, marbles and metabasalt rocks; and

(3) an intermediate Yumaguzin unit - metasedimentary rocks (quartzites and micaceous schists, without eclogite).

The lower unit of the complex is of the most petrological interest. Numerous mafic eclogite boudins, lenses and interlayers in host garnet-glaucophane-mica schists and the presence of olivine-enstatite, quartz-jadeite and lawsonite associations determine the culmination of prograde metamorphism in the range 550-700 °C and 0.8-2.4 GPa (Dobretsov et al., 1996, Lennykh et al., 1995, Beane, Connelly, 2000, Leech, Ernst, 2000). However, reports on mineralogical indicators of HP and UHP conditions (coesite and diamond) suggest

that lithostatic pressure at the early stage of mineral formation could reach at least 2.8-3.2 GPa. These data are confirmed by findings of jadeite eclogites in contact with ultramafic (Ol-Enst) UHP rocks (Valizer et al., 2015) and new data from mineralogical geothermobarometry (Fedkin et al., 2017), on the basis of which it is assumed that the peak parameters of the eclogitic metamorphism could reach values of $T = 550-700\text{ °C}$ and $P > 2.8-3.5\text{ GPa}$. During the first stage of exhumation, Maksyutov rocks were metamorphosed at a temperature increase up to 700-800 °C, and then decrease to 300-400 °C at pressure of 0.6-0.8 GPa (Beane, Leech, 2007, Valizer et al., 2011).

The most studied and informative part of the Maksyutov complex (the localities Shubino, Antingan, Novosimbirka, Karayanova and Ivanovka) was selected for detailed study of eclogites. Eighteen representative samples garnet-bearing mafic rocks were analyzed from different parts of large boudins, from eclogitic lenses and interlayers within Grt-Cpx-Gln-mica schists. High-quality XRF and ICP MS bulk-rock analyzes on the major-, trace-, and rare-earth elements were performed at the Geoanalytical Laboratory of Washington State University. Microprobe analysis of the compositions of coexisting minerals for thermobarometry purposes was carried out at the D.S.Korzinsky Institute of Experimental Mineralogy Russian Academy of Sciences.

New bulk-rock analyses reflect the presence of MORB, OIB, and IAT basaltic and andesitic series and their metasomatized equivalents. Wide scatter in the major, trace, and rare-earth bulk-rock elements probably reflects multiple metasomatic stages of alteration of the basaltic protoliths in contrasting oceanic and subduction-zone realms. The major component of the analyzed samples show a wide range of SiO₂ content: from 41.8-61.12 wt. %. However, all of the samples plot in the field of low potassium basalts, and only some of them correspond to andesite basalts (basaltic andesites). The element fractionation trends (FeO* (total) and MgO decrease with increasing SiO₂, increasing Na₂O with increasing SiO₂, FeO*-MgO reverse correlation) reflect the transition from basalt to andesite compositions. The AFM diagram (Fig.1) shows the eclogite field with clearly distinguished enriched and depleted basalt compositions forming a single trend of tholeiite and calc-alkaline petrogenetic series, which emphasizes a complex geodynamic setting for formation of their protoliths. At the same time, the alkali - silica correlation (Fig.2) reflects typical differentiation trends for a protolith of HP and UHP metamorphic rocks.

As for rare and trace elements, bulk-rock compositions of the analyzed samples (Fig. 3) overlap the fields of basalts of the oceanic islands (Fig. 3, OIT, OIA), the N-MORB and E-MORB fields, and island-arc tholeiites (Fig. 3, IAT), demonstrating a wide range of possible plate-tectonic settings. In such a situation, the composition of initial rocks could vary either due to the diversity of heterogeneous protoliths from a wide range of plate-tectonic environments from which they were subducted or because of the contrasting intensity of metasomatic processes at different stages of their recrystallization (metasomatism of the seabed, prograde and / or retrograde metamorphism during subduction).

Bulk-rock REE patterns normalized to chondrites show the same spread, but compositions of the N- and E-type MORBs are not widely divergent. Somewhat enrichment of the precursor rocks by light REE suggests a combination of subduction and metasomatic processes for the ocean metabasalts. Most of the analyzed garnet-bearing rocks (with the exception of one) of the Maksyutov complex apparently reflect transformation from a basaltic precursor because they lack positive Eu and Sr anomalies characteristic of crustal-level (moderate pressure) gabbroic intrusions. The REE patterns are similar to those for N-MORB and E-MORB types.

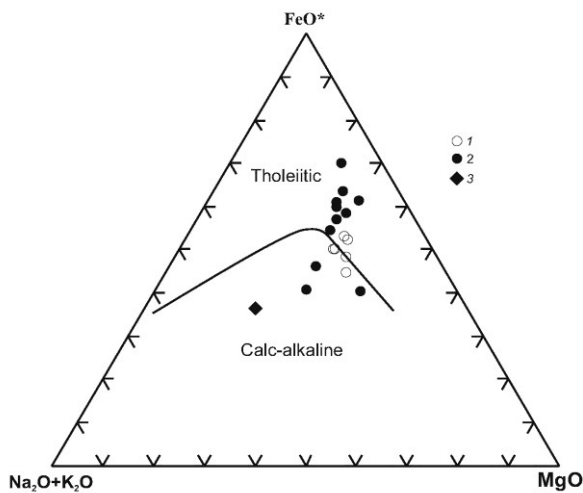


Fig. 1. AFM diagram for Maksyutov eclogite compositions. 1-2 - basalt compositions: 1 - depleted, 2 - enriched; 3 - andesite composition.

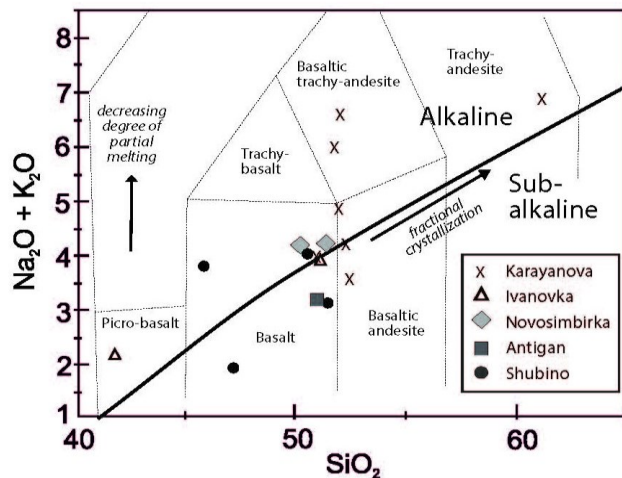


Fig. 2. Alkali vs. silica correlation of the Maksyutov eclogites.

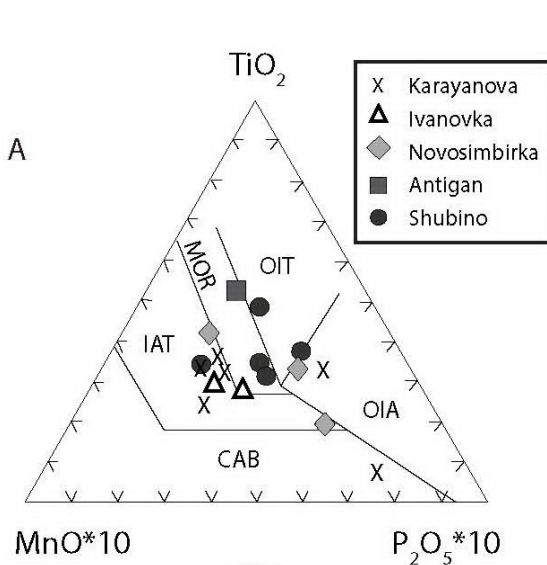


Fig. 3. Discrimination diagram for Maksyutov eclogites by rare and trace elements.

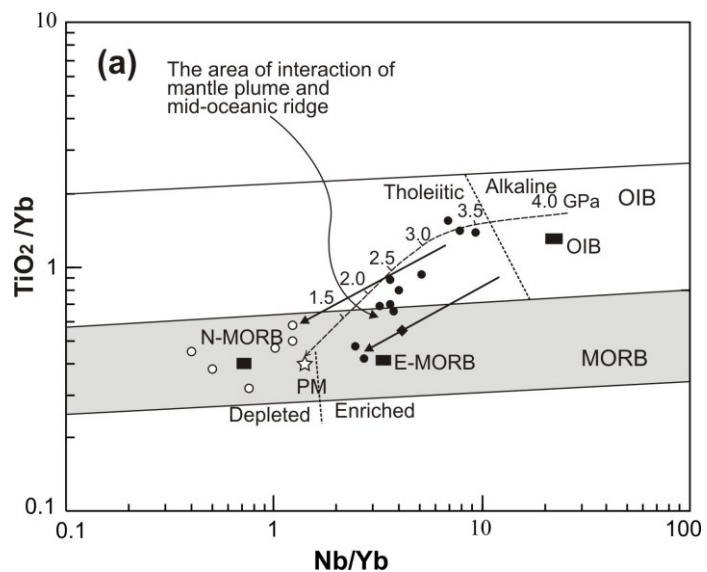


Fig. 4. $TiO_2/Yb-Nb/Yb$ diagram for Maksyutov eclogite compositions (Shchipansky, Fedkin et al., 2012). The field division and N-MORB, E-MORB, OIB, PM (primitive mantle) and CC (continental crust) mean values are from Pierce (2008).

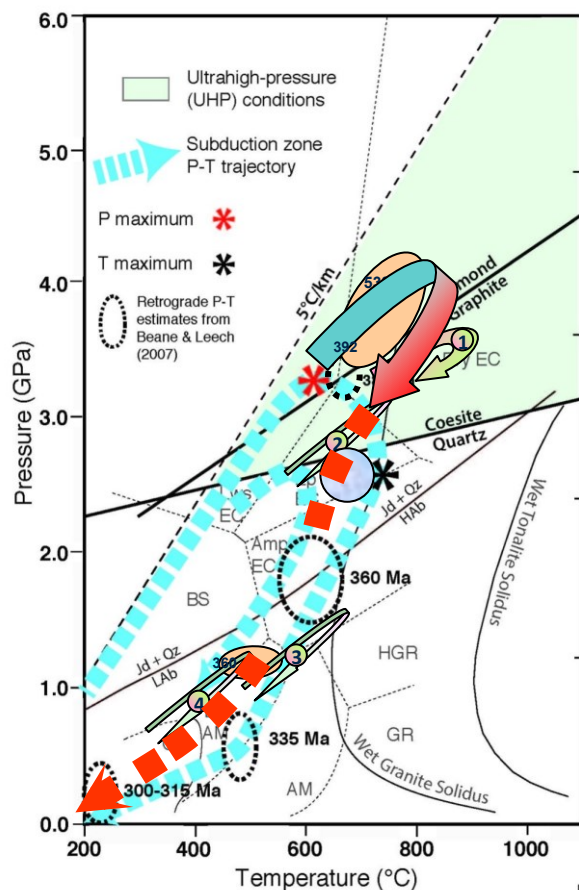


Fig. 5. Physicochemical conditions of the Maksyutov complex formation.

- * The maximum pressure in the early prograde stage in the subduction zone fixes the **geothermal gradient**
- P-T conditions for the formation of peak associations of eclogites - **the transition area from the subduction regime to exhumation** of the complex.
- Thermal maximum at the early stage of exhumation of the complex.
- * P-T-t trend evolution of metamorphism during the exhumation of the complex - **the gradient of the metamorphic field**
- Four episodes of conjugated prograde and retrograde metamorphism (Fedkin et al., 2017)
- Parameters Perple_X modeling: T = 650-675 C, P = 2.4-2.6 GPa (Burlik, Leech, Ernst, 2014)

Figure 9

Thus, bulk-rock geochemistry by major, trace and rare-earth elements for Maksyutov eclogites shows that their protoliths were tholeiite and subalkaline basalts of both enriched (OIB type) and depleted (N- and E-MORB types) compositions, which inherited features of subduction and further metasomatic processes. On the other hand, modeling of magma generation processes (Pierce, 2008) based on eclogite bulk-rock compositions clearly shows a possible interaction of a mantle plume source of OIB type and a depleted mantle source of MORB type in the pressure range of 1.5-4.0 GPa (Fig. 4). The possibility of such interaction is confirmed by new data on the ancient (≥ 533 Ma) UHP ultramafic rocks associated with eclogites at parameters up to 700-800 °C and $P > 3.2-4.0$ GPa (Valizer et al., 2015). According to the authors, the data give evidence to the participation of the ancient substratum tectonic mantle-crust inclusions in the complex formation. Bulk-rock geochemistry data of the eclogites of the Maksyutov complex shows that the geodynamics of the formation of their protoliths can not be reduced to any simple model. This process combined three different sources: the depleted N-MORB mantle, the enriched OIB mantle, and the contribution of the subduction component involving the process of crustal magma generation, which is estimated from 1 to 4% (Shchipsansky, Fedkin et al., 2012).

Coesite relics, micro-diamond aggregates and mantle-crust inclusions of ultrabasic rocks indicate a peak pressure $> 3.2-4$ GPa in the early prograde stage of metamorphism and define the geothermal gradient of the subduction zone (Fig. 5).

Mineralogical thermobarometry and the Perple_X modeling parameters reflect the initial stage of HP exhumation and the position of the metamorphic field gradient, within which at least four episodes of the metamorphic evolution of the complex are distinguished (Fedkin et al., 2017). Retrograde metamorphism of the last stages, which took place under blueschist and greenschist facies condition, was apparently accompanied by Na-metasomatism processes along the shear-zone-defined solution paths.

As can be seen from Fig. 5, all the main evolutionary events of the mafic eclogites of the Maksyutov complex proceeded under conditions close to the gradient line of the metamorphic field. Only relics of UHP minerals and mantle-crust inclusions of hyperbasitic rocks reflect the prograde stage of the subduction process. Thus, the final main events in the geodynamic history of the complex were the processes of pushing the Paleo-Asian oceanic plate under the continent and its exhumation. However, the details of the geodynamic model require further research.

Acknowledgements. The work was funded by Fulbright Program of the Institute of International Education (grants for 2011 and 2015). The author is grateful to Prof. W.G.Ernst (Stanford University), Prof. M.Leech (San Francisco State University), Dr. A.A.Shchipsansky (GIN RAS) and Dr. P.M.Valizer (Ilmen State Reserve, Ural branch, RAS) for initiating this research, support and help.

References:

- Beane, R.J., and Connelly, J.N., 2000, $^{40}\text{Ar}/^{39}\text{Ar}$, U-Pb, and Sm-Nd constraints on the timing of metamorphic events in the Maksyutov Complex southern Ural Mountains: *Journal of the Geological Society, London*, v. 157, p. 811-822.
- Beane, R.J., and Leech, M.L., 2007, The Maksyutov Complex: The first UHP terrane 40 years later, *in* Cloos, M., Carlson, W.D., Gilbert, M.C., Liou, J.G., and Sorensen, S.S., eds., *Convergent Margin Terranes and Associated Regions: A Tribute to W.G. Ernst*: Geological Society of America Special Paper no. 419, p. 153-169, doi: 10.1130/2006.2419(08)
- Bostick, B.C., Jones, R.E., Ernst, W.G., Chen, C., Leech, M. L., and Beane, R. J., 2003, Low-temperature microdiamond aggregates in the Maksyutov metamorphic complex, south Ural Mountains, Russia: *American Mineralogist*, v. 88, p. 1709-1717.
- Burlick, T.D., Leech, M.L., and Ernst, W.G., 2014, Eclogite-facies metamorphism in the Maksyutov Complex, south Ural Mountains, Russia. \ \ Goldschmidt conference abstract, 07f-79.
- Chesnokov, B.V., and Popov, V.A., 1965, Increasing volume of quartz grains in eclogites of the South Urals: *Doklady Akademiya Nauk SSSR*, v. 162, p. 176-178.
- Dobretsov, N.L., and Dobretsova, L.V., 1988, New mineralogical data on the Maksyutovo eclogite-glaucophane schist complex, southern Urals: *Doklady Akademiya Nauk SSSR*, v. 300, p. 111-116.
- Dobretsov, N.L., Shatsky, V.S., Coleman, R.G., Lennykh, V.I., Valizer, P.M., Liou, J.G., Zhang, R., and Beane, R.J., 1996, Tectonic setting of ultrahigh-pressure metamorphic rocks in the Maksutov Complex, Ural Mountains, Russia: *International Geology Review*, v. 38, p. 136-160.
- Fedkin, V. V., Leech, M. L., Shchipansky, A. A., Burlick, T. D., and Ernst, W. G., 2017, Coexisting zoned garnets and clinopyroxenes from mafic eclogites of the Maksyutov Complex, South Ural Mountains, Russia: *Experiment in Geosciences*, v. 23, no. 1, 10 p.
- Leech, M.L., and Ernst, W.G., 1998, Graphite pseudomorphs after diamond? A carbon isotope and spectroscopic study of graphite cuboids from the Maksyutov Complex, south Ural Mountains, Russia: *Geochemica et Cosmochimica Acta*, v. 62, p. 2,143-2,154.
- Leech, M.L., and Ernst, W.G., 2000, Petrotectonic evolution of the high- to ultrahigh-pressure Maksyutov Complex, Karayanova area, south Ural Mountains, Russia: structural and oxygen isotopic constraints: *Lithos*, v. 52, p. 235-252.
- Lennykh, V.I., Valizer, P.M., Beane, R., Leech, M., and Ernst, W.G., 1995, Petrotectonic evolution of the Maksyutov Complex, southern Urals, Russia: implications for ultrahigh-pressure metamorphism: *International Geology Review*, v. 37, p. 584-600.
- Pearce, J.A., 2008, Geochemical fingerprinting of oceanic basalts with applications to ophiolite classification and the search for Archean oceanic crust: *Lithos*, v. 100, p. 14-48.
- Shchipansky A.A., Fedkin V.V., Ernst E.G., and Leech M.L., 2012 Petrochemical and geochemical characteristic of eclogites of the Maksyutov complex (preliminary data). \ \ In: *Mineralogy in a whole space of the word. RMS Annual Session and Fedorov Session. Conference proceedings. St. Petersburg 9-11.10.2012.* Lemaprint publisher, p. 271-273.
- Valizer P.M., Krasnobaev, A.A., and Rusin A.I., 2011, Ultrahigh-Pressure (UHP) associations in ultramafites of the Maksyutov complex (southern Urals): *Transactions of the Doklady Earth Sciences, Geochemistry Section*, v. 441, p. 1,645-1,648.
- Valizer, P. M., Krasnobaev, A. A., and Rusin, A. I., 2015, UHPM eclogite of the Maksyutov Complex (Southern Urals): *Doklady Akademii Nauk*, v. 461, p. 316-321.

Gorbachev N.S., Kostyuk A.V., Sultantov D.M., Nekrasov A.N. Experimental investigation of peridotite-H₂O and eclogite-H₂O systems at T=1000-1400°C, P=4 GPA: phase composition and critical relations. UDC 550.4.02

Institute of Experimental Mineralogy RAS, Chernogolovka, Moscow district. (gor@iem.ac.ru)

Abstract. Phase relationships in peridotite-H₂O and eclogite-H₂O systems were studied at T=1000-1400°C, P=4 GPa. In the peridotite system at T = 1000-1300°C quenching samples were characterized by anomalous structure and phase composition. The quenching material is represented by compacted microgranular powder consisting of isolated relicts of liquidus minerals of peridotite Ol, Opx, Cpx composition. The individual fragments were characterized by a "brecciated" texture formed by inclusions of Ol relicts in the Grt-Cpx matrix. Silicate glass was found in the form of isolated microglobules. In the eclogite system quenching samples were characterized by a massive structure, due to the fact that the silicate glass-quenching silicate melt, localized in the intervals between the liquidus phases of the Cpx-Grt composition, cemented the sample. The anomalous structure and phase composition of quenching samples of the peridotite system indicate the existence of critical relationships between the silicate melt and fluid. The structure and phase composition of quenching samples of the peridotite and eclogite system at T = 1400 and 1200-1300°C respective indicate the absence of critical relationships between the silicate melt and fluid.

Keywords: *peridotite, eclogite, fluid, critical relations, experiment*

Introduction. The existence of critical relationships at high pressures and temperatures is a feature of fluid-containing silicate systems. At critical pressure and temperature (PkTk), complete miscibility between the melt (m) and the fluid (f) is observed, with the formation of a supercritical fluid-melt, and at the second final critical point (2PkTk), when the P-T solidus of silicate and PkTk of m-f equilibrium are equal, observed the total miscibility between the liquidus phases, melt and fluid. According to experimental data, critical PkTk and 2PkTk in H₂O-containing silicate systems of monomineral (SiO₂, albite, nepheline, jadeite) and granite compositions lie in the range P = 0.7-2.3 GPa, T = 550-1050°C, increasing in the sequence Q, Ne, Ab, Jd, granite (Bureau, Keppler, 1999). In systems of the basic and ultrabasic composition, PkTk and 2PkTk have higher values. Thus, in the Fo-En-H₂O system, the pressure at the second final critical point is estimated at 12-13 GPa (Stalder et al. 2001), basalt (eclogite) + H₂O-5-6 GPa (Kessel et al., 2005), basalt (eclogite) + peridotite + H₂O - 3.8-4.0 GPa

Mineral equilibria at high PT-parameters

(Gorbachev, 2000), peridotite + H₂O - 3.8-4 GPa (Mibe et al., 2007, Gorbachev et al., 2015). Considering the large temperature interval between the solidus and the liquidus in the systems of the basic and ultrabasic composition, as well as the formation of mantle magmas with partial melting of the mantle matter at wide T interval, it is of great interest to investigate the critical relationships between the partial melts and the fluid in the presence of restite minerals of the refractory residue. In this respect, silicate systems have been poorly studied. The partial melting of H₂O-containing peridotite and eclogite at P = 4 GPa, T = 1000-1400°C, close to the mantle adiabat, was studied to estimate the initial critical P-T and the features of the interaction of supercritical fluid melt with silicates.

Methodology. The experiments were carried out at the IEM RAS on the anvil-with-hole apparatus NL-10 using a multi-ampoule quenching technique. In the interval T=1000-1250°C – Au ampoules, at T=1300°C – Au-Pd ampoules, at T=1400°C – Pt ampoules were used. The starting materials were Grt peridotite from the xenolith in the Obnazhennaya kimberlite pipe (Yakutia), tholeiitic basalt ST-1, chemical analogue of the Siberian trap and distilled H₂O. The weight ratio of silicate-H₂O varied from 6 to 2. The temperature was measured by a Pt30Rh/Pt6Rh thermocouple, the pressure at high temperatures was calibrated by the quartz-coesite equilibrium curve. The accuracy of determining the temperature and pressure in the experiments is estimated at ±5°C and ±1 kbar (Litvin, 1991). The duration of the experiment was from 8 to 24 hours.

Polished preparations of quenching samples were studied and analyzed in the IEM RAS on CamScan MV2300 ECM.

Results. Representative compositions of coexisting phases are given in Table 1. In the peridotite-H₂O system at T = 1000-1300°C quenching samples were characterized by an anomalous structure and phase composition (Table 1, Fig. 1). Their main feature is the absence of intergranular quenching silicate glass - quenched silicate melt, a characteristic feature of partial melting. Its absence led to their disintegration, the quenching material, which is represented by compressed microgranular powder consisting of isolated precipitates or splices of liquidus minerals of disintegrated peridotite - olivine Ol, orthopyroxene Opx, clinopyroxene Cpx. At T = 1000-1100°C, separate fragments of the quenching sample close to the solidus temperature of the H₂O-containing peridotite were characterized by a "breccia" texture (Fig. 1a). In such fragments ("breccias"), the peridotite association Ol + Opx was replaced by the newly formed eclogite association Grt-Cpx composition. In "breccias", the inclusion of Ol ± Opx relics is localized in the Grt + Cpx matrix of the composition. Ol from the "breccia" and the main mass are similar in content of Fe and Mg. At higher T=1200-1300°C and degrees of melting, fragments with a "breccia-like" texture did not occur, although reaction relations between Ol and Cpx were observed. At these parameters, silicate glass was found in the form of isolated microglobules of Al-Si-Ca composition (Fig. 1b).

Table 1. Peridotite-H₂O system. Representative compositions of coexisting phases.

| T = 1000°C | | | | | | | | | | | |
|------------|------------------|------------------|--------------------------------|-------|------|-------|-------|-------------------|------------------|--------------------------------|--------|
| | SiO ₂ | TiO ₂ | Al ₂ O ₃ | FeO | MnO | MgO | CaO | Na ₂ O | K ₂ O | Cr ₂ O ₃ | Total |
| Ol | 40.51 | 0.0 | 0.32 | 7.89 | 0.21 | 50.95 | 0.11 | 0.16 | 0.00 | 0.0 | 100.17 |
| Gr | 40.95 | 0.21 | 19.19 | 8.31 | 0.38 | 17.66 | 8.80 | 0.21 | 0.08 | 4.15 | 99.95 |
| Cpx | 52.04 | 0.18 | 3.19 | 1.71 | 0.17 | 16.45 | 21.51 | 1.28 | 0.04 | 0.56 | 97.11 |
| Opx | 54.64 | 0.0 | 3.70 | 5.23 | 0.29 | 34.52 | 0.83 | 0.23 | 0.00 | 0.32 | 99.76 |
| Chr | 0.46 | 0.25 | 18.63 | 16.62 | 0.0 | 13.45 | 0.43 | 0.23 | 0.07 | 44.81 | 94.95 |
| T = 1100°C | | | | | | | | | | | |
| Ol | 41.11 | 0.02 | 0.09 | 8.22 | 0.06 | 49.78 | 0.03 | 0.04 | 0.03 | 0.20 | 99.59 |
| Gr | 41.83 | 0.03 | 22.17 | 5.58 | 0.45 | 19.94 | 7.99 | 0.17 | 0.00 | 2.37 | 100.54 |
| Cpx | 52.77 | 0.15 | 2.57 | 2.55 | 0.17 | 18.56 | 21.52 | 0.05 | 0.05 | 0.70 | 99.10 |
| Chr | 0.71 | 0.17 | 37.38 | 10.41 | 0.56 | 19.37 | 0.13 | 0.12 | 0.03 | 34.40 | 103.28 |
| T = 1200°C | | | | | | | | | | | |
| Ol | 40.79 | 0.05 | 0.12 | 4.97 | 0.12 | 52.47 | 0.13 | 0.04 | 0.05 | 0.20 | 99.05 |
| Cpx | 50.06 | 0.18 | 5.33 | 5.56 | 0.26 | 16.05 | 18.28 | 0.01 | 0.00 | 0.52 | 96.31 |
| K-Cpx | 49.62 | 2.71 | 13.86 | 9.80 | 0.25 | 4.50 | 13.77 | 1.24 | 1.36 | 0.00 | 97.61 |
| Chr | 0.08 | 0.00 | 4.23 | 9.57 | 0.44 | 15.43 | 0.16 | 0.27 | 0.00 | 68.10 | 98.37 |
| Gl | 73.65 | 0.19 | 6.89 | 0.41 | 0.25 | 4.03 | 2.09 | 0.05 | 0.47 | 0.03 | 88.16 |
| T = 1300°C | | | | | | | | | | | |
| Ol | 41.52 | 0.14 | 0.09 | 5.66 | 0.04 | 54.90 | 0.08 | 0.00 | 0.00 | 0.01 | 102.67 |
| Cpx | 53.18 | 0.08 | 3.49 | 4.17 | 0.62 | 20.08 | 19.63 | 0.00 | 0.00 | 0.87 | 102.12 |
| Opx | 54.35 | 0.17 | 5.96 | 8.54 | 0.27 | 31.29 | 2.31 | 0.07 | 0.03 | 0.00 | 102.99 |
| T = 1400°C | | | | | | | | | | | |
| Ol | 41.30 | 0.12 | 0.17 | 0.24 | 0.0 | 57.33 | 0.01 | 0.12 | 0.08 | 0.71 | 100.10 |
| Cpx | 48.30 | 0.62 | 15.90 | 0.72 | 0.43 | 11.17 | 23.79 | 0.27 | 0.0 | 0.28 | 101.52 |
| Gl | 49.78 | 0.44 | 15.84 | 0.17 | 0.05 | 0.02 | 8.56 | 0.28 | 0.41 | 0.08 | 81.82 |

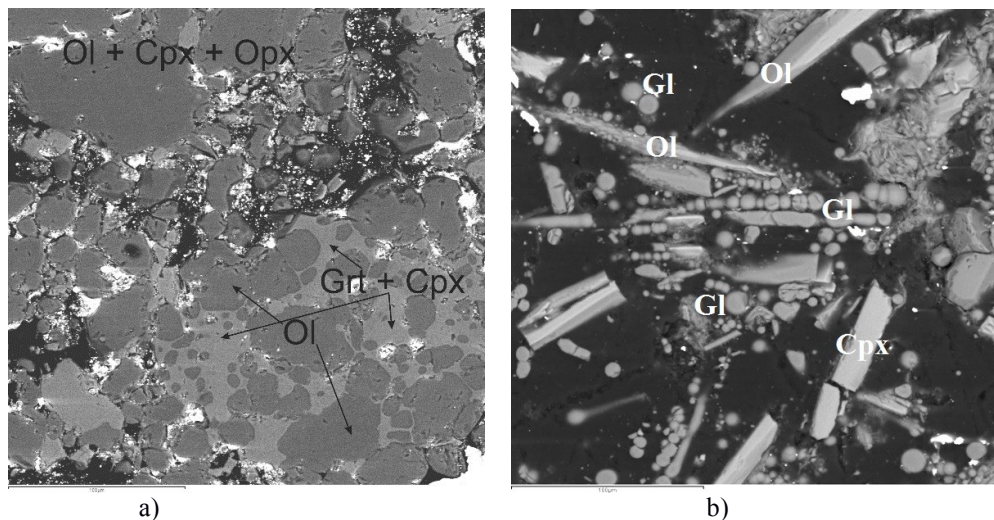


Fig. 1. BSE micrographs of quenching samples: a) $T = 1100^{\circ}\text{C}$, reaction "breccia", b) $T = 1300^{\circ}\text{C}$, disintegrated peridotite consisting of Ol and Cpx relics and Al-Si glass microglobules, quenching product of supercritical fluid-melt.

Table 2. The eclogite- H_2O system. Representative compositions of coexisting phases.

| | SiO ₂ | TiO ₂ | Al ₂ O ₃ | FeO | MnO | MgO | CaO | Na ₂ O | K ₂ O | Cr ₂ O ₃ | Total |
|-----|------------------|------------------|--------------------------------|------|------|-------|-------|-------------------|------------------|--------------------------------|-------|
| Cpx | 46.40 | 2.75 | 12.61 | 6.26 | 0.31 | 8.89 | 20.45 | 1.56 | 0.01 | 0.19 | 99.43 |
| Bt | 41.21 | 2.45 | 11.77 | 8.13 | 0.11 | 16.13 | 1.67 | 1.20 | 6.57 | 0.15 | 89.38 |
| Gl | 63.06 | 0.14 | 18.84 | 0.48 | 0.03 | 0.02 | 2.87 | 5.82 | 3.83 | 0.00 | 95.08 |

At $T = 1400^{\circ}\text{C}$, the samples were characterized by a massive texture. There was intergranular glass. Quenching samples consisted of Ol, with an uncharacteristic elongated, up to $400\ \mu\text{m}$, form cemented with silicate glass with inclusions of Cpx (Fig. 2a). On the polished surface of quenching samples, the oriented dendritic form of Ol conform a triangular or diamond-shaped pattern (Fig. 2 b).

In the eclogite- H_2O system in the interval $T = 1200\text{--}1400^{\circ}\text{C}$, quenching samples were characterized by a massive texture with characteristic features of partial melting – the matrix is represented by silicate glass of the trachyte-andesite composition with inclusions of clinopyroxene and mica (possibly quenched) (Fig. 2c). Representative compositions of coexisting phases are given in Table 2.

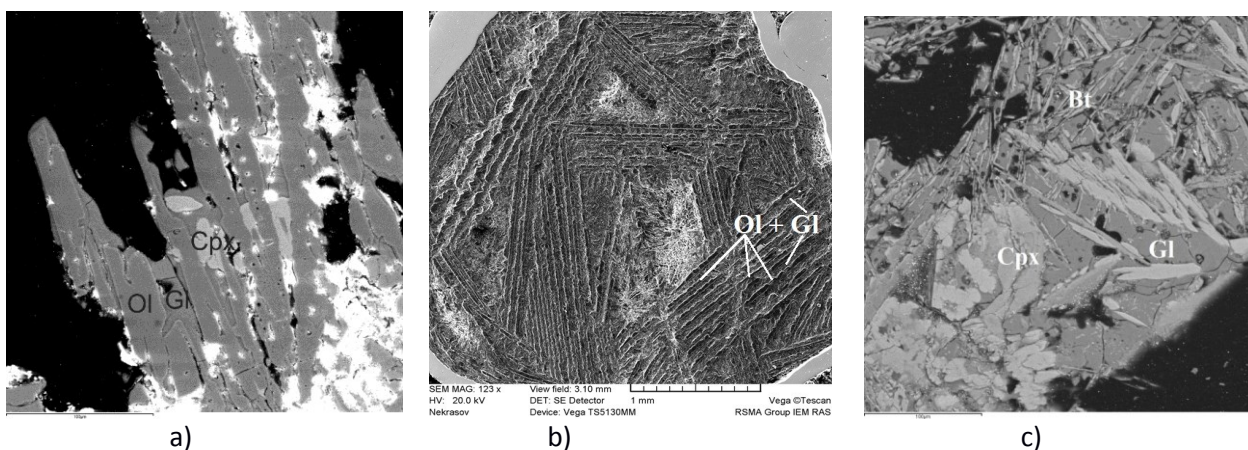


Fig. 2. BSE micrographs of quenching samples: a, b) peridotite- H_2O system, $T = 1400^{\circ}\text{C}$; c) system of eclogite- H_2O , $T = 1300^{\circ}\text{C}$.

Discussion. In most experimental studies, "remote" research methods were used, without material analysis, in which the transition from subcritical to supercritical state was fixed either optically in "hydrothermal diamond anvils" (Shen, Keppler, 1997), or by high-temperature X-ray radiography (Mibe et al., 2007). The use of these methods does not allow us to study matter. In

addition, the possibilities of the first method are limited to simple silicate systems with low T solidus, such as Ab, Ne, Jd, dacite, granite (Bureau, Keppler, 1999). The only exception is the study of critical ratios in the system $\text{SiO}_2\text{--H}_2\text{O}$, $\text{SiO}_2\text{--MgO--H}_2\text{O}$, eclogite- H_2O , peridotite-basalt- H_2O using the quenching method in which the test of the transition of the silicate- H_2O system from subcritical pressures

to supercritical were textures of quenching samples, the absence of quenching glass, and the composition of the quench phases (Kennedy et al., 1962, Stalder et al., 2001, Kessel et al., 2005, Gorbachev, 2000).

The anomalous texture and phase composition of quenching samples in the peridotite-H₂O system in the interval T = 1000-1300°C can be explained by the existence of critical relationships between the partial silicate melt and the fluid.

The massive texture of quenching samples with partial melting of peridotite and eclogite (at T = 1400 and 1300°C respectively), the presence of quenching intergranular glass cementing the liquidus minerals in them, indicate that under these conditions partial melting occurred under subcritical conditions. The experimentally observed eclogitization of peridotite in interaction with supercritical fluid melt with replacement of the peridotite association Ol + Opx with eclogite Grt + Cpx can serve as an effective mechanism for overcoming the "eclogite" barrier, and explaining the eclogite "paradox" - the joint existence of peridotite and eclogite parageneses in inclusions in diamonds.

The work was supported by RFBR grant 17-05-00930a

References:

- Gorbachev N.S. A supercritical state in the water-containing mantle (according to the experimental study of the fluid containing peridotite at P=40 kbar, T=1400°C) // Doklady Earth Sciences, 2000, Vol. 371, Part 3. pp. 362-365.
- N. S. Gorbachev, A. V. Kostyuk, Yu. B. Shapovalov. Experimental Study of the Peridotite-H₂O System at P = 3.8-4 GPa and T = 1000-1400°C: Critical Relations and Vertical Zoning of the Upper Mantle // Doklady Earth Sciences, 2015, Vol. 461, Part 2, pp. 360-363 DOI: 10.1134/S1028334X15040017
- Litvin Yu.A. (in rus.) Physicochemical studies of the melting of the Earth's deep matter. M. Izd. Nauka. 1991.
- Bureau H., H. Keppler. Complete miscibility between silicate melts and hydrous fluids in the upper mantle: experimental evidence and geochemical implications // Earth Planet Sci. Lett. 1999. 165. p.187-196.
- Kennedy G.C., Wasserburg G.J., Heard H.C., Newton R.C. The upper three-phase region in the system SiO₂-H₂O // Am J Sci. 1962. 260(7):501-521.
- Kessel R., P. Ulmer, T. Pettke, M.W. Schmidt, A.B. Thompson. The water-basalt system at 4 to 6 GPa: Phase relations and second critical endpoint in a K-free eclogite at 700 to 1400°C // Earth and Planetary Science Letters, 2005. V. 237. P. 873-892.
- Mibe K., Kanzaki M., Kawamoto T., Matsukage K. N., Fei Y. and Ono S. Second critical endpoint in the peridotite-H₂O system // J. Geophys. Res. 2007. 112, B03201.
- Shen A.H., Keppler H. Direct observation of complete miscibility in the albite-H₂O system // Nature. 1997. 386(6618):710-712.
- Stalder R., Ulmer P., Thompson A.B., Gunther D. High pressure fluids in the system MgO-SiO₂-H₂O under upper mantle conditions // Contrib. Mineral. Petrol. 2001. V.140. P. 607-618

Gorbachev N.S., Kostyuk A.V., Soultanov D.M., Nekrasov A.N. Eclogitization of peridotite at interaction with supercritical fluid-melts (for experimental data). UDC 550.4.02

Institute of Experimental Mineralogy RAS, Chernogolovka, Moscow district. (gor@iem.ac.ru, nastya@iem.ac.ru, dill@iem.ac.ru, alex@iem.ac.ru)

Abstract. The eclogitization of peridotite at interaction with supercritical fluid-melt was experimentally studied in the peridotite-H₂O system at P = 4.0 GPa, T = 1000-1200°C. Features of the texture of quenching samples, their low quality factor, absence of intergranular quenching glass indicate the existence of critical relationships between partial melts and fluid. Individual fragments were characterized by a "brecciated" texture, with the replacement of the peridotite association (Ol + Opx) with eclogite association (Grt-Cpx). The minerals of quenching "breccias" were characterized by high concentrations of microelements (Th, U, Nb, Ta, Zr, REE). The eclogitization of peridotite at interaction with supercritical fluid-melt can serve as an effective mechanism for overcoming the "eclogite barrier".

Keywords: peridotite, eclogite, fluid, critical relations, experiment

Introduction. Experimental study of the phase relations and melting of the peridotite-H₂O system at high P-T parameters is of special interest with account for the peridotitic composition of the mantle, the hydrous composition of mantle fluids, and the effective influence of H₂O on the phase composition, melting temperature of peridotite, composition, and physical properties of melts, and high extractive and transporting properties of hydrous fluid at high pressures. The critical relations between silicate melts and hydrous fluid resulting from the high relative solubility of the components of the silicate melt and fluid are an important feature of H₂O-bearing silicate systems. Complete miscibility between melt and fluid is observed at supercritical pressures (P_c) and temperatures (T_c) (Gorbachev et al., 2000, 2015). In this paper, we report the results of experimental study of partial melting in the peridotite at 4.0 GPa and 1000-1200°C, at which eclogitization of peridotite was observed during interaction with supercritical fluid melt.

Method and analysis of samples. Experiments were performed at the Institute of Experimental Mineralogy, Russian Academy of Sciences, on an anvil-with-hole apparatus NL-10 using the multi-ampoule quench methodology in Au ampoules. Grt peridotite from the xenolith in the Obnazhennaya kimberlite pipe (Yakutia) and distilled H₂O were used as the starting materials. The concentration of H₂O is 15 wt.%. The temperature was measured by the Pt30Rh/Pt6Rh thermocouple; at high temperatures, the pressure was calibrated by the quartz-coesite equilibrium curve. The accuracy of

temperature and pressure estimation in runs was estimated as $\pm 5^{\circ}\text{C}$ and ± 1 kbar (Litvin, 1991). The duration of experiments ranged from 8 to 24 h. Quenching samples were polished and analyzed at the Institute of Experimental Mineralogy on a CamScan MV2300 scanning electron microscope and on ICP MS in the Yaroslavl Branch of the Physical–Technological Institute, Russian Academy of Sciences.

Results. The compositions of coexisting phases in quenched experimental samples and concentration of microelements are given in Table 1; their photomicrographs illustrating the textural and phase relationships are shown in Fig. 1.

The quenched samples at $T=1000\text{--}1100^{\circ}\text{C}$ are characterized by an anomalous texture and phase composition. Their major peculiarity is the absence of intergranular silicate glass – the quenched silicate

melt formed by partial melting of peridotite. The absence of intergranular glass in quenched samples resulted in their disintegration. The quenched material is represented by a pressed microgranular powder composed of isolated segregations or intergrowths of liquidus minerals of disintegrated peridotite (olivine Ol, orthopyroxene Opx, clinopyroxene Cpx, and corroded chromite Cht – Fig. 1a). Individual fragments are characterized by a "brecciated" structure (Fig. 1b). Inclusions of Ol relics in such fragments ("breccias") are overgrown by the Grt–Cpx aggregate. In such areas - reactionary "breccias", the peridotite association Ol–Opx replaced the eclogite Grt–Cpx (Fig. 1b). At $T = 1200^{\circ}\text{C}$, fragments with a "brecciated" texture did not occur, although the reaction relations between Ol and Cpx were observed (Fig. 1c).

Table 1. Representative chemical compositions of coexisting phases in the peridotite– H_2O system.

| | T=1000°C | | T=1100°C | | | T=1200°C | |
|--------------------------------|----------|--------|----------|--------|--------|----------|--------|
| | Ol | Grt | Ol | Cpx | Opx | Ol | Cpx |
| SiO ₂ | 38.99 | 41.92 | 41.11 | 52.77 | 54.64 | 41.41 | 51.53 |
| TiO ₂ | 0.00 | 0.04 | 0.02 | 0.15 | 0.00 | 0.00 | 0.37 |
| Al ₂ O ₃ | 0.33 | 21.93 | 0.09 | 2.57 | 3.70 | 0.20 | 6.13 |
| FeO | 8.05 | 8.05 | 8.22 | 2.55 | 5.23 | 7.22 | 5.59 |
| MnO | 0.05 | 0.25 | 0.06 | 0.17 | 0.29 | 0.02 | 0.57 |
| MgO | 50.53 | 18.22 | 49.78 | 18.56 | 34.52 | 50.61 | 14.62 |
| CaO | 0.00 | 10.44 | 0.03 | 21.52 | 0.83 | 0.12 | 20.46 |
| Na ₂ O | 0.02 | 0.03 | 0.04 | 0.05 | 0.23 | 0.07 | 0.01 |
| K ₂ O | 0.09 | 0.05 | 0.03 | 0.05 | 0.00 | 0.04 | 0.00 |
| Li | 0.38 | 0.82 | 0.61 | 1.02 | 1.96 | 0.79 | 4.16 |
| Be | 0.01 | 0.02 | 0.003 | 0.02 | 0.09 | - | 0.1 |
| Ba | 1.69 | 16.6 | 0.91 | 7.08 | 26.9 | 0.36 | 164.65 |
| Th | 2.92 | 1.08 | 0.04 | 0.37 | 0.69 | 0.01 | 0.94 |
| U | 1.86 | 0.67 | 0.1 | 0.23 | 0.38 | 0.03 | 0.35 |
| Nb | 35.43 | 15.86 | 1.21 | 2.44 | 6.86 | 0.69 | 9.89 |
| Ta | 0.93 | 0.39 | 0.38 | 0.08 | 0.18 | 0.02 | 0.23 |
| La | 3.3 | 2.72 | 0.18 | 1.49 | 3.02 | 0.02 | 5.66 |
| Ce | 16.25 | 9.71 | 1.1 | 4.55 | 4.78 | 0.02 | 10.89 |
| Pb | 0.29 | 0.82 | 0.08 | 0.26 | 0.91 | 0.25 | 1.02 |
| Sr | 4.44 | 32.67 | 2.27 | 46.5 | 19.28 | 1.07 | 228.67 |
| Nd | 24.02 | 12.37 | 3.02 | 2.3 | 2.18 | 0.01 | 4.17 |
| Hf | 0.78 | 0.31 | 0.91 | 0.16 | 0.19 | - | 0.34 |
| Sm | 6.44 | 2.72 | 1.75 | 0.53 | 0.57 | 0.02 | 0.77 |
| Eu | 1.43 | 0.61 | 0.57 | 0.18 | 0.17 | 0.004 | 0.96 |
| Gd | 8.93 | 4.41 | 3.37 | 1.45 | 1.3 | 0.01 | 2.62 |
| Ti | 1181.27 | 730.67 | 549.49 | 248.04 | 393.57 | 51.0 | 416.08 |
| Dy | 2.19 | 1.08 | 3.87 | 0.47 | 0.44 | - | 0.54 |
| Y | 9.49 | 4.3 | 26.03 | 2.87 | 2.35 | 0.05 | 3.82 |
| Er | 1.29 | 0.59 | 3.35 | 0.41 | 0.3 | - | 0.38 |
| Yb | 1.25 | 0.68 | 4.1 | 0.47 | 0.43 | - | 0.46 |
| V | 181.22 | 207.8 | 173 | 97.29 | 147.15 | 17.61 | 86.53 |
| B | 6.23 | 16.86 | 9.48 | 17.28 | 21.2 | 3.01 | 29.07 |
| Zr | 32.59 | 9.65 | 12.5 | 3.74 | 4.47 | 0.32 | 8.72 |

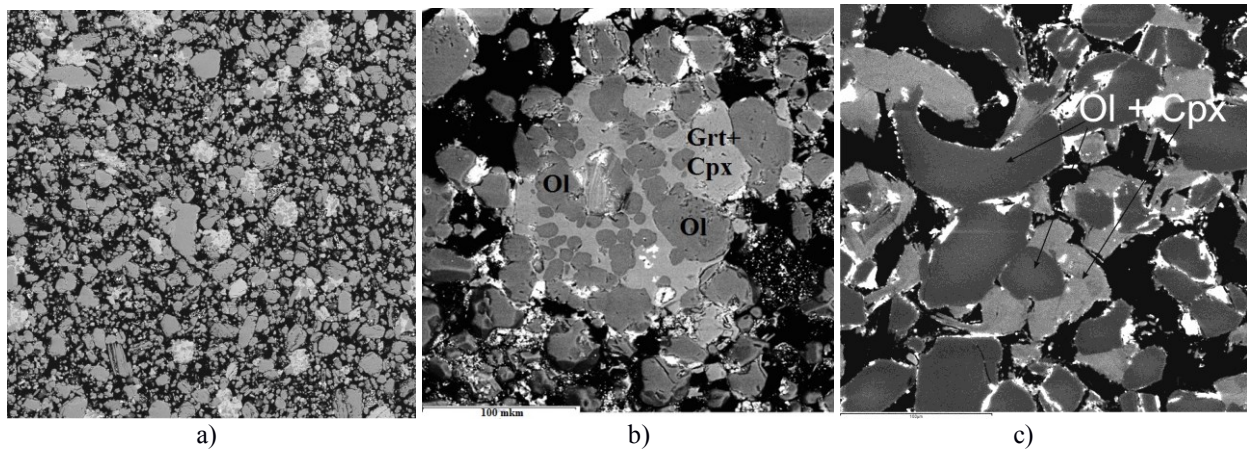
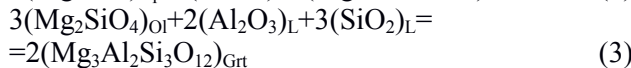
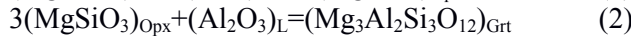
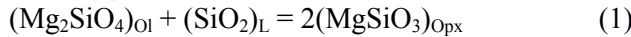


Fig. 1. BSE micrographs of quenching experimental samples: a) general view, isolated discharges of liquidus minerals of disintegrated peridotite (T=1000°C) with fragments of the reactionary "breccia"; b) reaction "breccia", relics of the liquidus Ol are included in the matrix Grt-Cpx composition (T = 1100°C); c) Ol relics overgrow Cpx (T = 1200°C).

The formation of Grt in the interaction of melts with Ol and Opx is modeled by reactions 1-3 in which the fully mobile components are SiO₂ (L) and Al₂O₃ (L).



The equilibria of the triple point Fo + En + Pyr is $(Mg_2SiO_4)_{Ol} + (MgSiO_3)_{Opx} + (Al_2O_3)_L + (SiO_2)_L = 2(Mg_3Al_2Si_3O_{12})_{Grt}$. The coordinates of this point are $\log a(SiO_2)_L = -1.13$ и $\log a(Al_2O_3)_L = -0.49$ at T=1373°K, P=4 GPa (Fig. 2).

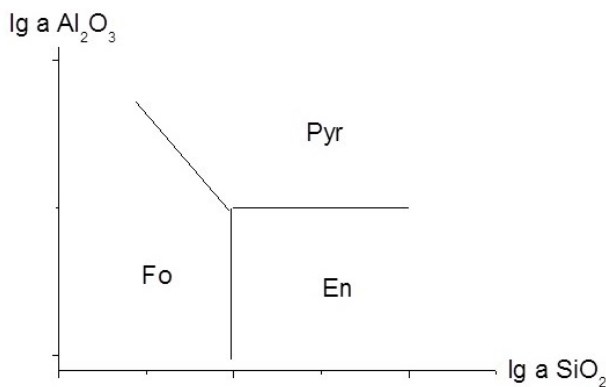


Fig. 2. The coordinates of the triple point Fo+En+Pyr

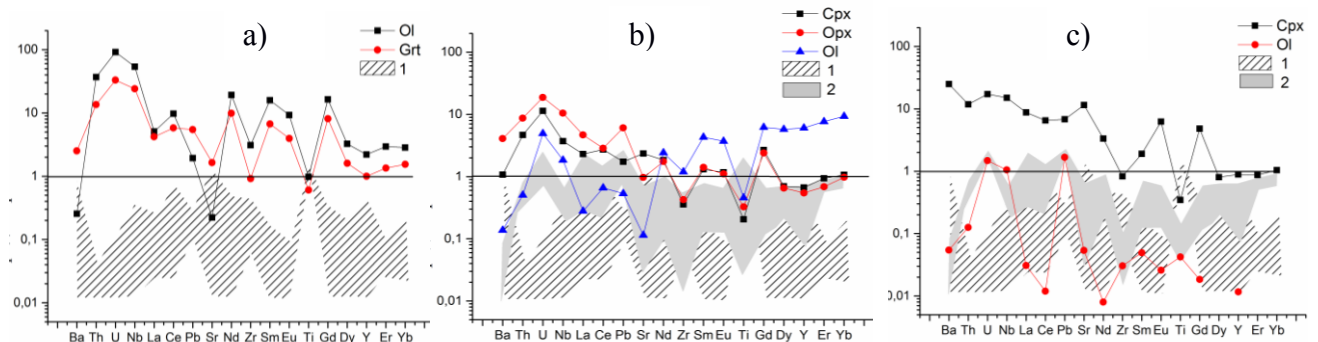


Fig.3. The microelement concentrations normalized in primitive mantle in Ol, Grt, Opx, Cpx at temperatures: a) 1000°C, b) 1100°C, c) 1200°C for comparison, data are given (filled areas 1 - Ol and 2 - Cpx) from peridotites of mantle xenoliths (Gregoire, 2000).

Discussion. The anomalous structure and the phase composition of quenched samples obtained in the temperature range of 1000–1300°C may be explained by the critical relations between the silicate melt formed by partial melting of peridotite and the aqueous fluid. The supercritical fluid-melt interacted with peridotitic minerals, which resulted in their dissolution, in the formation of a reactional Grt + Cpx matrix around relict Ol ± Opx, and in enrichment in trace elements. This enrichment is more effective at low volume of nearsolidus supercritical fluid-melt at low degree of melting (T=1000-1100°C). At increase of temperature (up to 1200°C), degree of melting and volume of supercritical fluid-melt this effect are decrease (dilution effect). The eclogitization of peridotite in interaction with supercritical fluid-melt with replacement of peridotite association Ol+Opx with eclogite Grt+Cpx can serve as an effective mechanism for overcoming the "eclogite" barrier, explaining the eclogite "paradox" – the joint existence of peridotite and eclogite parageneses in inclusions in diamonds. The enrichment of the minerals of quenching "breccias" of trace elements indicates a high extracting and reactivity of nearsolidus supercritical fluid-melt.

The work was supported by RFBR grant 17-05-00930a

References:

- Gorbachev N.S. A supercritical state in the water-containing mantle (according to the experimental study of the fluid containing peridotite at P=40 kbar, T=1400°C) // Doklady Earth Sciences, 2000, Vol. 371, Part 3. pp. 362-365.
- Gorbachev N. S., A. V. Kostyuk, Yu. B. Shapovalov. Experimental Study of the Peridotite–H₂O System at P = 3.8–4 GPa and T = 1000–1400°C: Critical Relations and Vertical Zoning of the Upper Mantle // Doklady Earth Sciences, 2015, Vol. 461, Part 2, pp. 360–363 DOI: 10.1134/S1028334X15040017
- Litvin Yu.A. (in rus.) Physicochemical studies of the melting of the Earth's deep matter. M. Izd. Nauka. 1991.
- Gregoire M., B.N. Moine, Suzanne Y. O'Reilly et al. Trace element residence and partitioning in mantle xenoliths metasomatized by highly alkaline, silicate-and carbonate-rich melts (Kerguelen Islands, Indian Ocean) // Journal of Petrology. 2000. T. 41. № 4. C. 477-509.

Khodorevskaya L.I. Compositions of solutions and phases minerals in the amphibol-fluid system: application to the acid metasomatism. UDC 553.065.1

D.S. Korzhinskii Institute of Experimental Mineralogy RAS, Chernogolovka Moscow district. khodorevskaya@mail.ru

Abstract. Experiments, simulating the interaction of amphibole and H₂O-HCl solutions at a temperature of 650-750°C and a pressure of 7 kbar, were conducted. The

results obtained show that as m_{HCl} increases, amphibole is replaced by chlorite, orthoamphibole and cordierite. The concentrations of major petrogenic elements in coexisting solutions were measured. More Ca and Fe and less Mg are shown to be removed from amphibole because Mg is re-precipitated into chlorite. As a result of the precipitation of Ca, Fe and Mg from amphibole, the residual matrix is enriched in alumina, contributing to corundum formation. f_{HCl}, at which amphibole-plagioclase associations are succeeded by chlorite associated with gedrite or cordierite, were calculated. f_{HCl} values, most probable upon high-temperature metasomatism of metabasic rocks, were estimated.

Keywords: amphibole, fluid, HCl, metasomatism, metabasites, fluid interaction, experimental modeling.

Estimation of HCl fugacity in deep-seated fluids is essential for an understanding of the mechanisms of chlorine transportation from the deep layers of the Earth. HCl is also an essential constituent of ore fluids (Hedenquist and Lowenstern, 1994; Simon et al., 2005 и др.). Estimation of a chlorine constituent in a fluid phase is based on exchange reactions of the type M-OH + HCl = M-Cl + H₂O. The f_{H₂O}/f_{HCl} ratio in fluid coexisting with biotite is now calculated from experimental data (Munoz & Swenson, 1981). f_{H₂O}/f_{HCl} ratio is fluid coexisting with apatite is calculated from experimental data (Korzhinsky, 1981). f_{HCl} was estimated quantitatively more seldom than f_{H₂O}/f_{HCl} because f_{H₂O}/f_{HCl} ratio can be estimated from the chemical compositions of biotite and apatite, which often occur in rocks, while to calculate f_{HCl}, one needs to independently estimate f_{H₂O}, which is not always possible.

The interaction of amphibole with H₂O-HCl solutions have not been studied earlier. The results of the experimental study of the reactions of amphibole with HCl-bearing fluids are reported in the present paper. The goal of the experiments was to determine and analyze the compositions of the phases formed at varying solution acidity and to calculate f_{HCl} –values in the fluids.

The experiments were conducted at a temperature of 650°C and a pressure of 7 kbar. HCl concentration in reference solution was 0.05-2.0 mol/kg H₂O (m). The composition of reference amphibole (mas. %) was: SiO₂ – 44.11, TiO₂ – 0.95, Al₂O₃ – 15.12, FeO – 12.08, MnO – 0.13, MgO – 12.05, CaO – 11.74, Na₂O – 1.66, K₂O – 0.49, total 98.32. According to (Leake et al., 1997), amphibole is consistent with tschermakite.

25–40 mg of reference amphibole were placed into a vertically positioned ampoule (5 mm in diameter and 50 mm in height). HCl solutions, varying in concentration from 0.05 to 2.81m, were then poured into the ampoule. Standard 1m and 0.1m solutions were used. Solutions with HCl concentration in excess of 1m were prepared by diluting certified 14 mas. % (4.46 m) HCl. 10-20-fold excess of fluid relative to a mineral sample was created in the ampoule to be able to diagnose the

Mineral equilibria at high PT-parameters

number of newly-formed phases. Upon filling, the ampoules were weighed, sealed, overturned and shaken vigorously for a more uniform solution-rock distribution. The experiments were carried out in gold ampoules to avoid losses of iron in walls of ampoules. Oxygen fugacity was not controlled and was assumed to be close to the buffer Ni-NiO (Helz, 1976). The experiments were conducted in apparatuses with gas pressure and internal heating (gas bombs) at the Institute of Experimental Mineralogy, RAS. The experiments were carried out for 4 days, and then hardening was done. The temperature controlling and measuring error was $\pm 7^\circ$, the pressure measurement error was ± 10 MPa, and the hardening rate was $100^\circ/\text{min}$. After the experiments the ampoules were re-weighed to see if they are intact. The ampoules were opened, and the solution extracted from the ampoules was diluted with 1 ml of distilled water and analyzed. Element analysis of the samples was done at the Analytical Certification Testing Centre in the Institute of Technology of Microelectronics and Specially Pure Materials, RAS (ACIS IPTM RAS) using the mass-spectral (X-7, Thermo Elemental, USA) and atomic emission (ICAP-61, Thermo Jarrell Ash, USA) analytical methods. Chlorine concentration in solution after the experiments was not estimated. A preset considerable excess of fluid relative to the weighed portion amphibole and the absence of solid chlorine-bearing phases after the experiments suggested that Cl concentration in the fluid after the experiments did not differ greatly from the reference concentration. A solid sample was extracted from the ampoule. Each sample was then placed into a container, was filled epoxy glue, polished and analyzed by a method for local X-ray spectrographic microanalysis using a CamScan MV2300 (VEGA TS 5130MM) scanning electron microscope equipped with an INCA-350 Energy dispersion X-ray spectrometer (Laboratory of Electron Microscopy and Microanalysis, IEM, RAS). The time taken for spectrum collecting is 70 s for various phases.

The main results of the experiments conducted at $650\text{-}750^\circ\text{C}$ are reported in (Khodorevskaya, Varlamov, 2017). They can be described briefly as follows. After P1 and P2 experiments (initial concentration $m_{\text{HCl}} = 0.05$ and 0.1 mol/kg H_2O) Ca-amphibole – tschermakite (*Tsch*) with $f = \text{FeO}/(\text{FeO}+\text{MgO}) = 0.25\text{-}0.35$ remained a clearly dominant phase (over 90%). The amphiboles did not differ in composition from the initial amphibole. Chlorite (*Chl*) was present in all experiments, regardless of HCl concentration. It was present as single crystals measuring 10 to ≈ 80 μm or rosettes, up to 100 μm in size, consisting of fine acicular

laminae. The formula of chlorites is: $(\text{Mg}_{2.93}\text{Fe}_{1.59}\text{Al}_{1.4})(\text{Si}_{2.68}\text{Al}_{1.32})\text{O}_{10}(\text{OH})_8$. As HCl concentration in chlorites rises, isomorphic replacement $\text{Fe}\rightarrow\text{Mg}$, $\text{Fe}\rightarrow\text{Al(VI)}$, and $\text{Al(IV)}\rightarrow\text{Si}$ in chlorites takes place, and the general formula of chlorites at $m_{\text{HCl}} = 1\text{m}$ (experiment P4) $(\text{Mg}_{3.43}\text{Fe}_{0.95}\text{Al}_{1.57})_{5.95}(\text{Si}_{2.92}\text{Al}_{1.08})\text{O}_{10}(\text{OH})_8$.

In addition to amphiboles and chlorites, plagioclase (*Pl*) $\text{An}_{95\text{-}100}$ was revealed. Fine (≈ 10 μm) spherical shapes of melt or quench products of the fluid phase were observed. After P3, P4 and P5 experiments, carried out at $m_{\text{HCl}} = 0.5, 1$ and 2 mol/kg H_2O , respectively, Ca-amphibole persists, but its quantity decreases considerably. Clusters, consisting of small spherical forms of quartz (*Qtz*), phases of the type $\text{Al}_2\text{SiO}_n \times m\text{H}_2\text{O}$ and thinly-fibrous Al_2SiO_5 , are formed. Scarce very coarse (> 200 μm) quartz, chlorite and corundum (*Crn*) crystals are occasionally encountered.

As the acidity of the solutions is changed, amphibole composition varies several times the centre of the grains to their rim; Na, Fe and Mg decrease, while SiO_2 increases. In addition to Ca-amphiboles in P3 experiment ($m_{\text{HCl}} = 0.5\text{m}$), scarce orthorhombic amphibole (*oAmph*) $\text{Mg}_5(\text{Mg}_{0.65}\text{Al}_{0.98}\text{Fe}_{0.10})_5\text{Si}_8\text{O}_{22}(\text{OH})_2$ crystals, similar in composition to anthophyllite or cummingtonite but with a considerable admixture of Al, are observed. Small ($2\text{-}3$ μm) Fe oxide (ox.Fe) globules are encountered.

Na and Ca concentrations in solutions after the experiments increase as the preset m_{HCl} rises (Fig. 1). In this case, Ca and Na, unlike other petrogenic elements, will completely pass into solution, rather than precipitate in newly-formed mineral phases.

Fe concentration in solutions increases by several orders of magnitude, while Mg concentration remains low (Fig. 2). Fe concentration values in solutions within the error limits coincide with the data presented in (Purtov, Yatluk, 1982, 3 in Fig. 2). Mg concentrations in our 1m HCl solutions are 4-5.5 times lower than those in the studies carried out by (Purtov, Yatluk, 1982) because in our experiments Mg is re-precipitated into chlorite and orthoamphibole. Our data and those obtained by Purtov, Yatluk show that in the diluted m_{HCl} range ($\leq 0.01\text{m}$) Mg concentration values in solutions coincide within the calculation limits.

In all the experiments Si and Al concentrations in hardening solutions remain low (Si = $100\text{-}400$ ppm, Al - < 40 ppm) because at HCl concentrations of ≤ 0.1 mol/l) amphibole is poorly dissolved (P1-P2 experiments); at higher m_{HCl} (P3-P2 experiments) Si and Al are not dissolved either, forming alumosilicate matrix.

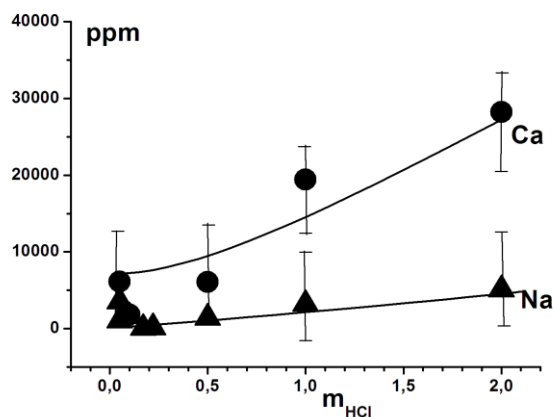


Fig. 1. $m_{\text{HCl}} - \text{ppm}_{(\text{Ca, Na})}$ ratio in solution

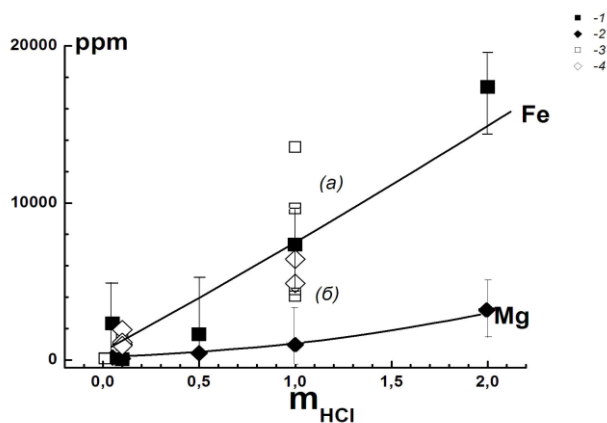


Fig. 2. $m_{\text{HCl}} - \text{ppm}_{(\text{Fe, Mg})}$ ratio in solution: 1 – Fe, 2 – Mg, 3-4 – data (Purtov, Yatluk, 1982): 3 – Fe concentrations equiponderous with gabbro (a) and dunite (b); 4 – Mg concentrations.

HCl and H_2O fugacity in fluid during the experiments was estimated from the equations: $f_{\text{HCl}} = X_{\text{HCl}}^0 \gamma_{\text{HCl}}^0 P_{\text{total}}^0$, $f_{\text{H}_2\text{O}} = X_{\text{H}_2\text{O}}^0 \gamma_{\text{H}_2\text{O}}^0 P_{\text{total}}^0$,

where γ_{HCl}^0 , $\gamma_{\text{H}_2\text{O}}^0$ are the fugacity coefficients of pure HCl and H_2O and P_{total}^0 is total pressure. γ_{HCl}^0 was estimated from (Mel'nik, 1978) and $\gamma_{\text{H}_2\text{O}}^0$ from (Kestin et al., 1984). X_{HCl} , $X_{\text{H}_2\text{O}}$ are molar fractions of HCl and H_2O . As a considerable excess of solutions was preset in the experiments, it is assumed that the dissolution of amphibole and the precipitation of the elements have not markedly changed the preset initial HCl concentration in fluid during the experiments. In other words, the authors admit that X_{HCl} and $X_{\text{H}_2\text{O}}$ values depend on the ratio of the number of HCl or H_2O moles to the total $\text{HCl} + \text{H}_2\text{O}$ moles in the reference solutions.

($\text{Hbl} + \text{Pl} + \text{Melt} + \text{ox.Fe}$) and without it ($\text{Crn} + \text{Qtz} \pm \text{oHbl} + \text{Chl} \pm \text{Crd}$), obtained in our experiments, are separated by a dotted line. The delineated fields show f_{HCl} values in the fluids detached at a late magmatic stage of syenite (S) and charnockite (TC) crystallization in intrusions and host metapelites (M) (Markl, Piazzolo, 1998). It follows from Fig. 3 that $\lg f_{\text{HCl}} - T$ ratio estimates at natural localities are limited dominantly by the $\lg f_{\text{HCl}} - T$ ratios of plagioclase resistance obtained from the experiments (dotted line in Fig. 3). In other words, at $T = 650-830^\circ\text{C}$ f_{HCl} values in fluids that provoke metasomatism are most probably limited by the values of ≤ 600 bar. Higher f_{HCl} values seem to occur in nature in exceptional cases or do not occur at all.

Thus, as a result of amphibole-HCl solution interaction, Ca, Fe and Mg are precipitated to a greater extent than Si and Al. Re-precipitation of Mg from solutions into chlorite contributes to Ca and Fe accumulation in solutions. These elements then contribute to the formation of metasomatic rocks. In metabasic rocks, it is primarily the formation of melanocratic veins with minerals that contain higher $f = \text{FeO}/(\text{FeO} + \text{MgO})$ and Ca concentrations (e.g. elevated grossular concentration in garnet) than host rocks and zoisite formation. The removal of Ca, Fe and lesser Mg results in alumina accumulation in the residual matrix, contributing to corundum formation. Similar corundum in metasomatic rocks, evolving after gabbroic rocks, are described in (Serebryakov, Aristov, 2004; Khodorevskaya, Varlamov, 2018 et al.).

References:

- Hedenquist, J.W., Lowenstern, J.B. The role of magmas in the formation of hydrothermal ore deposits // Nature. 1994. Vol. 370. P. 519–526.
 Helz R.T. Phase relations of basalts in their melting ranges at $P = 5$ kb as a function of oxygen fugacity. Part I. Mafic phases // J. Petrol. 1973. Vol. 14. P. 249-302.

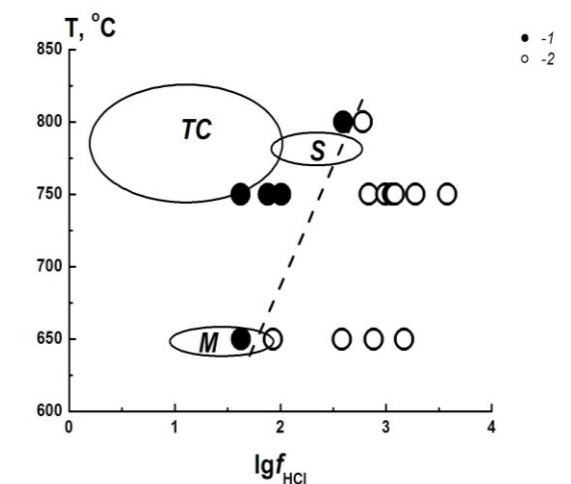


Fig. 3. $\lg f_{\text{HCl}} - T^\circ\text{C}$ ratio. 1 – amphibole-plagioclase associations are stable; 2 – plagioclase-free associations are stable. According to (Markl, Piazzolo, 1998), the composition fields of the fluids associated with syenite (S), charnockite (TC) and metapelite (M) are delineated and indicated by letters.

Fig. 3 shows a $\lg f_{\text{HCl}} - T$ ratio created in our experiments and estimated for various natural localities. Associations with plagioclase

- Kestin J., Sengers J.V., Kamgar-Parsi B., Levelt Sengers J.M.H. Thermophysical Properties of fluid H₂O // J. Phys. Chem. Ref. Data. 1984. Vol. 13. № 1. P. 175–183.
- Khodorevskaya L. I., Varlamov D. A. Experimental investigation of interaction of amphibole with H₂O-HCl fluid under 650-750°C, 7 kbar: application to high-temperature metasomatism // Trudy VESEMPG-2017 (Moscow: Vernadsky Institute RAS). 2017. P. 92-95. [in Russian].
- Khodorevskaya L. I., Varlamov D. A. High-Temperature Metasomatism of the Layered Mafic–Ultramafic Massif in Kiy Island, Belomorian Mobile Belt // Geochemistry Intern. 2018. Vol. 56. № 6. P. 535–553. [in Russian]
- Korzhinsky M.A. Apatite solid solution as indicator of fugacity of HCl⁰ и HF⁰ in hydrothermal fluids // Geokhimiya. 1981. № 5. P. 689-706. [in Russian].
- Markl G., Piazzolo S. Halogen-bearing minerals in syenites and high-grade marbles of Dronning Maud Land, Antarctica: monitors of fluid compositional changes during late-magmatic fluid-rock interaction processes // Contrib. Mineral. Petrol. 1998. Vol. 132. P. 246-268.
- Mel'nik Yu.P. Thermodynamic properties of gases in conditions of deep petrogenesis. 1978. Kiev: Naukova Dumka, 150 p. [in Russian].
- Munoz J.L., Swenson A. Chloride–hydroxyl exchange in biotite and estimation of relative HCl/HF activities in hydrothermal fluids // Econ. Geol. 1981. Vol. 76. P. 2212–2221.
- Purtov B.K., Yatluk G.M. Experimental studies of processes of mobilization of petrogenic components in hydrothermal systems. 1982. Sverdlovsk: URC of the USSR Academy of Sciences. [in Russian].
- Serebryakov N.S., Aristov V.V. Conditions of localization of gem-quality corundum in rocks of Chupa sequence of the Belomorian complex of Northern Karelia // Izvestiia Visshikh Uchebnikh Zavedenii. 2004. Geol. I Razvedka, 4, 36–42. [in Russian].

Konogorova D.V.¹, Kriulina G.Yu.¹, Garanin V.K.¹ Peculiar properties of the formation of unique russian diamonds

¹M.V. Lomonosov Moscow State University, Department of Geology, Moscow, (diana-96perm@mail.ru).

The object of the study was data about unique diamond Russia (more than 550 crystals weighing more than 50 ct) obtained for 1959-2016 gg company AK ALROSA (OAO) of the main handles tubes: jubilee, Udachnaya, Sitakanta, Nyurba, Zarnitsa, Mir, International, Aikhal and Komsomol.

Unique diamond makes the presence of characteristics such as rare color, shape, and nuggets weighing more than 50 ct name. Nominal diamonds have always been evaluated individually by a team of experts. When evaluating named diamonds, they are always strictly related to such characteristics as unusual color and shape, as well as purity and absence of defects. In the first years of development of the Yakut fields the names given to the stones weighing more than 15 ct. However, when such

diamonds were found several dozen a year, it was decided to "raise the bar" to 50 ct. This condition is valid today. Nominal diamonds are often called in honor of the great events. In the Soviet Union they are usually called in honor of the anniversaries of the October revolution, the Congress of the Communist party and Komsomol. So, found in 1989, the diamond weighing 320.65 ct wanted to give the name "Unbreakable Soviet Union", but "unbreakable" turned out to be a fragment of a larger stone, and moreover, pressed, and it was called "Alexander Pushkin". For 40 years of development of the Yakut deposits more than 200 diamonds received names. ALROSA company notes in its sources that in recent years the number of large crystals increases. So in 2016 the company ALROSA produced 7 unique crystals weighing from 51.5 to 235.65 ct (mainly in the jubilee tube).

Large diamonds are of great value from the point of view of science for studying of laws of formation and placement in diamondiferous breeds. But unfortunately, mineralogists do not have the opportunity to study the internal features of these crystals, however, to date, there are data on the time and place of their production, which makes it possible to make assumptions about the laws of formation, availability and distribution of large diamonds in the fields.

Modern researchers (Bogatikov et al., 2010; Kononova, 2009, 2011; Kostrovitskiy, 2009; Tretyachenko, 2008; Garanin et al., 2009; etc.) in the selection of varieties of kimberlites preference indicator of the role of TiO₂. The basis of the common classification of kimberlites (Bogatikov et al., 2007, 2010) is rooted in the separation of kimberlites into three geochemical type, conventionally called low by titaniferous (TiO₂<1.0 wt.%) (NTT), moderately Titanic (1.0<TiO₂<2.5 wt.%) (UTT) and high-Titanic (TiO₂>2.5 wt.%). However, high by titaniferous type of kimberlite diamondiferous rock is pathetic, so are not considered.

UTT. This type of kimberlites are pipe: World, anniversary, Sitakanta, Udachnaya, Zarnitsa, Aikhal and Komsomolskaya. As shown in work (Kriulina, 2012), and also in experimental works on synthesis of a diamond (Synthesis of minerals, 2000) the moderate content of the Titan in a diamond-forming medium renders positive influence on quality of a diamond, reducing its ability to be enriched with nitrogen and reducing supersaturation of a medium by carbon. Usually the diamonds from kimberlites of UTT (range of diamond potential from high to miserable), mostly colorless layers with the octahedral character of the growth facets. Characterized by low content of nitrogen impurities (N_{tot}<500 at.ppm.) with a high proportion of B-form (25-80%), which corresponds to the conditions of

long-term high-temperature annealing. And large diamonds from these kimberlites are characterized by prevalence of yellow shades and crystals of transitional forms meet more often. The largest number of nominal diamonds is recorded in the tube Mir (189 PCs.). Diamonds weighing between 50.05 and 342.50 ct, average weight 94 ct.

NTT. This type of kimberlite pipes include: Nuremberg and International. For low-Titanic kimberlites in addition to low titanium content, characterized by low concentrations of rare elements, such rocks are found mainly on Northern continents: on VEP and Yakutia. Perhaps this geochemical feature of kimberlites reflects the global heterogeneity of the earth's mantle. Usually the diamonds from kimberlites of NTT (range of

diamond from organosilicas to miserable) have a relatively low quality, due to lower-temperature conditions of formation and the shortness of the annealing. And especially large diamonds in kimberlites NTT are characterized by transparent-translucent color and crystals of octahedral habit are more frequent. Diamonds weighing 51.5 to 241.65 ct, with an average weight of 108 ct.

For fig. 1 we see that unique extra large diamonds are found in NTTS, but they are rare. The number and weight of large diamonds are characteristic of tubes with a moderate content of titanium oxide. This fact testifies to the existence of specific conditions for the formation of a large diamond.

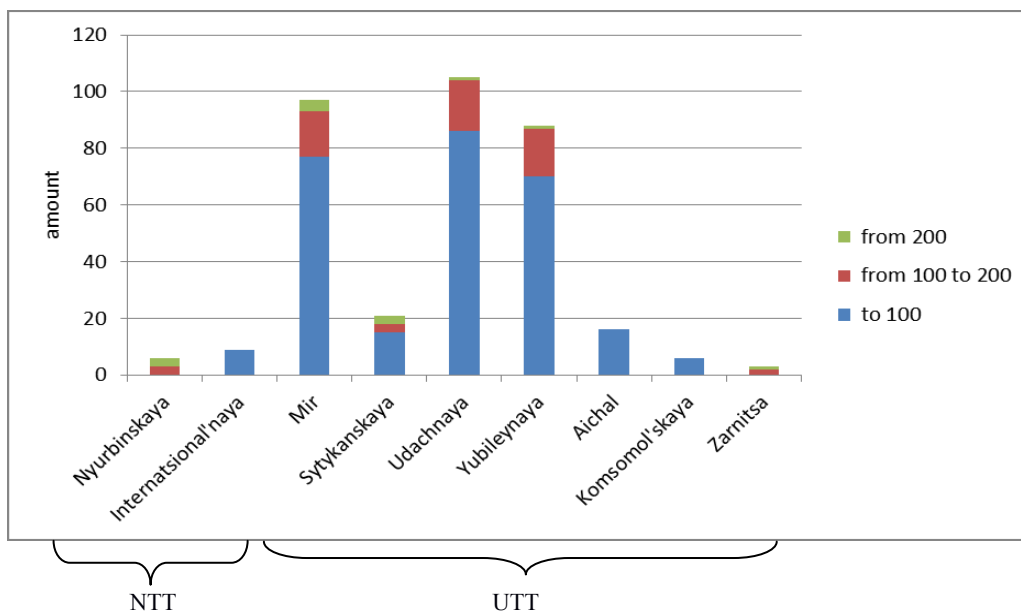


Fig. 1. Diagram of distribution of mined diamonds through the tubes.

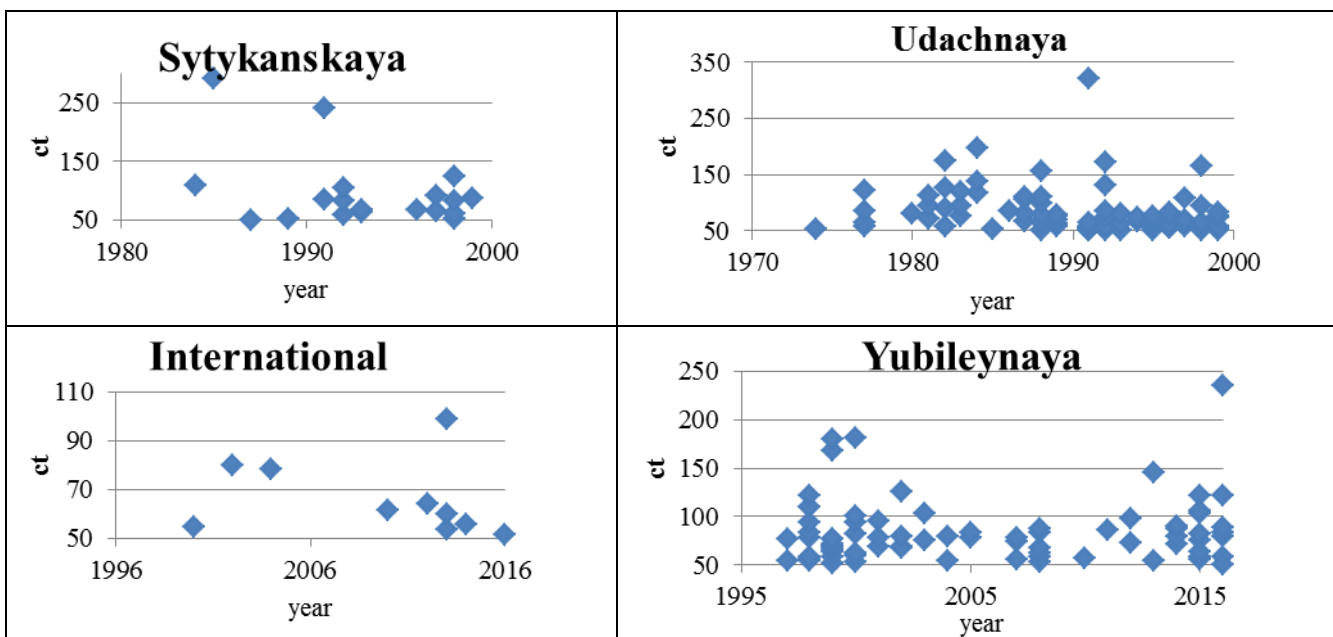


Fig. 2. Graphs of the distribution of large diamonds mined at the time.

Tube leader in the extraction of large crystals is "jubilee". Since the beginning of 2017, 20 diamonds weighing more than 50 ct have been produced at Yubileynaya.

It was noted that in recent years the number of large diamond crystals extracted increased (fig. 2). Probably, it is connected with depth of working off of tubes. This fact testifies to the existence of specific super-deep conditions for the formation of a large diamond.

References:

- Belyakova Yu. A. synthesis of minerals volume 3.. M: Subsoil, 1987, 256 p.
- Bogatikov O. A., Kononova V. A., Nosova A. A., Kondrashov I. A. Kimberlites and lamproites of the Eastern European platform: Petrology and Geochemistry. 2007. T. 15. No. 4. C. 339-360.
- Garanin K. V. kimberlite Classifications // Abstracts of the scientific conference Lomonosov readings (Geology section). - Moscow state University, 2009.
- Kononova V. A., Bogatikov O. A., Kondrashov I. A.. Kimberlites and lamproites: criteria of similarity and differences // Petrology. 2011. Vol. 19. № 1, p. 35-55
- Kostrovitsky S. I. Mineralogy and Geochemistry of kimberlites of Western Yakutia. Abstract. dis. doctor. gay.-miner. Sciences'. Institute of Geochemistry SB RAS, Irkutsk, 2009. 44 PP.
- Kriulina G. Yu, V. K. Garanin, G. G. Samsonov Prediction quality diamond raw materials in the petrochemical fields of different type //Izvestiya of higher educational institutions. Geology and exploration. - 2013. — No. 6.
- V. V. Tretyachenko Mineragenic zoning of the kimberlite region of South-Eastern white sea area. Abstract. Diss. kand. gay.- min. Sciences. Moscow: 2008. 28 p.

Marchenko E.I.¹, Ismailova L.S.², Eremin N.N.¹, Bobrov A.V.^{1,2}. Computer modeling of the influence of cation ordering effects on structural characteristics of skiaigite-Fe-majorite solid solution. UDC 548.3

¹M.V. Lomonosov Moscow State University, Department of Geology, Moscow,

²Vernadsky Institute of Geochemistry and Analytical Chemistry RAS, Moscow (marchenko-ekaterina@bk.ru)

Abstract. The effects of Fe²⁺, Fe³⁺ and Si cations ordering at 16a crystallographic positions on the structure and the elastic properties in skiaigite-Fe-majorite solid solution system were studied by atomistic semi-empirical modeling.

Keywords: *skiaigite-Fe-majorite, solid solution, computer modeling, cation ordering.*

With the help of atomistic semi-empirical modeling using GULP code (Gale and Rohl, 2003) we studied the effect of Fe²⁺, Fe³⁺ and Si cations ordering at 16a crystallographic positions on the structure and the elastic properties in ski-Fe-maj solid solution system.

The semi-empirical self-consistent partially ionic interatomic potential model (Pedone et al., 2006) was used as a basis of our set. Si-O and O-O pair potentials from this work were used unchanged. Fe^{II}-O and Fe^{III}-O Morse type pair potentials parameters were optimized using X-ray sample structural data in the *ski - Fe-maj* system (Ismailova et al., 2017).

$$V(r) = D[\exp(-2\sigma(r-r_0)) - 2\exp(-\sigma(r-r_0))].$$

Here r – is the interatomic distance (Å), D – dissociation bond energy (eV), σ – bond softness parameter (Å⁻¹), r_0 – optimal interatomic distance for atomic pair (Å). For Fe^{II}-O pair interaction the following potential parameters were obtained using structure fitting procedure in *ski - Fe-maj* solid solution: $D=0.426155$ eV, $\sigma=1.620517$ Å⁻¹, $r_0=2.394132$ Å; and for Fe^{III}-O these values were as follows: $D=0.070493$ eV, $\sigma=1.866179$ Å⁻¹, $r_0=2.636605$ Å; Si-O: $D=0.340554$ eV, $\sigma=2.006700$ Å⁻¹, $r_0=2.092033$ Å; O-O: $D=0.042399$ eV, $\sigma=1.379316$ Å⁻¹, $r_0=3.618816$ Å. Cutoff for all potentials was 12.0 Å, and the ionicity degree for all bonds according to Pedone et al. (2006) charge model was assigned as 0.6. Thus the effective charges of atoms in the model were the following: $Z(\text{Fe}^{\text{II}}) = 1,2e$, $Z(\text{Fe}^{\text{III}}) = 1,8e$, $Z(\text{Si}) = 2,4e$, $Z(\text{O}) = -1,2e$.

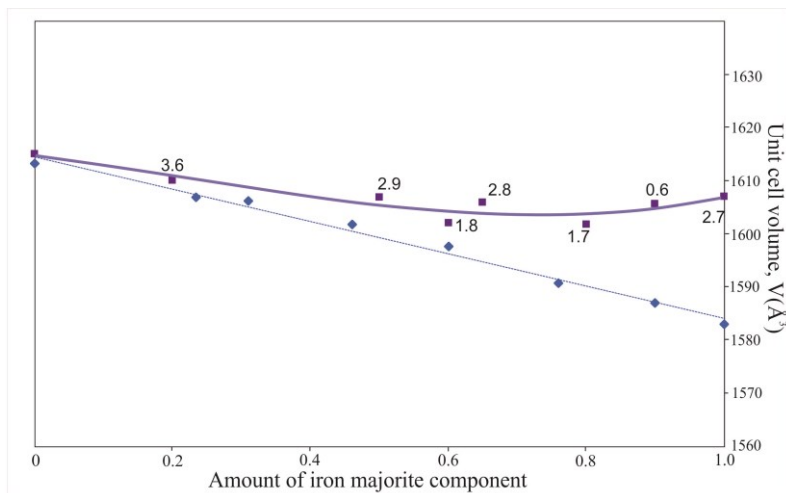
As is seen from Fig. 1 (dashed line) this interatomic potential model allowed to reproduce all experimental structural characteristics of *ski - Fe-maj* solid solution for all compositions using virtual crystal approximation with high accuracy.

However, in the virtual crystal approximation, the crystallographic positions are statistically populated, which can greatly differ from the real local structure in the solid solution.

Therefore, in order to accurately predict the properties of the solid solution, we used the supercells simulation procedure with the representational atomic configurations. The algorithm for such a configuration choose is realized in the Binar code (Eremin et al., 2008). The supercell dimension for configurations with different degree of order (χ^2) in the current procedure ranged from $2 \times 2 \times 2$ (1536 atoms) to $3 \times 3 \times 3$ (5184 atoms).

The dependence of the volume on the composition of the solid solution over the entire range of compositions, including the experimentally unimplemented *Fe-maj* was estimated. Figure 1 demonstrates the dependence of the ski-Fe-maj unit cell volume on the composition and degree of order. As is seen from the figure the virtual crystal approximation yields a linear dependence, which is well reproduced with high accuracy by the developed interatomic potentials model taking into consideration partially populations of octahedral positions by of different types of atoms. Note that the disordering effects lead to a sufficient increase of the unit cell volumes and a change from the linear dependence to a nonlinear one with increasing Fe-maj component.

Fig. 1. *Ski* - *Fe-maj* unit cell volume – composition and order degree dependence. The rhombuses show the virtual crystal model results, squares represent the supercell calculations of the disordered configurations. The figures show the χ^2 values of the selected atomic configuration in the supercell.



In addition to disordered configurations, various variants of Fe and Si ordering by octahedral positions in *Fe-maj* were tested: chess ordering of SiO_6 and FeO_6 octahedra in the supercell, layered ordering of SiO_6 and FeO_6 octahedra, layered ordering with conjugate replacement $1\text{SiO}_6 \leftrightarrow 1\text{FeO}_6$ and $2\text{SiO}_6 \leftrightarrow 2\text{FeO}_6$ in each layer and double layered ordering. As is seen from table 1 the most energetically favorable

is single layered ordering of SiO_6 and FeO_6 octahedra (fig. 2). Note that unit cell volumes of all ordered configurations are less than disordered ones with high scattering of values. This fact can explain the experimental data of Akaogi and Akimoto (1977), where a sufficiently smaller unit cell volume of *Fe-maj* was reported (1558.89 \AA^3).

Table 1. Structure energies, unit cell volumes and bulk modulus of *Fe-maj* supercells with different atomic configurations.

| Ordering scheme | E/unit cell, eV | V/unit cell, \AA^3 | Bulk modulus (Hill approximation), GPa |
|--|-----------------|-----------------------------|--|
| Disordered configuration ($\chi^2=2.7$) | -2243.97 | 1607.00 | 128.5 |
| Chess ordering of SiO_6 and FeO_6 octahedra | -2244.87 | 1594.65 | 146.1 |
| Layered ordering of SiO_6 and FeO_6 octahedra | -2273.68 | 1577.57 | 159.1 |
| Layered ordering of SiO_6 and FeO_6 octahedra with conjugate replacement $1\text{SiO}_6 \leftrightarrow 1\text{FeO}_6$ in each layer | -2243.64 | 1579.81 | 156.7 |
| Layered ordering of SiO_6 and FeO_6 octahedra with conjugate replacement $2\text{SiO}_6 \leftrightarrow 2\text{FeO}_6$ in each layer | -2243.70 | 1581.45 | 154.9 |
| Double layered ordering of SiO_6 and FeO_6 octahedra | -2244.30 | 1586.78 | 150.4 |

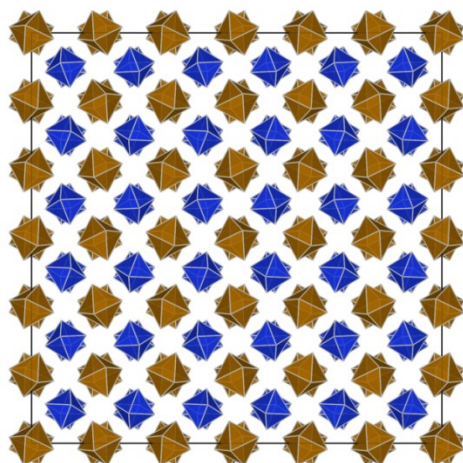


Fig. 2. Layered ordered SiO_6 and FeO_6 octahedra sublattice in the 3×3 majorite supercell. (a-b projection). SiO_6 octahedra are shown as blue ones, FeO_6 octahedra are brown.

Acknowledgments. The work was supported by RFBR grant № 16-05-00419. The work was carried out using the equipment of the Center of the collective using of Ultra-High-Performance Computational Resources of the Moscow State University.

References:

- Akaogi M., Akimoto S. (1977) Pyroxene-garnet solid-solution equilibria in the systems $\text{Mg}_4\text{Si}_4\text{O}_{12}$ - $\text{Mg}_3\text{Al}_2\text{Si}_3\text{O}_{12}$ and $\text{Fe}_4\text{Si}_4\text{O}_{12}$ - $\text{Fe}_3\text{Al}_2\text{Si}_3\text{O}_{12}$ // *Physics of the Earth and Planetary Interiors*. V. 15. Pp. 90–106.
 Gale J.D., Rohl A.L. (2003) The General Utility Lattice Program (GULP) // *Mol. Simul.* V. 29. Pp. 291–341.
[doi:10.1080/0892702031000104887](https://doi.org/10.1080/0892702031000104887)

Eremin N.N., Deyanov R.Z., Urusov V.S. (2008) Choice of the supercell with the optimum atomic configuration in simulation of disordered solid solutions // *Glass Physics and Chemistry*. Maik Nauka/Interperiodica Publishing. V. 34. № 1. Pp. 9-18. DOI [10.1134/S1087659608010021](https://doi.org/10.1134/S1087659608010021)

Ismaililova L., Bykov M., Bykova E., Bobrov A., Kupenko I., Cerantola V., Vasiukov D., Dubrovinskaia N., McCammon C., Hanfland M., Glazyrin K., Liermann H.-P., Alexander Chumakov A., and Dubrovinsky L. (2017) Effect of composition on compressibility of skiaegite-Fe-majorite garnet // *American mineralogist*. V. 102. Pp. 184-191.

Pedone A., Malavasi G., Menziani M.C., Cormack A.N., and Segre U. (2006) A new self-consistent empirical interatomic potential model for oxides, silicates, and silica-based glasses // *J. Phys. Chem. B*. V. 110. Pp. 11780-11795.

Martirosyan N. S.^{1,2}, Podborodnikov I.V.^{1,2}, Shatskiy A.F.^{1,2}, Litasov K. D.^{1,2}, Yoshino T.³ Phase relations in the CaCO₃–olivine–Fe system: implication for the formation of the Ca-rich inclusions in diamonds UDC 551.14:544.015.4

¹ Sobolev Institute of Geology and Mineralogy SB RAS, Novosibirsk, Russia (martirosyan_naira@igm.nsc.ru)

² Novosibirsk State University, Pirogova st., 2, Novosibirsk 630090, Russia

³ Institute for Planetary Materials, Okayama University, Misasa, Tottori 682-0193, Japan

Abstract. The CaCO₃-olivine-Fe system, which allows to model phase relations in the carbonate-silicate system in the presence of metallic iron, was studied at 6 GPa, 1100-1300°C. Formation of merwinite, monticellite, ferropericlase, graphite and silicate-bearing carbonate-oxide melt was observed. Crystallization of carbide and graphite occurs due to carbonate-iron redox reaction. In this case, carbide is an intermediate phase, which forms only in excess of iron and it is further replaced by graphite upon interaction with the carbonate. The present experimental data indicate that the interaction of carbonate-bearing subduction rocks with Fe-bearing peridotitic mantle would lead to the crystallization of diamond, merwinite, monticellite and formation of Ca-rich carbonatite melt at temperatures of hot subduction geotherm. Thus, merwinite and monticellite can be considered as an indicators of the CaCO₃ metasomatic activity in the ultramafic assemblages.

Keywords: carbonate, redox conditions, iron, olivine, diamond, carbide, monticellite, merwinite, carbonatite melt, CaCO₃ metasomatic activity

Introduction The occurrence of CaCO₃ in the mantle follows from its observation in syngeneic inclusions in diamonds (Bulanova and Pavlova, 1987; Sobolev et al., 1997, 2004, 2009; Stachel et al., 1998; Leost et al., 2003). Ca-carbonate is often found together with Ca-rich suite of mineral inclusions, including dolomite, merwinite, CaSiO₃, CaTiO₃, CaSi₂O₅, and Ca₂SiO₄, which indicate an existence of a distinct Ca-rich carbonate-silicate reservoir in the sublithospheric mantle (Brenker, et al., 2007; Bulanova, et al., 2010; Kaminsky, et al., 2013,

Nestola, et al., 2018; Walter, et al., 2008; Zedgenizov, et al., 2014). The C-isotopic composition of the host diamonds (Walter, et al., 2008; Zedgenizov, et al., 2014) and Eu-anomalies of CaSiO₃ (Stachel, et al., 2000), attribute the Ca-rich lithologies to the subduction processes.

Carbonate inclusions in diamonds indicate the heterogeneity of the redox conditions in the mantle and possibility of the redox reactions with the formation of diamond. Thermodynamic calculations and experiments show that the mantle rocks may contain metallic Fe or Fe-Ni alloy at ~250 km depth and in all mantle regions below (Frost, et al., 2004). An occurrence of metallic iron and iron carbides as inclusions in diamonds (Kaminsky, Wirth, 2011; Smith, et al., 2016) is in agreement with this concept. Under such conditions, carbonates and carbonatite melts will react with iron to form diamonds (Palyanov, et al., 2013).

In the present work, we studied CaCO₃-olivine-Fe system, which allows to model phase relations in the carbonate-silicate system in the presence of metallic iron.

Experimental Experiments were conducted at 6 GPa and 1100-1300°C with run duration of 2-24 h. For high-pressure generation we used uniaxial split-sphere multianvil apparatus USSA-1000 (IPM, Okayama University, Misasa, Japan). Two types of capsules were used (Fig. 1a; g): (1) double capsule with 1 mm thick MgO outer capsule (Fig. 1g), and 0.1 mm thick Fe inner capsule; (2) Ta capsule for experiment at 1300°C (Fig. 1a). Initial reactants, synthetic CaCO₃ (99.9 %, Wako Pure Chem. Ind., Ltd., Japan), San Carlos olivine and Fe powder (99.9 %, Rare Metallic Co) were loaded into the capsules in layered configuration in the following order: (1) CaCO₃, (2) olivine+3 wt% Fe. Au foil was placed on olivine-Fe layer from both sides marking the boundary with carbonate and with iron capsule (Fig. 1 a; g). Samples were analyzed using scanning electron microscope with energy-dispersive spectrometer and Raman spectroscopy.

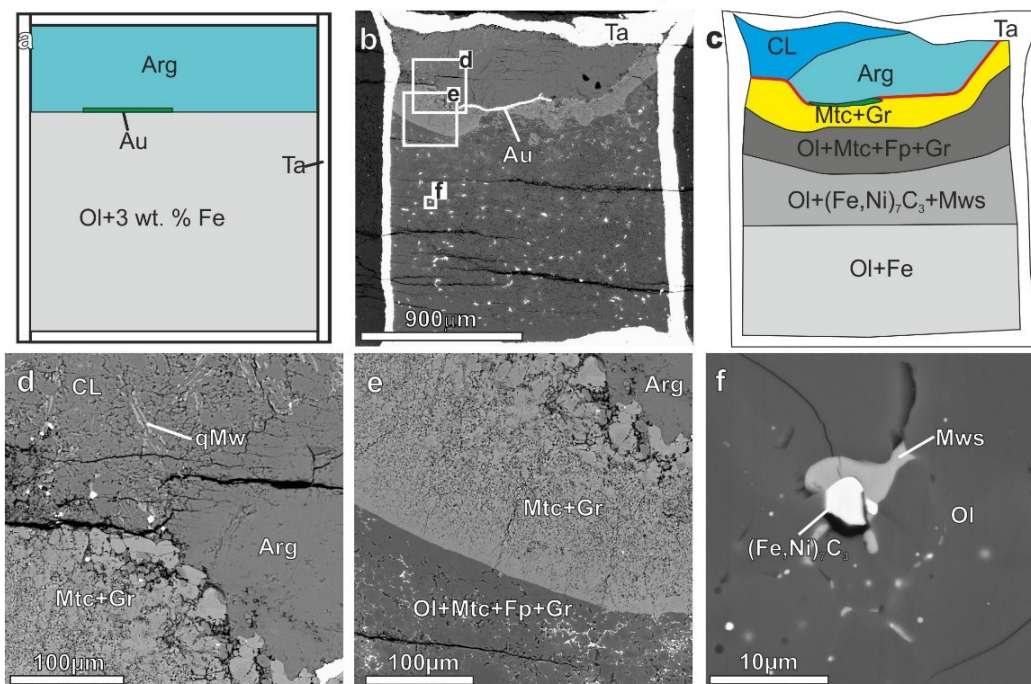
Results In all samples, substantial amount of pure CaCO₃ aragonite was preserved in crystalline form (Fig. 1). Iron was detected only in the experiment with the shortest duration (2 h at 1300°C) (Fig. 1b). In the longer runs (12-24 h, 1100°C), only relicts of Fe-Au alloy, that formed at the contact of Fe capsule with Au foil, were observed, while iron capsule all over the sample was substituted by magnesiowustite and graphite (Fig. 1h, l). The formation of merwinite, monticellite, ferropericlase, graphite and silicate-containing carbonate-oxide melt was observed. All samples have a zoned structure with phase assemblages changing with the distance from the initial boundary between carbonate and olivine-Fe mixture (Fig. 1).

In the shortest run (2 h at 1300°C) (Fig. 1b-f), at the upper part of the capsule, which was adjacent to the thermocouple, we observed segregated silicate-

containing carbonate-oxide melt and unreacted aragonite (Fig. 1d). The melt is calcium-rich ($\text{Ca}\# = 80\text{--}90$) with concentration of $\text{SiO}_2 = 2\text{--}4$ wt.%; $\text{MgO} = 6\text{--}8$ wt.%; and $\text{FeO} = 1\text{--}2$ wt.%. Merwinite and pure CaCO_3 were detected among dendrites of quenched melt. We observed monticellite-graphite layer, 200 μm thick (Fig. 1c) beneath the Au-foil that separates carbonate and silicate containing parts (Fig. 1b) and marks the

initial boundary between CaCO_3 and olivine-Fe mixture. Its edge is marked by the presence of olivine. The predominantly olivine containing part of the sample can also be separated into three zones according to the accessory phases (Fig. 1c): (1) monticellite+ferropericlasite+graphite, 250 μm thick; (2) $(\text{Fe,Ni})_7\text{C}_3$ +magnesiowustite, 300 μm thick (Fig. 1f); and (3) metallic Fe, 600 μm thick.

1300°C; 6 GPa; 2h; Ta capsule



1100°C; 6 GPa; 12h; double capsule: MgO - outer, Fe - inner

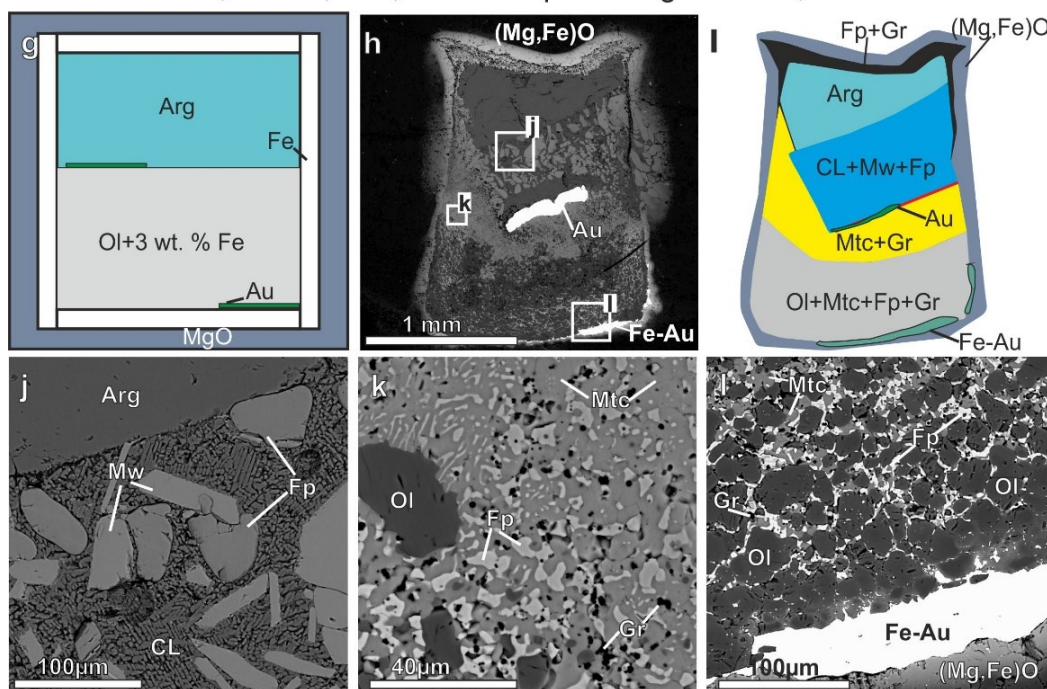
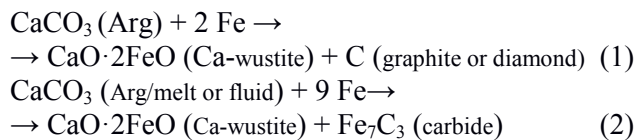


Fig. 1. Representative images and BSE microphotographs of the experimental samples: b, d–f – at 1300°C and 2h; h, j–l – 1100°C and 12h. a, g – schemes of sample loading before experiment; c, i – after experiment. Abbreviations: Ol – olivine; Arg – aragonite; CL – silicate containing carbonate-oxide melt; Mtc – monticellite; Mw, qMw – merwinite; Gr – graphite; Fp – ferropericlasite; Mws – magnesiowustite.

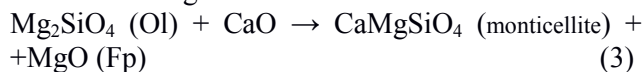
In the experiment conducted at 1100°C with duration of 12 h 4 zones can be distinguished: (1) unmodified pure CaCO₃ aragonite (Fig. 1j); (2) silicate-containing carbonate-oxide melt with large ferropericlasite and merwinite crystals (Fig. 1j); (3) monticellite, ferropericlasite and graphite with relicts of olivine (Fig. 1k); and (4) layer predominantly composed of isometric olivine crystals with monticellite, ferropericlasite and graphite situated in interstices (Fig. 1l). With the increase of run duration up to 24 h monticellite is substituted by merwinite all over the sample. No signs of carbide were detected. Composition of silicate-containing carbonate-oxide melt is similar to that formed at 1300°C.

Discussion Based on the experimental results, we can further explain the observed regularities by separating them into the elemental reactions. First of all, formation of oxides, graphite and carbide requires occurrence of the redox reactions, that according to the previous experimental studies in CaCO₃-Fe system (Martirosyan, et al., 2015, Martirosyan, et al., 2016) can be represented as follows:



In the sample from the experiment with 2 h heating duration at 1300°C (Fig 1c), carbide-bearing layer was found in contact with unreacted metallic iron, while only graphite was observed near aragonite. It can be suggested, that the formation of graphite and carbide occurs at different local concentrations of iron and carbon: an excess of carbonate leads to the crystallization of graphite, whereas in the case of iron-rich environment carbide forms. Since in the long experiments (12 and 24 h at 1100°C) we do not detect carbide, it can be suggested that it is an intermediate phase, and under conditions of an excess of carbonate, it is replaced by graphite.

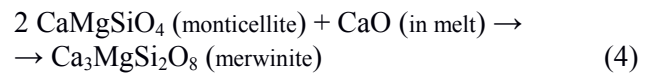
Ca-wüstite, which can be formed by the redox reactions (1 and 2) is not stable in silicate-bearing systems and it is replaced by monticellite, according to the following reaction:



Silicate-bearing carbonate-oxide melt with high Ca# (80-90) was detected in the present experiments already at 1100°C, which is 100°C lower than the temperature of CaCO₃-CaO melt formation in the CaCO₃-Fe system (Martirosyan, et al., 2015), and 600°C below the melting point of CaCO₃ at 6 GPa (Shatskiy, et al., 2014). It is known that the CaO-CaCO₃ at high pressure has eutectic type diagram. The difference in melting temperatures of CaCO₃ and CaO-CaCO₃ eutectic increases with pressure, reaching 200 K at 3 GPa (Huang, Wyllie, 1976). The reduction of CaCO₃ occurs with the formation of

CaO and the exchange reactions of oxide with olivine lead to the formation of ferropericlasite and monticellite. These reactions could be accompanied by the generation of a high-calcium melt at temperatures well below the melting point of CaCO₃.

Merwinite in all samples is confined to the zone with a melt and is found either in the form of dendrites or in the form of large crystals crystallizing from the melt (Fig. 1j). The formation of merwinite is probably associated with the interaction of monticellite with a silicate-bearing carbonate-oxide melt:



In the recent work Sharygin et al (2018) argued that the formation of merwinite, can occur in olivine-alkali-carbonate melt reaction under the oxidized conditions. The present work shows another mechanism of the merwinite crystallization, which is more relevant to the redox conditions of the diamond formation. In our experiments, merwinite does not replace olivine directly. Its formation occurs only at the conditions of the local excess of calcium due to the interaction of monticellite with a carbonate-oxide melt, according to reaction (4). In turn, monticellite replaces olivine directly, and thus forms at the local Mg-, and Si-rich conditions.

The present experimental data indicate that at the upper mantle conditions, merwinite and monticellite can be considered as an indicator of the CaCO₃ metasomatic activity in the ultramafic assemblages. Moreover, formation of merwinite requires specific, Ca-rich and Mg- and Si-depleted environments, which differ from the basic mantle lithologies (peridotite and eclogite). Such chemical conditions can occur during interaction of carbonate-bearing subduction rocks with Fe-bearing peridotitic mantle, which would eventually lead to the crystallization of diamond, Ca-silicates and formation of Ca rich carbonatite melt at rather modest temperatures, corresponding to the «hot» subduction geotherm (1100°C, 6GPa) (Syracuse, et al., 2010).

The work was supported by Russian foundation of basic research No.18-35-00104 and the RF state assignment project No. 0330-2016-0012.

References:

- Brenker F. E., Vollmer C., Vincze L., Vekemans B., Szymanski A., Janssens K., Szaloki I., Nasdala L., Joswig W., Kaminsky F. Carbonates from the lower part of transition zone or even the lower mantle // *Earth and Planetary Science Letters*. – 2007. – V. 260. – P. 1-9.
- Bulanova G. P., Walter M. J., Smith C. B., Kohn S. C., Armstrong L. S., Blundy J., Gobbo L. Mineral inclusions in sublithospheric diamonds from Collier 4 kimberlite pipe, Juina, Brazil: subducted protoliths, carbonated melts and primary kimberlite magmatism // *Contributions to Mineralogy and Petrology*. – 2010. – V. 160. – P. 489-510.
- Frost D. J., Liebske C., Langenhorst F., McCammon C. A., Tronnes R. G., Rubie D. C. Experimental evidence for

the existence of iron-rich metal in the Earth's lower mantle // *Nature*. – 2004. – V. 428. – P. 409-412.

Huang W.-L., Wyllie P. J. Melting relationships in the systems CaO-CO₂ and MgO-CO₂ to 33 kilobars // *Geochimica et Cosmochimica Acta*. – 1976. – V. 40. – P. 129-132.

Kaminsky F. V., Wirth R. Iron carbide inclusions in lower-mantle diamond from Juina, Brazil // *Canadian Mineralogist*. – 2011. – V. 49. – P. 555-572.

Kaminsky F. V., Wirth R., Schreiber A. Carbonatitic inclusions in deep mantle diamonds from Juina, Brazil: new minerals in the carbonate-halide association // *Canadian Mineralogist*. – 2013. – V. 51. – P. 669-688.

Martirosyan N., Litasov K., Shatskiy A., Ohtani E. Reactions of iron with calcium carbonate at 6 GPa and 1273–1873 K: implications for carbonate reduction in the deep mantle // *Russian Geology and Geophysics*. – 2015. – V. 56. – P. 1322-1331.

Martirosyan N. S., Yoshino T., Shatskiy A., Chanyshv A., Litasov K. The CaCO₃-Fe interaction: Kinetic approach for carbonate subduction to the deep Earth's mantle // *Physics of the Earth and Planetary Interiors*. – 2016. – V. 259. – P. 1-9.

Nestola F., Korolev N., Kopylova M., Rotiroti N., Pearson D., Pamato M., Alvaro M., Peruzzo L., Gurney J., Moore A. CaSiO₃ perovskite in diamond indicates the recycling of oceanic crust into the lower mantle // *Nature*. – 2018. – V. 555. – P. 237.

Palyanov Y. N., Bataleva Y. V., Sokol A. G., Borzdov Y. M., Kupriyanov I. N., Reutsky V. N., Sobolev N. V. Mantle-slab interaction and redox mechanism of diamond formation // *Proceedings of the National Academy of Sciences*. – 2013. – V. 110. – P. 20408-20413.

Sharygin I. S., Shatskiy A., Litasov K. D., Golovin A. V., Ohtani E., Pokhilenko N. P. Interaction of peridotite with Ca-rich carbonatite melt at 3.1 and 6.5 GPa: Implication for merwinite formation in upper mantle, and for the metasomatic origin of sublithospheric diamonds with Ca-rich suite of inclusions // *Contributions to Mineralogy and Petrology*. – 2018. – V. 173. – P. 22.

Shatskiy A., Borzdov Y. M., Litasov K. D., Kupriyanov I. N., Ohtani E., Palyanov Y. N. Phase relations in the system FeCO₃-CaCO₃ at 6 GPa and 900–1700° C and its relation to the system CaCO₃-FeCO₃-MgCO₃ // *American Mineralogist*. – 2014. – V. 99. – P. 773-785.

Smith E. M., Shirey S. B., Nestola F., Bullock E. S., Wang J., Richardson S. H., Wang W. Large gem diamonds from metallic liquid in Earth's deep mantle // *Science*. – 2016. – V. 354. – P. 1403-1405.

Stachel T., Harris J. W., Brey G. P., Joswig W. Kankan diamonds (Guinea) II: lower mantle inclusion parageneses // *Contributions to Mineralogy and Petrology*. – 2000. – V. 140. – P. 16-27.

Syracuse E. M., van Keken P. E., Abers G. A. The global range of subduction zone thermal models // *Physics of the Earth and Planetary Interiors*. – 2010. – V. 183. – P. 73-90.

Walter M. J., Bulanova G. P., Armstrong L. S., Keshav S., Blundy J. D., Gudfinnsson G., Lord O. T., Lennie A. R., Clark S. M., Smith C. B., Gobbo L. Primary carbonatite melt from deeply subducted oceanic crust // *Nature*. – 2008. – V. 454. – P. 622-630.

Zedgenizov D. A., Shatskiy A., Ragozin A. L., Kagi H., Shatsky V. S. Merwinite in diamond from Sao Luiz, Brazil: A new mineral of the Ca-rich mantle environment // *American Mineralogist*. – 2014. – V. 99. – P. 547-550

Minin D.A.^{1,2}, Shatskiy A.F.^{1,2}, Litasov K.D.^{1,2}
^{1,2} The phase diagram Fe-Ni-P at 6 GPa UDC
550.4.02:544.344.015.3:546.181.1

¹ Sobolev Institute of Geology and Mineralogy SB RAS, Novosibirsk

² Novosibirsk State University, Novosibirsk
(daniil_minin@igm.nsc.ru)

Abstract. We have experimentally determined the phase diagram Fe-Ni-P in the compositional range of 0-33 mol% P at 900-1600 °C and 6 GPa. At subsolidus conditions, the Metal (Me)-rich side of the ternary has three phases: Fe-Ni alloy, (Fe,Ni)_{3-x}P, where $x \leq 0.7$, and (Fe,Ni)₂P. The first melting occurs at 950 °C at the Ni-P join and is controlled by the Ni₂P-Ni eutectics with composition of 18 mol% P. The melt field expands toward Fe-P side as temperature increases and the Fe₂P-Fe eutectic appears at 1100 °C and 16 mol% P. The maximum phosphorus content in metallic Fe is 5 mol%, whereas for metallic nickel it is 3 mol% P.

Keywords: *high-pressure experiments, phase diagram, iron-nickel phosphides, meteorites, core formation.*

Introduction The Fe-Ni-P is one of the basic phase diagrams for understanding core formation processes in planets and asteroids. Recent finding of high-pressure minerals in iron meteorites (Holtstam et al., 2003; Litasov, Podgornykh, 2017) and abundance of complex Fe-Ni-P-S quench textures with unusual bulk compositions indicate an importance of the study of related systems at elevated pressures. Although most high-pressure minerals in meteorites originate under shocked conditions of impact during short time, static high-pressure experiments are more relevant for interpretation of these processes relative to shock wave experiments, where durations of shock is too short to model meteorite impacts (10⁻⁷ sec).

Cosmochemical data indicate that about 90 % P in our planet is concentrated in the core (e.g., Litasov, Shatskiy, 2016). Occurrence of schreibersite ((Fe,Ni)₃P), allabogdanite ((Fe,Ni)₂P) and perryite ((Ni,Fe)₈(Si,P)₃) in iron and chondritic meteorites suggests that metallic cores of other planetary bodies including small planetoids with core pressure ≤ 6 GPa may contain significant amount of phosphorus. Typical P concentration in iron meteorites does not exceed 1 wt%, however due to poor solubility in iron phases it form own minerals and locally its concentration may exceed 20-30 wt% (Britvin et al., 2002). Therefore, the study of phase relations in the Fe-Ni-P system under high-pressures is important to understand differentiation of phosphorus in planetary bodies and its possible impact on the structure of metallic core of small planets.

Fe-Ni-P phase relations were determined at 1 atm with phosphorus content range up to 26 mol% P (Doan, Goldstein, 1970) and up to 28 mol% P (Romig, Goldstein, 1980). Here, we present experimental results of Fe-Ni-P system at 6 GPa.

Experimental procedure Experiments were carried out using a DIA-type multianvil apparatus «Discoverer-1500» installed at Sobolev Institute of Geology and Mineralogy (Novosibirsk, Russia). «Fujillo N-05» 26-mm tungsten carbide cubes with truncation edge length of 12 mm were employed as Kawai-cell anvils. Pressure medium shaped as 20.5

Mineral equilibria at high PT-parameters

mm octahedron with cut edges and corners were ground from semi-sintered ZrO_2 ceramics. Pyrophyllite gaskets, 4.0 mm in both width and thickness were used to seal the compressed volume and support the anvil flanks.

The design of the cell assembly is shown in Fig. 1. The cell contains 16 samples, 1.0 mm in diameter and length, loaded into $3MgO \cdot 4SiO_2$ ceramics cassettes. The cassettes were made of talc dehydrated by annealing at 1000 °C for 1 h. The high temperature was generated using a tubular graphite heater, 4.0/4.5 mm in inner/other diameter and 11 mm in length. The sample temperature was monitored via a $W_{97}Re_3-W_{75}Re_{25}$ thermocouple, inserted through the heater walls and electrically insulated from the heater by Al_2O_3 tubes.

Starting materials were prepared by blending reagent grade Fe_3P (99.5 %), Ni_2P (98%), Fe (99.9 %) and Ni (99.9 %) powders (Alfa Aesar) in an agate mortar with acetone to obtain homogeneous mixtures containing 2, 5, 10, 20, 25, 30, and 33 mol% P. The mixtures were loaded as a powder into the cassettes. The loaded samples were covered by thin layer of MgO powder (99.9% purity fired at 1000 °C) for better sealing and closed by cup made of $3MgO \cdot 4SiO_2$ ceramics (Fig. 1).

Recovered samples were mounted into epoxy and polished using anhydrous lubricants following to the procedure described by (Shatskiy et al., 2017). Samples were studied using a MIRA 3 LMU scanning electron microscope (Tescan Orsay Holding) coupled with an INCA 450 energy-dispersive X-ray microanalysis system equipped with the liquid nitrogen-free large area EDS X-Max-80 Silicon Drift Detector (Oxford Instruments Nanoanalysis Ltd) at IGM SB RAS. The run products were also examined by a micro-focused X-ray diffractometer (Rugaku MicroMax-007HF) at the Geodynamic Research Center, Ehime University,

Matsuyama, Japan. The measurements were performed from the central portion of the samples using Cu X-ray source at 40 kV tube voltage and 30 nA tube current in reflection mode and stage angle of 20°. The diffraction time was 60 min and collimator diameter was 100 μm .

Results and Discussion Phase relations in the Fe-Ni-P system at 6 GPa and temperature range 900-1600 °C are illustrated in Fig. 2. Examples of backscattered electron (BSE) images of samples are shown in Fig. 3. At 900 °C, the subsolidus phase assemblages are represented by homogeneous aggregates of metals, phosphides and $Me_{3-x}P$ solid solution, with grain size varying from 5 to 70 μm . First melt appears at 950 °C on the Ni- Ni_2P side, which extends with further temperature increasing toward Fe- Fe_2P .

At 900 °C the system has three P-bearing compounds: Me_3P , $Me_{3-x}P$ and Me_2P . At $X(P) = 100P/(P+Fe+Ni) = 30$ mol% and $\#Fe = 100 Fe/(Fe+Ni) = 100, 75$ and 50 mol%, Me_3P coexists with Me_2P (Fig. 3 a,b), whereas at $X(P)/\#Fe = 30/25$ and 30/0, $Me_{3-x}P$ solid solution coexists with Me_2P . Consequently, $Me_{3-x}P$ solid solution in Fe-Ni-P system is controlled by Fe content from 0 to 25 mol%. At $X(P) = 10$ and 20 mol% and subsolidus conditions, the phase assemblage was represented by Me and Me_3P compounds. The Ni- Ni_2P compounds are more fusible than Fe- Fe_2P compounds and first melt appears on Ni- Ni_2P side at 950 °C and $X(P) = 20$ mol%. The $Me_{3-x}P$ phase remains stable up to 1150 °C and completely melts at 1200 °C (Fig. 2). The Me_3P , on the Ni- Ni_2P side, melts at 1200 °C, whereas at $\#Fe = 100-50$ mol% it still remains solid and on the Fe- Fe_2P side completely melts at 1300 °C. The Me_2P phosphide on the Ni- Ni_2P side is already melted, whereas on the Fe- Fe_2P side it is still stable. The Me_2P phase field shrinks with increasing temperature and completely disappears at 1600 °C on the Fe- Fe_2P side.

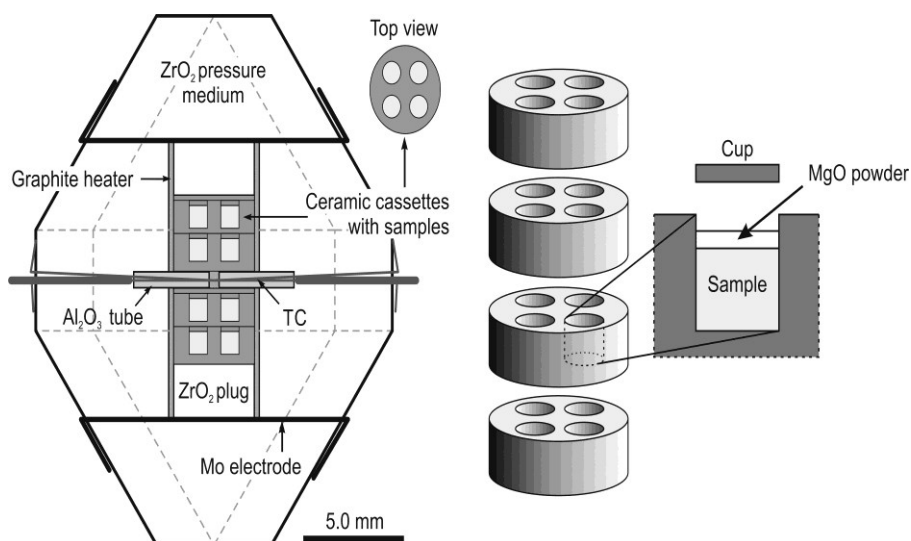


Fig.1. High-pressure cell assembly. TC – thermocouple.

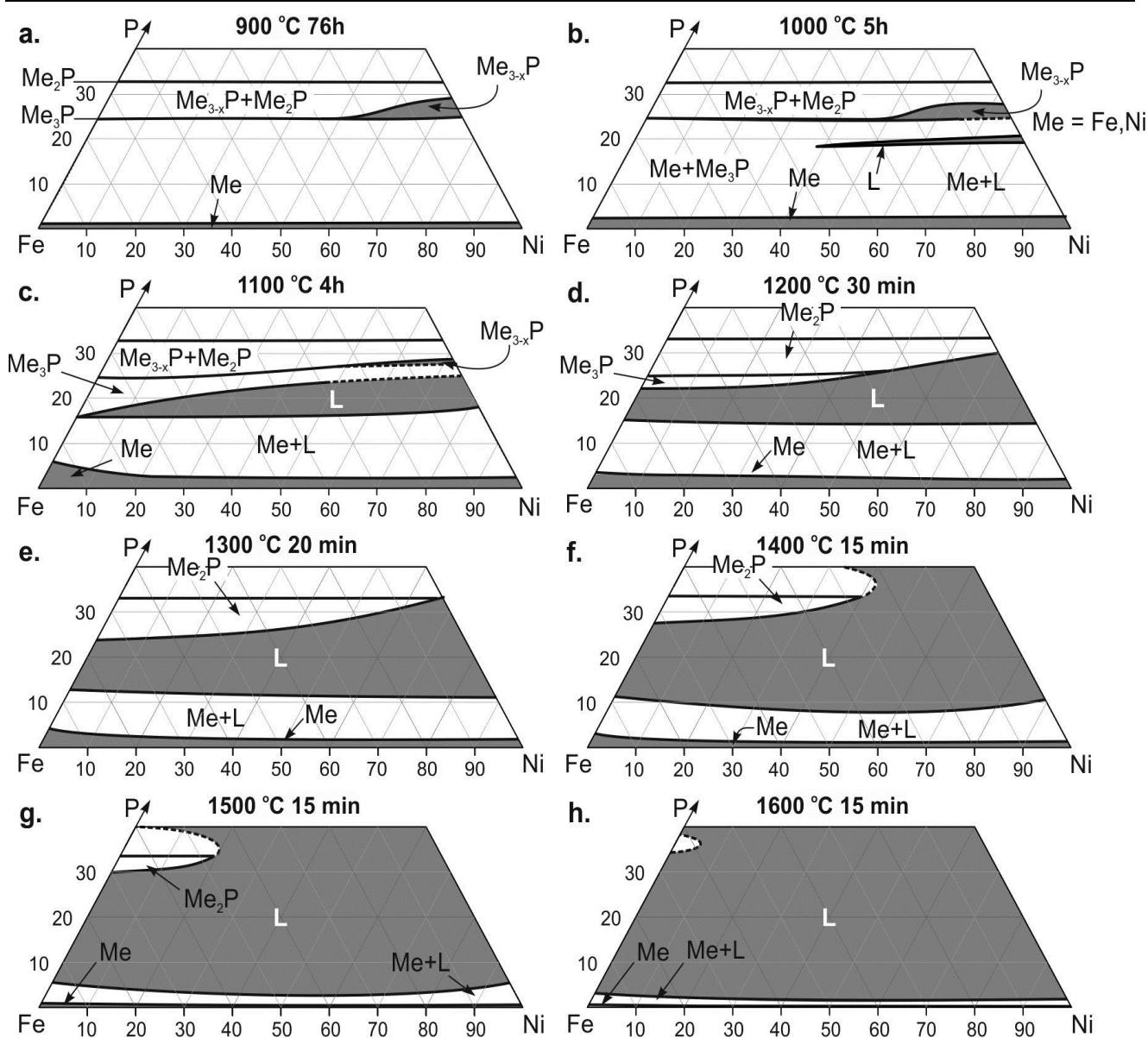


Fig.2. Isothermal sections of the Fe-Ni-P phase diagrams at 6 GPa.

Our results are in good agreement with the melting temperature of pure Fe and Ni, 1668 °C and 1532 °C, respectively, at 6 GPa. Measurable amounts of P in metallic phase suggest an existence of limited solid solutions of P in metals under given conditions. In the temperature range of 900-1050 °C, the iron contains 1-2 mol% P. The maximum phosphorus solubility in iron, 4-6 mol%, is established at 1100-1250 °C. The phosphorus solubility in metallic nickel increases from 2 mol% P at 900 °C to maximum of 3.5 mol% P at 950 °C.

The subsolidus samples and residue crystalline phosphides in subliquidus runs were examined using microfocus X-ray diffraction. Phosphides correspond to the ambient pressure phases of $(Fe,Ni)_2P$ with space group $P62m$ (barringerite) (Hendricks, Kostig, 1930; Rundqvist, 1961) and $(Fe,Ni)_3P$ with space group $I4$ (schreibersite) (Rundqvist, 1962; Skála, Císařová, 2005).

A number of tiny spots and worms, 1-30 μm in size, represented by Fe-Ni phosphates with secondary Mg content, were observed along the grain boundaries of metallic phases and phosphides in subsolidus samples (Fig. 3). As temperature increases, the number of phosphate inclusions decreases, but their size increases. In subliquidus runs, the phosphate globules appear among residual phosphide crystals and suspended in phosphide liquid. At temperatures exceeding 1050 °C, on the Fe- Fe_2P side, phosphates appear either as single-phase inclusions of Mg-poor $Fe_3(PO_4)_2$ or as Fe-Mg phosphate melt. The total amount of phosphates varies in 1-3 vol.% of the sample. Taking into account that observed phosphates are immiscible with phosphide and metal, this amount is not critical for the determined Fe-Ni-P phase diagram.

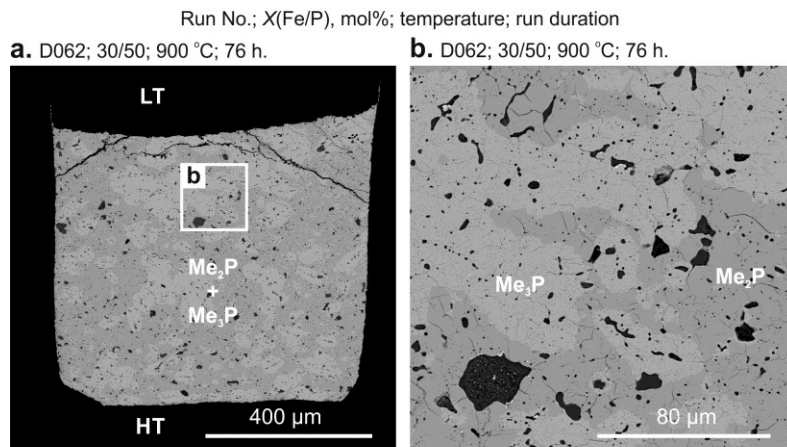


Fig.3. Representative BSE images of samples from subsolidus experiments in the system Fe-Ni-P at 6 GPa. HT = high-temperature side. LT = low-temperature side.

The work is supported by Russian Science Foundation (project No 17-17-01177)

References:

- Britvin S.N., Rudashevsky N.S., Krivovichev S.V., Burns P.C., Polekhovskiy Y.S. Allabogdanite, $(\text{Fe,Ni})_2\text{P}$, a new mineral from the Onello meteorite: The occurrence and crystal structure // *American Mineralogist*. – 2002. – V. 87. – P. 1245-1249.
- Doan A.S., Goldstein J.I. The ternary phase diagram, Fe-Ni-P // *Metallurgical Transactions*. – 1970. – V. 1. – P. 1759-1767.
- Hendricks S.B., Kosting P.R. The crystal structure of Fe_2P , Fe_2N , Fe_3N and FeB // *Zeitschrift für Kristallographie*. – 1930. – V. 74. – P. 511-533.
- Holtstam D., Broman C., Söderhielm J., Zetterqvist A. First discovery of stishovite in an iron meteorite // *Meteoritics & Planetary Science*. – 2003. – V. 38. – P. 1579-1583.
- Litasov K.D., Podgornykh N.M. Raman spectroscopy of various phosphate minerals and occurrence of tuite in the Elga IIE iron meteorite // *Journal of Raman Spectroscopy*. – 2017. – V. 48. – P. 1518-1527.
- Litasov, K.D., Shatskiy, A.F., Composition of the Earth's core: A review // *Russian Geology and Geophysics*. – 2016. – V. 57. – P. 22-46.
- Romig A.D., Goldstein J.I. Determination of the Fe-Ni and Fe-Ni-P phase diagrams at low temperatures (700 to 300 °C) // *Metallurgical Transactions A*. – 1980. – V. 11. – P. 1151-1159.
- Rundqvist S. X-ray investigation of Mn_3P , Mn_2P , and Ni_2P // *Acta Chem. Scand.* – 1961. – V. 16. – P. 92.
- Rundqvist S. X-ray investigations of the ternary system Fe-P-B. some features of the systems Cr-P-B, Mn-P-B, Co-P-B and Ni-P-B // *Acta Chem. Scand.* – 1962. – V. 16. – P. 1-19.
- Shatskiy A., Sharygin I.S., Gavryushkin P.N., Litasov K.D., Borzdov Y.M., Shcherbakova A.V., Higo Y., Funakoshi K., Palyanov Y.N., Ohtani E. The system $\text{K}_2\text{CO}_3\text{-MgCO}_3$ at 6 GPa and 900–1450°C // *American Mineralogist*. – 2013. – V. 98. – P. 1593-1603.
- Skála R., Čisářová I. Crystal structure of meteoritic schreibersites: determination of absolute structure // *Physics and Chemistry of Minerals*. – 2005. – V. 31. – P. 721-732.

Podborodnikov I.V.^{1,2}, Rashchenko S.V.^{1,2}, Arefiev A.V.^{1,2}, Shatskiy A.F.^{1,2}, Litasov K.D.^{1,2} Stoichiometry OF Na-Ca double carbonates versus pressure and temperature
UDC 551.14:544.015.4

¹V.S. Sobolev Institute of Geology and Mineralogy SB RAS, Novosibirsk,
²Novosibirsk State University, Novosibirsk
(podborodnikov@igm.nsc.ru)

Abstract. Considering experimental data on phase relations in the system $\text{Na}_2\text{CO}_3\text{-CaCO}_3$, a range of the intermediate compounds changes as pressure and temperature increases in the following sequence: $\text{Na}_2\text{Ca}_2(\text{CO}_3)_3$ (0.1 GPa, <400 °C) → $\text{Na}_2\text{Ca}(\text{CO}_3)_2$ (0.1 GPa, 400-725 °C) → $\text{Na}_2\text{Ca}(\text{CO}_3)_2$, $\text{Na}_2\text{Ca}_3(\text{CO}_3)_4$ (3 GPa) → $\text{Na}_4\text{Ca}(\text{CO}_3)_3$, $\text{Na}_2\text{Ca}_3(\text{CO}_3)_4$ (6 GPa). Based on these data we can model composition of carbonatite melt formed by incipient melting of carbonated mantle rocks at pressures up to 6 GPa.

Keywords: Na-Ca double carbonates; high-pressure; multianvil experiment; Earth's mantle

Alkali elements (Na and K) in their natural abundances could account for lowering of the solidus temperatures of carbonated silicate mantle by several hundred degrees (Litasov et al., 2013). Partial melting of carbonated peridotites and eclogites at ≥ 3 GPa yields Na- and K-bearing carbonatite melts (Dasgupta et al., 2005, Thomson et al., 2016). Mass-balance calculations of samples obtained below apparent solidi often produce clear deficits of alkalis (Dasgupta, Hirschmann, 2007), suggesting the presence of minor alkali-rich liquid or solid carbonate phases (Litasov et al., 2013). Identification and precise determination of the compositions of these phases are problematic due to their trace amounts in the natural-like systems. Phase equilibria in simple carbonate systems are therefore important to facilitate interpretation of the complex carbonated silicate systems. Particularly, it is essential to know crystal chemistry and Raman spectra of high-pressure alkali-bearing carbonate phases.

As part of an investigation of those systems, Na_2CO_3 – CaCO_3 is important, given the Na and Ca abundances in the mantle-derived carbonatite melts (Kaminsky et al., 2009) and in the groundmass of fresh kimberlites (Kamenetsky et al., 2004, Golovin et al., 2017). The given system is also important in view of the Na and Ca abundances in carbonatite melt inclusions in kimberlite-hosted phenocrysts (Golovin et al., 2007, Kamenetsky et al., 2009) and mantle xenoliths derived from depths varying from 110–115 km (spinel harzburgite: 3.4–3.5 GPa, 860 °C) (Giuliani et al., 2012) to 140 km (garnet wehrlite: 4.3 GPa, 1060 °C), and 180–240 km (sheared garnet harzburgite and lherzolites: 5.7–7.3 GPa, 1230–1360 °C) (Golovin et al., 2017, Golovin et al., 2018).

Phase relations for the join Na_2CO_3 – CaCO_3 have been previously determined at 0.1 and 6 GPa (Cooper et al., 1975, Shatskiy et al., 2013). Although the end members, CaCO_3 and Na_2CO_3 , reveal quite high melting temperatures (Li et al., 2017), which are 400–800 °C higher than the typical shield geotherm (40 mW/m²), the Na_2CO_3 – CaCO_3 system forms fusible intermediate compounds (Na–Ca double carbonates) and eutectics, which are several hundreds of degrees lower than melting temperatures of the end members (Fig. 1). Yet, significant difference in intermediate compounds stable at pressures of 0.1

and 6 GPa does not allow reliable interpolations between these pressures. Based on the phase relations established at 6 GPa, shortite $\text{Na}_2\text{Ca}_2(\text{CO}_3)_3$ and nyerereite $\text{Na}_2\text{Ca}(\text{CO}_3)_2$, the double carbonates observed at 0.1 GPa (Cooper et al., 1975), are not stable at the pressure and temperature conditions of sublithospheric mantle (Shatskiy et al., 2013). At the same time, findings of these minerals in coexistence with aragonite among daughter phases in the melt inclusions in olivine from the sheared garnet peridotites (Golovin et al., 2017, Golovin et al., 2018) may indicate that their stability fields could extend at least to *P*–*T* conditions of the shallow mantle.

In this paper we show preliminary data on phase relations in Na_2CO_3 – CaCO_3 system at 3 GPa. The experiments were performed using multianvil apparatus Discoverer 1500 installed at IGM SB RAS, Novosibirsk. The details of the experiments were reported elsewhere (Shatskiy et al., 2018).

Fig. 1 shows the isobaric *T*–*X* phase diagrams for the Na_2CO_3 – CaCO_3 system, which were experimentally established at 0.1 GPa (Cooper et al., 1975), 3 GPa (Podborodnikov et al., 2018), and 6 GPa (Shatskiy et al., 2013). These data are also summarized on the *P*–*T* plot in Fig. 2.

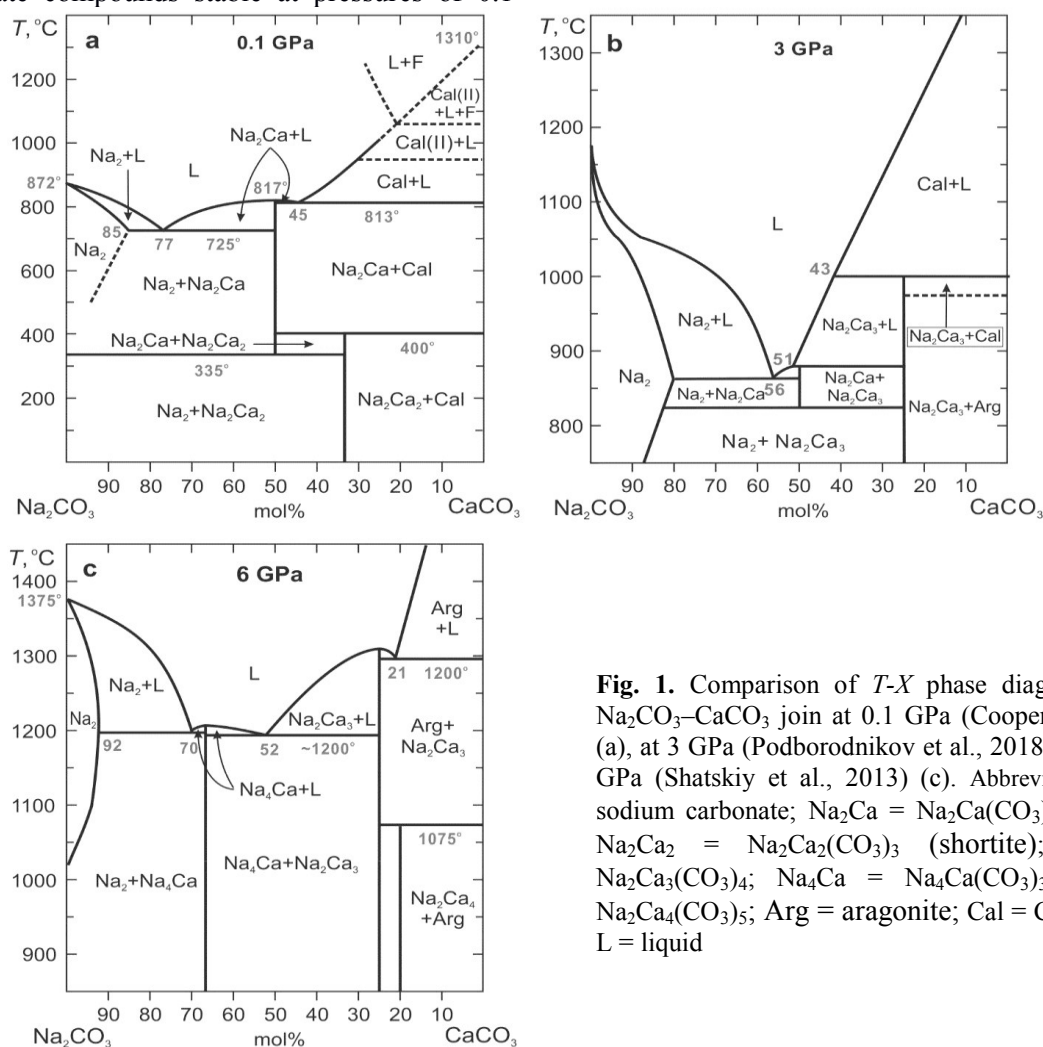
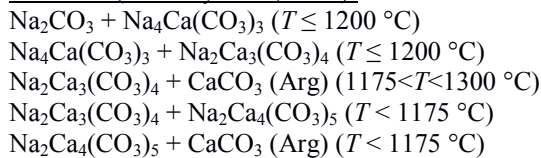


Fig. 1. Comparison of *T*–*X* phase diagrams for the Na_2CO_3 – CaCO_3 join at 0.1 GPa (Cooper et al., 1975) (a), at 3 GPa (Podborodnikov et al., 2018) (b), and at 6 GPa (Shatskiy et al., 2013) (c). Abbreviations: Na_2 = sodium carbonate; Na_2Ca = $\text{Na}_2\text{Ca}(\text{CO}_3)_2$ (nyerereite); Na_2Ca_2 = $\text{Na}_2\text{Ca}_2(\text{CO}_3)_3$ (shortite); Na_2Ca_3 = $\text{Na}_2\text{Ca}_3(\text{CO}_3)_4$; Na_4Ca = $\text{Na}_4\text{Ca}(\text{CO}_3)_3$; Na_2Ca_4 = $\text{Na}_2\text{Ca}_4(\text{CO}_3)_5$; Arg = aragonite; Cal = CaCO_3 calcite; L = liquid

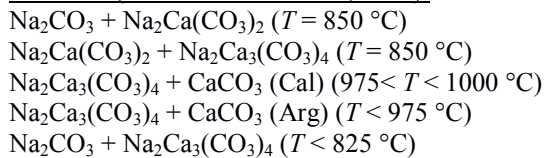
Mineral equilibria at high PT-parameters

According to the phase diagrams presented in Figs. 1 and 2, equilibrium subsolidus associations in the Na_2CO_3 - CaCO_3 binary can be summarized as follows:

At 6 GPa (Shatskiy et al., 2013):



At 3 GPa (Podborodnikov et al., 2018):



At 0.1 GPa (Cooper et al., 1975):

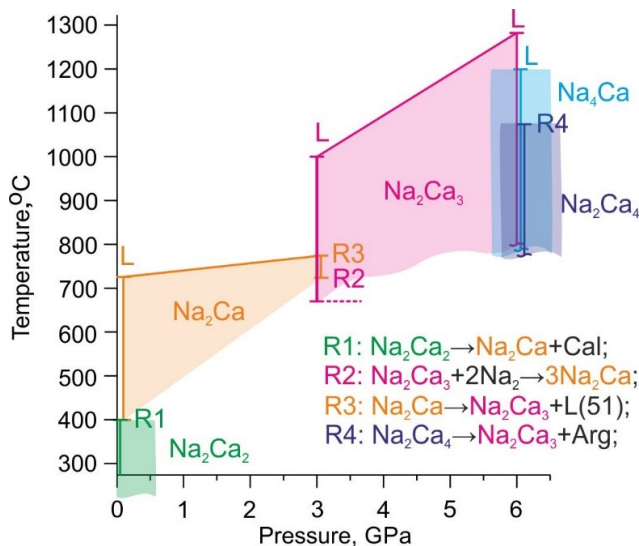
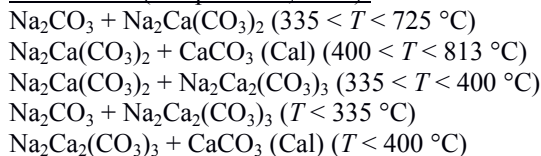
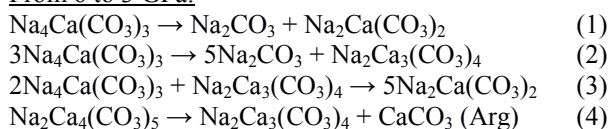


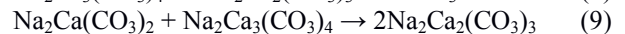
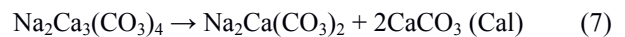
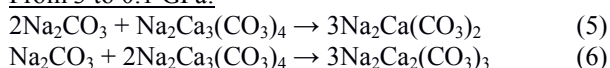
Fig. 2. Variety of double carbonates established in the Na_2CO_3 - CaCO_3 system at ≤ 0.1 GPa (Cooper et al., 1975), 3 GPa (Podborodnikov et al., 2018), and 6 GPa (Shatskiy et al., 2013).; $\text{Na}_2\text{Ca} = \text{Na}_2\text{Ca}(\text{CO}_3)_2$ (nyererite); $\text{Na}_2\text{Ca}_2 = \text{Na}_2\text{Ca}_2(\text{CO}_3)_3$ (shortite); $\text{Na}_2\text{Ca}_3 = \text{Na}_2\text{Ca}_3(\text{CO}_3)_4$; $\text{Na}_4\text{Ca} = \text{Na}_4\text{Ca}(\text{CO}_3)_3$; $\text{Na}_2\text{Ca}_4 = \text{Na}_2\text{Ca}_4(\text{CO}_3)_5$; L = liquid.

The listed associations assume that following solid-state reactions can occur upon pressure decrease:

From 6 to 3 GPa:



From 3 to 0.1 GPa:



We roughly estimated the volume effects of the reactions (1-9) using unit cell volumes of involved phases at ambient conditions (Dickens et al., 1971, Dusek et al., 2003, Gavryushkin et al., 2014, Gavryushkin et al., 2016, Rashchenko et al., 2017, Rashchenko et al., 2018). All obtained reaction volumes are positive, supporting the possibility of the discussed solid-phase transformations upon release of pressure. The latter suggest that association of Na_2CO_3 , $\text{Na}_2\text{Ca}(\text{CO}_3)_2$, $\text{Na}_2\text{Ca}_2(\text{CO}_3)_3$, and CaCO_3 reported for inclusions in superdeep diamonds (Kaminsky et al. 2009), kimberlitic olivines (Golovin et al. 2016), and kimberlite groundmass (Golovin et al., 2018) may actually represent breakdown products of high-pressure minerals identical to synthetic phases described here.

This study was financially supported by the Russian Foundation for Basic Research (project No 17-05-00501) and partially by the state assignment project no. 0330-2016-0006.

References:

- Cooper A.F., Gittins J. and Tuttle O.F. The system Na_2CO_3 - K_2CO_3 - CaCO_3 at 1 kilobar and its significance in carbonatite petrogenesis // *American Journal of Science*. - 1975. - V. 275. - № 5. - P. 534-560.
- Dasgupta R., Hirschmann M.M. and Dellas N. The effect of bulk composition on the solidus of carbonated eclogite from partial melting experiments at 3 GPa // *Contributions to Mineralogy and Petrology*. - 2005. - V. 149. - № 3. - P. 288-305.
- Dasgupta R. and Hirschmann M.M. Effect of variable carbonate concentration on the solidus of mantle peridotite // *American Mineralogist*. - 2007. - V. 92. - № 2-3. - P. 370-379.
- Dickens B., Hyman A. and Brown W.E. Crystal structure of $\text{Ca}_2\text{Na}_2(\text{CO}_3)_3$ (shortite) // *Journal of Research of the National Bureau of Standards Section A-Physics and Chemistry*. - 1971. - V. A 75. - № 2. - P. 129-140.
- Dusek M., Chapuis G., Meyer M. and Petricek V. Sodium carbonate revisited // *Acta Crystallographica Section B-Structural Science*. - 2003. - V. 59. - № - P. 337-352.
- Gavryushkin P.N., Bakakin V.V., Bolotina N.B., Shatskiy A.F., Seryotkin Y.V. and Litasov K.D. Synthesis and crystal structure of new carbonate $\text{Ca}_3\text{Na}_2(\text{CO}_3)_4$ homeotypic with orthoborates $\text{M}_3\text{Ln}_2(\text{BO}_3)_4$ (M = Ca, Sr, and Ba) // *Crystal Growth & Design*. - 2014. - V. 14. - № 9. - P. 4610-4616.
- Gavryushkin P.N., Thomas V.G., Bolotina N.B., Bakakin V.V., Golovin A.V., Seryotkin Y.V., Fursenko D.A. and Litasov K.D. Hydrothermal synthesis and structure solution of $\text{Na}_2\text{Ca}(\text{CO}_3)_2$: "Synthetic Analogue" of Mineral Nyererite // *Crystal Growth & Design*. - 2016. - V. 16. - № 4. - P. 1893-1902.
- Giuliani A., Kamenetsky V.S., Phillips D., Kendrick M.A., Wyatt B.A. and Goemann K. Nature of alkali-carbonate fluids in the sub-continental lithospheric mantle // *Geology*. - 2012. - V. 40. - № 11. - P. 967-970.

Golovin A., Sharygin I., Kamenetsky V., Korsakov A. and Yaxley G. Alkali-carbonate melts from the base of cratonic lithospheric mantle: links to kimberlites // *Chemical Geology*. - 2018. - V. 483. - № 4. - P. 261-274.

Golovin A.V., Sharygin V.V. and Pokhilenko N.P. Melt inclusions in olivine phenocrysts in unaltered kimberlites from the Udachnaya-East pipe, Yakutia: Some aspects of kimberlite magma evolution during late crystallization stages // *Petrology*. - 2007. - V. 15. - № 2. - P. 168-183.

Golovin A.V., Sharygin I.S. and Korsakov A.V. Origin of alkaline carbonates in kimberlites of the Siberian craton: Evidence from melt inclusions in mantle olivine of the Udachnaya-East pipe // *Chemical Geology*. - 2017. - V. 455. - № - P. 357-375.

Kamenetsky M.B., Sobolev A.V., Kamenetsky V.S., Maas R., Danyushevsky L.V., Thomas R., Pokhilenko N.P. and Sobolev N.V. Kimberlite melts rich in alkali chlorides and carbonates: A potent metasomatic agent in the mantle // *Geology*. - 2004. - V. 32. - № 10. - P. 845-848.

Kamenetsky V.S., Kamenetsky M.B., Weiss Y., Navon O., Nielsen T.F.D. and Mernagh T.P. How unique is the Udachnaya-East kimberlite? Comparison with kimberlites from the Slave Craton (Canada) and SW Greenland // *Lithos*. - 2009. - V. 112. - № - P. 334-346.

Kaminsky F., Wirth R., Matsyuk S., Schreiber A. and Thomas R. Nyerereite and nahcolite inclusions in diamond: evidence for lower-mantle carbonatitic magmas // *Mineralogical Magazine*. - 2009. - V. 73. - № 5. - P. 797-816.

Li Z., Li J., Lange R., Liu J. and Militzer B. Determination of calcium carbonate and sodium carbonate melting curves up to Earth's transition zone pressures with implications for the deep carbon cycle // *Earth and Planetary Science Letters*. - 2017. - V. 457. - № - P. 395-402.

Litasov K.D., Shatskiy A., Ohtani E. and Yaxley G.M. The solidus of alkaline carbonatite in the deep mantle // *Geology*. - 2013. - V. 41. - № 1. - P. 79-82.

Podborodnikov I.V., Shatskiy A., Arefiev A.V., Rashchenko S.V., Chanyshv A.D. and Litasov K.D. The system $\text{Na}_2\text{CO}_3\text{-CaCO}_3$ at 3 GPa // *Physics and Chemistry of Minerals*. - 2018. - V. - № - P. DOI: 10.1007/s00269-018-0961-2.

Rashchenko S.V., Bakakin V.V., Shatskiy A.F., Gavryushkin P.N., Seryotkin Y.V. and Litasov K.D. Noncentrosymmetric $\text{Na}_2\text{Ca}_4(\text{CO}_3)_3$ carbonate of "M1₃M2₃XY₃Z" structural type and affinity between borate and carbonate structures for design of new optical materials // *Crystal Growth & Design*. - 2017. - V. 17. - № 11. - P. 6079-6084.

Rashchenko S.V., Shatskiy A.F., Seryotkin Y.V. and Litasov K.D. $\text{Na}_4\text{Ca}(\text{CO}_3)_3$ and carbonate analogs of borate optical materials // *Crystal Growth & Design*. - 2018. - V. Under review. - № -

Shatskiy A., Sharygin I.S., Litasov K.D., Borzdov Y.M., Palyanov Y.N. and Ohtani E. New experimental data on phase relations for the system $\text{Na}_2\text{CO}_3\text{-CaCO}_3$ at 6 GPa and 900-1400 °C // *American Mineralogist*. - 2013. - V. 98. - № 11-12. - P. 2164-2171.

Shatskiy A., Podborodnikov I.V., Arefiev A.V., Minin D.A., Chanyshv A.D. and Litasov K.D. Revision of the $\text{CaCO}_3\text{-MgCO}_3$ phase diagram at 3 and 6 GPa // *American Mineralogist*. - 2018. - V. 103. - № 3. - P. 441-452.

Thomson A.R., Walter M.J., Kohn S.C. and Brooker R.A. Slab melting as a barrier to deep carbon subduction // *Nature*. - 2016. - V. 529. - № - P. 76-79.

Shatskiy A.F.^{1,2}, Litasov K.D.^{1,2} Experimental view on mineral inclusions of "mixed" paragenesis in diamonds UDC 551.14:544.015.4

¹V.S. Sobolev Institute of Geology and Mineralogy SB RAS, Novosibirsk,

²Novosibirsk State University, Novosibirsk (shatskiy@igm.nsc.ru, klitasov@igm.nsc.ru)

Abstract. The natural diamonds could be formed during reduction of carbonate-silicate melts, which can be derived by partial melting of carbonated eclogites in subducted slabs. The partial reduction of these melts should cause precipitation of silicate solutes simultaneously with diamond. Decreasing of the bulk CO_2 content, which accompanies reduction, changes the mineral assemblage co-precipitating with diamond in following sequence: eclogite (Coe + Cpx + Grt) → pyroxenite (Cpx + Opx + Grt) → lherzolite (Ol + Opx + Cpx + Grt) → wehrlite (Ol + Cpx + Grt). This would explain the formation of diamonds from group A eclogite with mineral inclusions of "mixed" paragenesis, where two-phase coesite + clinopyroxene ($\text{Jd}_{7}\text{Di}_{85}\text{En}_5\text{Fs}_3$) inclusions and garnet ($\text{Prp}_{74}\text{Alm}_{17}\text{Grs}_9$) inclusions are located at the central zone and olivine (Fo_{93}) inclusions are much closer to periphery. In our study clinopyroxene with close composition ($\text{Jd}_{10}\text{Di}_{83}\text{En}_3\text{Fs}_4$) was observed in coexistence with coesite at bulk CO_2 content of 15 wt%, whereas olivine appears at bulk CO_2 content of 15–23 wt%.

Keywords: diamond; mixed paragenesis; high-pressure; multianvil apparatus; Earth's mantle

Two diamond paragenesis, eclogitic and peridotitic, were distinguished based on the study of mineral inclusions in kimberlitic diamonds (Sobolev, 1977). According to current concept (Palyanov et al., 2013), lithospheric diamonds were crystallized from essentially carbonate melts during their partial reduction. These melts acted both as a carbon source and a solvent-catalyst lowering kinetic barrier of diamond formation. The essentially carbonate melts could be derived by partial melting of carbonated eclogites subducted down to the mantle transition zone (Thomson et al., 2016). Alternatively, such melts could be generated by means of redox melting in the upwelling mantle domains at depth of 660 km, where iron disproportionation reaction occurs resulting in carbon oxidation and carbonate formation (Stagno et al., 2013).

Experimental reconstruction of the composition of the deepest known melts (kimberlites) (Shatskiy et al., 2017) has shown that the liquid coexisting with garnet lherzolite mineral assemblage in the mantle source region contains (mol%): $\text{SiO}_2 = 9$, $\text{FeO} = 6\text{--}7$, $\text{MgO} = 23\text{--}26$, $\text{CaO} = 16$, $\text{Na}_2\text{O} = 4$, $\text{K}_2\text{O} = 1$, and $\text{CO}_2 = 30\text{--}35$ suggesting essentially carbonatitic composition of primary kimberlite melt similar to that of kimberlite-associated diamondiferous magnesiocarbonatites (Agashev et al., 2008) in terms of $\text{CaO}\text{-MgO}\text{-FeO}\text{-SiO}_2\text{-CO}_2$ system.

It was argued that the precursor kimberlite melt (i.e., alkali-rich carbonatite melt) can represent a liquid component of thermochemical plumes, which were more oxidized than ambient mantle and depleted cratonic roots (Sharygin et al., 2015) (Fig. 1). Infiltration of such melts in the base of subcontinental lithospheric mantle should cause partial reduction of carbonate component resulting in carbon precipitation.

Mineral equilibria at high PT-parameters

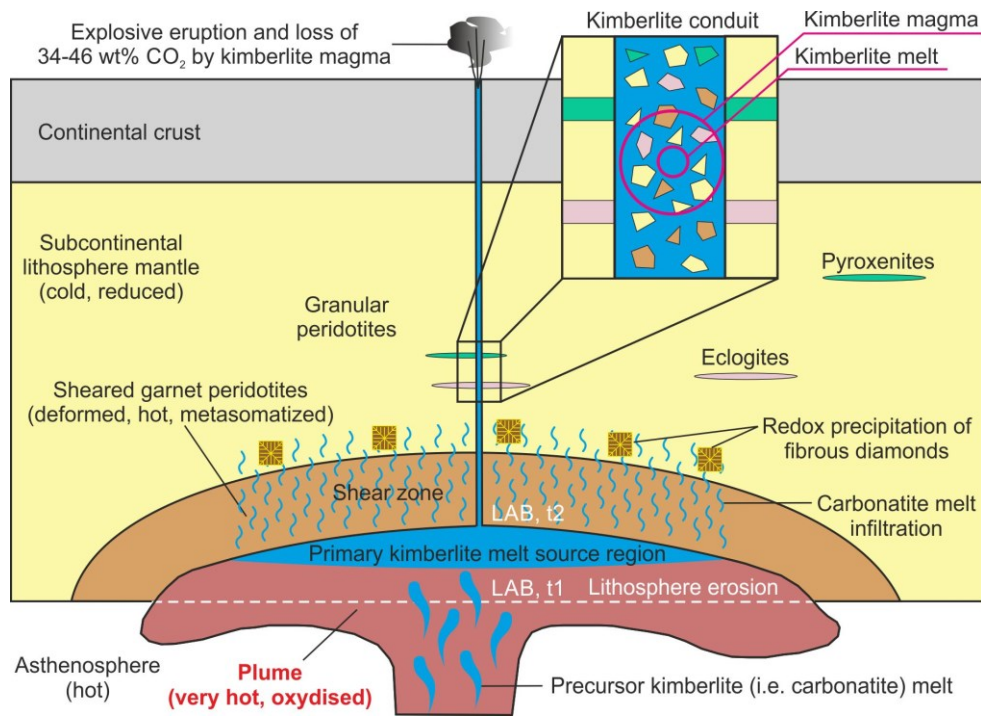


Figure 1. Schematic diagram illustrating kimberlite origin and its relation to the plume–subcontinental lithosphere mantle (SCLM) interaction and fibrous diamond genesis. Precursor kimberlite (i.e., carbonatite) melt of a deeper origin accumulates at the plume head. Plume head meets the cratonic root and creates shear zone at the base of SCLM. Carbonatite melt together with plume heat promotes thermo-mechanical erosion of lithosphere shifting up the lithosphere–asthenosphere boundary. The primary kimberlite melt was in equilibrium with the four-phase peridotitic mineral assemblage prior to its violent ascent. Kimberlite/carbonatite melt percolated through shear zone causes metasomatic modifications depleted mantle rocks (granular peridotites). Since only the base of SCLM is cold enough to retain diamonds, the partial reduction of kimberlite/carbonatite melt infiltrated into SCLM should cause precipitation of diamonds. Our experimental results suggest that the primary kimberlite melt was alkali-rich carbonatitic in composition, whereas the kimberlite magma was a mixture of this melt and mantle xenogenic material. Peridotites are predominant among the mantle xenoliths and represent accidental inclusions of mantle rocks plucked from the magmatic conduit. An abundance of mantle xenogenic material (≥ 35 wt%) and loss of substantial amount of CO_2 (34–46%) by kimberlite magma resulted in a significant difference in compositions of kimberlite rock (carbonate-bearing ultramafic) and primary kimberlite melt (alkali-rich carbonatitic) (Shatskiy et al., 2017).

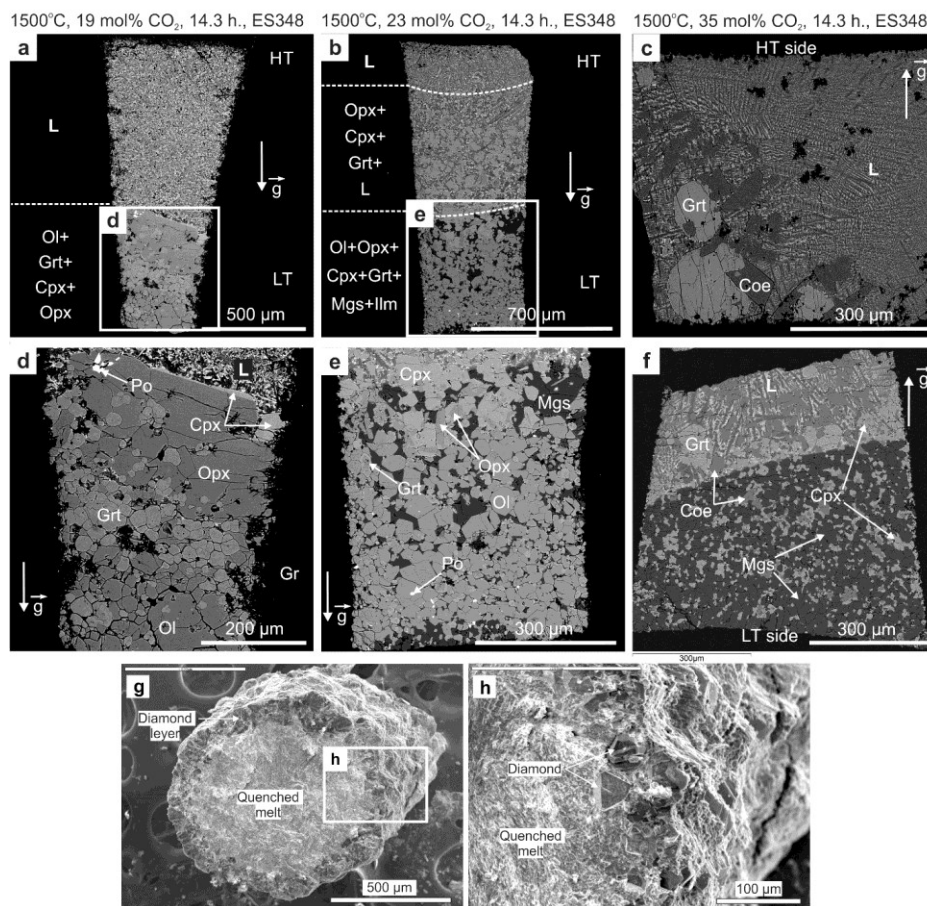


Figure 2. Back-scattered electron (a–f) images of run products recovered from Udachnaya-East kimberlite melting experiments at pressure of 6.5 GPa and temperature of 1500 °C and bulk CO_2 contents of 19 mol% (a, d), 23 mol% (b, e), 35 mol% (c, f). (a–c) General view of sample cross-sections with carbonatite melts pool (L) at high-temperature side (HT) and residual minerals at lower temperature side (LT). g – Gravity vector; OI – olivine; Opx – orthopyroxene; Cpx – clinopyroxene; Grt – garnet; Coe – coesite; Mgs – magnesite; Ilm – picroilmenite; Rt – rutile; Po – pyrrhotite; Gr – graphite. (g, h) Scanning electron micrographs of diamond-containing UEK sample with bulk CO_2 of 31 mol% (27 wt%) annealed at 1600 °C and 6.5 GPa for 5.5 h. (a) General view and (b) close view. Diamond crystals formed at the partial melt-graphite capsule interface. The layer of polycrystalline diamond formed at the partial melt-graphite capsule interface.

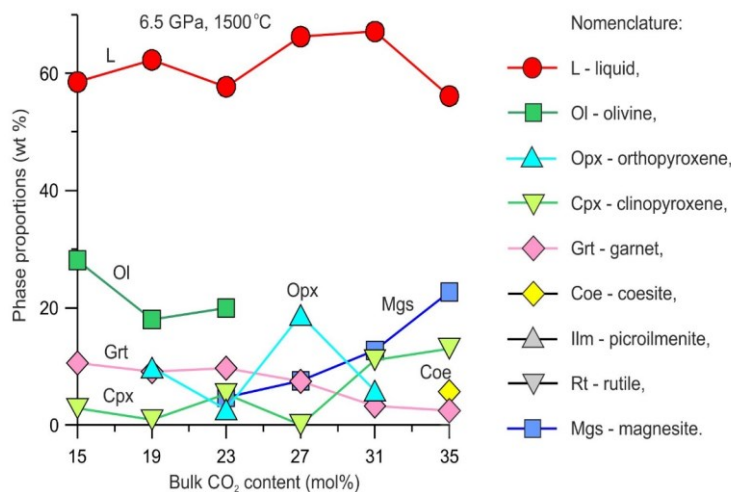


Figure 3. Modal proportions of phases in kimberlite melting experiments at 6.5 GPa pressure and temperature of 1500 °C. Modes were determined from the bulk compositions and phase compositions measured by electron microprobe.

Under high-pressures (> 3 GPa) most of carbonate-silicate systems have $T-X$ phase diagrams with eutectic shifted to carbonate component (Lee et al., 2000). Thus, under mantle pressures carbonate melts act as a solvent for refractory silicate minerals. Partial reduction of carbonate component of carbonate-silicate melt during its interaction with reduced iron saturated ambient mantle decreases the amount of solvent. As a result, carbonate-silicate melts become saturated with silicate minerals. Thus, diamond crystallization should be accompanied by nucleation and growth of silicate minerals.

Experimental results at 6.5 GPa and 1500 °C (Shatskiy et al., 2017) suggest that the decreasing bulk CO_2 , which accompanies reduction, changes the mineral assemblage co-precipitating with diamond in following sequence: eclogite (Coe + Cpx + Grt) → pyroxenite (Cpx + Opx + Grt) → lherzolite (Ol + Opx + Cpx + Grt) → wehrlite (Ol + Cpx + Grt). This would explain the formation of diamonds from group A eclogite (Shatskiy et al., 2008) with mineral inclusions of “mixed” paragenesis, where two-phase coesite + clinopyroxene ($\text{Jd}_{7}\text{Di}_{85}\text{En}_{5}\text{Fs}_{3}$) inclusions and garnet ($\text{Prp}_{74}\text{Alm}_{17}\text{Grs}_{9}$) inclusions are located at the central zone and olivine (Fo_{93}) inclusions are much closer to periphery (Ragozin et al., 2006). Shatskiy et al. (2017) observed clinopyroxene with close composition ($\text{Jd}_{10}\text{Di}_{83}\text{En}_{3}\text{Fs}_{4}$) in coexistence with coesite at bulk CO_2 of 31 wt%, whereas olivine appears at bulk CO_2 of 15–23 wt%. (Fig. 2 and 3).

Thus, successive decrease of bulk CO_2 during reduction of carbonate-silicate melt should change assemblage of minerals co-precipitating with diamond, from coesite-bearing eclogitic toward olivine-bearing peridotitic.

the geochemistry of kimberlite-carbonatite assemblages, Snap Lake dyke system, Canada // *Chemical Geology*. – 2008. – V.255. – P.317-328.

Lee W.J., Huang W.L., Wyllie P. Melts in the mantle modeled in the system $\text{CaO-MgO-SiO}_2\text{-CO}_2$ at 2.7 GPa // *Contributions to Mineralogy and Petrology*. – 2000. – V.138. – P.199-213.

Palyanov Y.N., Bataleva Y.V., Sokol A.G., Borzdov Y.M., Kupriyanov I.N., Reutsky V.N., Sobolev, N.V. Mantle–slab interaction and redox mechanism of diamond formation // *Proceedings of the National Academy of Sciences*. – 2013. – V.110. – P.20408-20413.

Ragozin A., Shatskiy V., Zetgenizov D., Mityukhin S. Evidence for evolution of diamond crystallization medium in eclogite xenolith from the Udachnaya kimberlite pipe, Yakutia // *Doklady Earth Sciences*. – 2006. – V.407. – P.465-468.

Sharygin I., Litasov K., Shatskiy A., Golovin A., Ohtani E., Pokhilenko N. Melting phase relations of the Udachnaya-East group-I kimberlite at 3.0-6.5 GPa: experimental evidence for alkali-carbonatite composition of primary kimberlite melts and implications for mantle plumes // *Gondwana Research*. – 2015. – V.28. – P.1391-1414.

Shatskiy A., Litasov K.D., Sharygin I.S., Ohtani E. Composition of primary kimberlite melt in a garnet lherzolite mantle source: constraints from melting phase relations in anhydrous Udachnaya-East kimberlite with variable CO_2 content at 6.5 GPa // *Gondwana Research*. – 2017. – V.45. – P.208-227.

Shatskiy V., Ragozin A., Zedgenizov D., and Mityukhin S. Evidence for multistage evolution in a xenolith of diamond-bearing eclogite from the Udachnaya kimberlite pipe // *Lithos*. – 2008. – V.105. – P.289-300.

Stagno V., Ojwang D.O., McCammon C.A., Frost D.J. The oxidation state of the mantle and the extraction of carbon from Earth’s interior // *Nature*. – 2013. – V.493. – P.84.

Thomson A.R., Walter M.J., Kohn S.C., Brooker R.A. Slab melting as a barrier to deep carbon subduction // *Nature*. – 2016. – V.529. – P.76-79.

Sobolev N.V. Deep seated inclusions in kimberlites and the problem of the composition of the upper mantle // *American Geophysical Union, Washington, D.C.* – 1977.

Spivak A.V.¹, Litvin Y.A.¹, Zakharchenko E.S.¹, Dubrovinsky L.S.² Peritectic decomposition of ringwoodite (Mg, Fe) $_2\text{SiO}_4$ with the formation of stishovite within the transition zone of the mantle (experiment at 20 GPa)

¹Institute of Experimental Mineralogy (IEM RAS), (spivak@iem.ac.ru)

The work was supported by the state assignment project no. 0330-2016-0006.

References:

Agashev A.M., Pokhilenko, N.R., Takazawa, E., McDonald, J.A., Vavilov, M.A., Watanabe, I., Sobolev, N.V. Primary melting sequence of a deep (> 250 km) lithospheric mantle as recorded in

Mineral equilibria at high PT-parameters

² Bavarian Research Institute of Experimental Geochemistry and Geophysics (BGI) University of Bayreuth

Abstract. Experimental studies of phase relations of the diamond-forming system MgO-FeO-SiO₂-Carb* - C [where Carb* = (Na,Ca,K)CO₃] were carried out in its polythermal section (Mg₂SiO₄ + Carb*) - (2FeO-SiO₂ + Carb*) at 20 GPa. In the region of high-iron compositions with Mg₂SiO₄ contents in the range 5-25 wt. %, the peritectic reaction of ringwoodite (Mg,Fe)₂SiO₄ and silicate-carbonate melt was established with the formation of magnesiowustite (Fe,Mg)O, stishovite SiO₂ and carbonate phases of Na, Ca and K. A reaction with formation of Ca-perovskite CaSiO₃ was also realized.

Keywords: substance of the transition zone of the mantle, magmatic evolution, stishovite paradox, parental melts-solutions, carbonatite parental medium, fractional ultrabasic-basite evolution, physico-chemical experiment.

Ringwoodite (Mg,Fe)₂SiO₄ has provided evidences as the main ultrabasic phase of the transition zone of the mantle within depths 400 – 660 km (19 – 24 GPa). Ringwoodites was identified in diamonds only as paragenetic inclusions. Basic stishovite is also discovered among inclusions in diamonds. This is a feature of ultrabasic to basic evolution of both, diamondiferous silicate-carbonate-carbon melts and derivate silicate magmas of the transition zone (Spivak, Litvin, 2018). Mineralogical researching data of syngenetic inclusions in diamonds, which genesis is connected with related horizons of the Earth mantle, have the main importance at estimating of base chemical and phase composition of diamond forming media of the mantle transition zone. The major minerals in inclusions in diamonds formed at depths of the transition zone of the mantle are presented with wadsleite and ringwoodite (high pressure polymorphic species of olivine composition) and majoritic garnet, as well as oxides – magnesiowustite (Fe,Mg)O and stishovite SiO₂, and carbonates of Na, Mg, Fe, Ca and K (Kaminsky, 2012). By mineralogical data, ultrabasic and basic oxide-silicate and carbonatite associations arranged as derivated material of the lower mantle.

The main primary minerals in inclusions in deep diamonds coincide in modal terms with experimentally proved rock forming mantle minerals at related depths (Akaogi, 2007). Experimental studies of subsolidus reactions in the system Mg₂SiO₄ – Fe₂SiO₄ (Ito, Takahashi, 1989) revealed for PT conditions of ringwoodite stability that iron component is unstable and disproportionates to stishovite and wustite. This is a reason for formation of two stishovite containing subsolidus associations: (1) ringwoodite (Mg,Fe)₂SiO₄ + stishovite SiO₂ + ferropericlae-magnesiowustite solid solutions (MgO/FeO ↔ FeO/MgO) and (2) magnesiowustite (Fe,Mg)O + stishovite SiO₂. However, data on phase relations at subsolidus conditions do not reveal physico-chemical mechanism of a formation of the associations.

The main goal of the work is in experimental evidence of the physico-chemical mechanism of decomposition of ringwoodite with a formation of a stable association of stishovite and phases of solid solutions periclae-wustite as a result of ultrabasic-basic evolution at conditions within the Earth transition zone.

Experimental studies of melting phase relations were carried out at 20 GPa, that corresponds to conditions of ringwoodite stability (it is stable within 18-24 GPa at depths 520-660 km). The experiments were done using high pressure-high temperature cubic apparatus multianvil press at 20 GPa and 1000 – 1700°C at BGI, University of Bayreuth, Germany. There was used a standard cell 7/3 with heater made of lanthan chromite LaCrO₃ and a capsule made of Pt or Re foil for researching substances in experiments. The method of high-velocity quenching of samples was applied. Accuracies at pressure and temperature measurements are estimated as ± 0.5 GPa и ± 50°C, correspondingly. A complete describing of methodical features and experimental procedures is in work (Frost at al., 2004). Experimental conditions and results are in table 1.

Table 1. Conditions and results of representative experiments on studying of system MgO – FeO – SiO₂ – (Na,Ca,K)CO₃ at 20 GPa

| № sample | T, °C | t, min | Experimental results | | | | | | | | |
|---|-------|--------|----------------------|------------------|-------|-------|-------|-------------------|------------------|-------------------|--------|
| | | | Phase | SiO ₂ | FeO | MgO | CaO | Na ₂ O | K ₂ O | CO ₂ * | Sum |
| | | | | wt. % | | | | | | | |
| I - (Fe₂SiO₄)_{52.5}(Mg₂SiO₄)_{17.5}(Carb*)₃₀ | | | | | | | | | | | |
| S6873-1 | 1700 | 30 | L | 10.47 | 9.79 | 8.70 | 18.57 | 18.69 | 12.47 | 21.32 | 100.00 |
| | | | Rwd | 34.42 | 34.73 | 27.02 | 1.55 | 0.95 | 1.32 | - | 99.99 |
| S6880-1 | 1500 | 20 | L | 7.26 | 10.63 | 11.64 | 11.97 | 6.16 | 8.80 | 43.54 | 100.00 |
| | | | Rwd | 33.12 | 35.20 | 25.39 | 2.45 | 1.64 | 2.19 | - | 99.98 |
| | | | MWus | 0.49 | 87.47 | 5.50 | 2.25 | 2.55 | 1.73 | - | 99.98 |
| | | | Sti | 98.15 | 1.27 | n.d. | 0.14 | n.d. | n.d. | - | 99.56 |
| S6877-1 | 1200 | 40 | L | 12.64 | 5.40 | 7.79 | 18.33 | 9.32 | 12.72 | 33.52 | 100.00 |
| | | | Rwd | 31.85 | 21.01 | 35.39 | 4.75 | 2.76 | 4.20 | - | 99.96 |
| | | | MWus | 0.55 | 92.68 | 5.33 | 0.49 | 0.23 | 0.32 | - | 99.84 |
| | | | Sti | 95.93 | 1.82 | 0.29 | 0.84 | 0.63 | 0.47 | - | 99.99 |

| № sample | T, °C | t,min | Experimental results | | | | | | | | |
|---|-------|-------|----------------------|------------------|-------|-------|-------|-------------------|------------------|-------------------|--------|
| | | | Phase | SiO ₂ | FeO | MgO | CaO | Na ₂ O | K ₂ O | CO ₂ * | Sum |
| | | | | wt. % | | | | | | | |
| | | | CaPrv | 48.57 | 1.64 | 0.55 | 46.32 | 0.92 | 1.79 | - | 99.97 |
| | | | Mgs | 0.43 | 2.40 | 40.27 | 0.35 | 0.16 | 0.22 | 56.00 | 100.00 |
| | | | K-Arg | 0.73 | 1.43 | 6.72 | 12.27 | 5.31 | 17.82 | 55.69 | 100.00 |
| S6886-1 | 1000 | 60 | MWus | 2.93 | 87.49 | 2.79 | 1.36 | 2.08 | 3.35 | - | 99.99 |
| | | | Sti | 93.12 | 1.20 | 1.16 | 1.14 | 1.61 | 1.77 | - | 99.98 |
| | | | CaPrv | 48.70 | 1.27 | 0.24 | 46.26 | 0.99 | 2.13 | - | 99.59 |
| | | | Mgs | 1.81 | 3.27 | 42.25 | 0.90 | 1.18 | 1.69 | 48.91 | 100.00 |
| | | | Na,K-Arg | 1.44 | 1.68 | 1.03 | 20.21 | 9.59 | 8.57 | 57.48 | 100.00 |
| II - (Fe₂SiO₄)_{66.5}(Mg₂SiO₄)_{3.5}(Carb*)₃₀ | | | | | | | | | | | |
| S6873-2 | 1700 | 30 | L | 11.66 | 18.62 | 1.94 | 10.26 | 6.66 | 8.89 | 41.85 | 100.00 |
| | | | MWus | 0.82 | 97.43 | 1.13 | 0.22 | 0.34 | n.d. | - | 99.95 |
| | | | Sti | 98.43 | 1.39 | n.d. | n.d. | n.d. | n.d. | - | 99.82 |
| S6875-2 | 1400 | 10 | L | 3.19 | 5.74 | 2.89 | 19.62 | 9.58 | 11.72 | 47.26 | 100.00 |
| | | | MWus | 0.44 | 98.15 | 0.98 | 0.15 | 0.26 | n.d. | - | 99.98 |
| | | | Sti | 96.92 | 2.28 | n.d. | 0.36 | 0.15 | 0.21 | - | 99.92 |
| S6877-2 | 1200 | 40 | L | 11.28 | 4.39 | 3.44 | 17.12 | 6.00 | 10.69 | 47.08 | 100.00 |
| | | | MWus | 0.50 | 97.26 | 1.46 | 0.39 | 0.16 | 0.17 | - | 99.98 |
| | | | Sti | 95.27 | 1.29 | 0.32 | 1.39 | 0.85 | 0.87 | - | 99.99 |
| | | | K-Cal | 0.74 | 3.45 | 3.01 | 21.20 | 9.49 | 13.53 | 48.59 | 100.00 |
| S6886-2 | 1000 | 60 | MWus | 0.62 | 92.06 | 0.79 | 0.20 | 1.05 | 0.41 | - | 99.99 |
| | | | Sti | 97.88 | 1.06 | 0.33 | 0.18 | n.d. | 0.53 | - | 99.99 |
| | | | Mag | n.d. | 4.83 | 36.94 | 7.33 | 1.10 | 3.60 | 46.21 | 100.00 |
| | | | K-Cal | 0.58 | 0.89 | 0.20 | 38.67 | 3.04 | 14.62 | 42.01 | 100.00 |
| | | | Na, K-Cal | 0.95 | 1.13 | 0.64 | 19.51 | 15.72 | 12.18 | 49.87 | 100.00 |

Phase relations of diamond forming oxide-silicate-carbonate system MgO – FeO - SiO₂ - (Na,Ca,K)CO₃ are the most interesting in point of diamond genesis.

Model fusible composition Na₂CO₃-CaCO₃-K₂CO₃ (cation part of oxide-silicate components doesn't repeat) was used as carbonate component. Homogenized gel mixtures Mg₂SiO₄, Fe₂SiO₄ and carbonates CaCO₃, Na₂CO₃ и K₂CO₃ of boundary compositions of binary polythermal section (Mg₂SiO₄)₇₀(Carb*)₃₀ – (Fe₂SiO₄)₇₀(Carb*)₃₀, where Carb* - CaCO₃ 34, Na₂CO₃ 33, K₂CO₃ 33 (wt %) were derivate materials for starting compositions. Two experimental compositions were used: I - Mg₂SiO₄ 17,5; Fe₂SiO₄ 52,5; CaCO₃ 10,2; Na₂CO₃ 9,9; K₂CO₃ 9,9 (wt %) and II – Mg₂SiO₄ 3,5; Fe₂SiO₄ 66,5; CaCO₃ 10,2; Na₂CO₃ 9,9; K₂CO₃ 9,9 (wt %). Experimental samples were investigated by scanning electron microscope CamScanM2300 (VEGA TS 5130MM) with spectral analyzer Link INCA at Institute of Experimental Mineralogy RAS.

Experimental (at 20 GPa) and theoretical studies of liquidus phase relations in system ringwoodite Rw (Mg₂SiO₄) – iron component (2FeO·SiO₂) were carried out with an emphasis on physico-chemical behavior of its silicate components, especially within an area of high content of iron components. It should be accentuated that system Mg₂SiO₄ – 2FeO·SiO₂ represents a polythermal section of a key importance for rock forming system of derivate substance of the transition zone of the Earth mantle at conditions of

ringwoodite stability (within 18 – 24 GPa at depths 520-660 km), whereas iron component Fe₂SiO₄ is unstable at the conditions and decomposes into 2FeO+SiO₂.

In results of carried out works we have received experimental samples, that we can trace the following chains of crystallization of studied carbonate-silicate systems by: for composition I - L + Rwd → L+Rwd+Sti+MWus → L+Rwd+Sti+MWus+Carb*+CaPrv → Sti+MWus+Carb*+CaPrv; for composition II - L+Sti+MWus → L+Sti+MWus+Carb* → Sti+MWus+Carb*+CaPrv (table 1). They lead to a formation of basic paragenesis containing stishovite at subsolidus conditions. Oxide-silicate-carbonate melts are completely miscible at melting of multicomponent oxide-silicate-carbonate diamond-forming system, herewith high solubility ultrabasic minerals as well as basic ones is provided. Lower melting temperatures of diamond forming multicomponent compositions relatively to geothermal values are substantially more significant. For example, there observed a partial melting of both starting compositions at 1200 °C. As both starting compositions are enriched in iron component, magnesiowustite is a prevailing mineral in each experimental samples (excluding sample S6873-1). Magnesiowustites of I series contain MgO upto 6.51 wt%, on an average 4.10 wt%, II series – on the average 0.99 wt% up to 2.11 wt %.

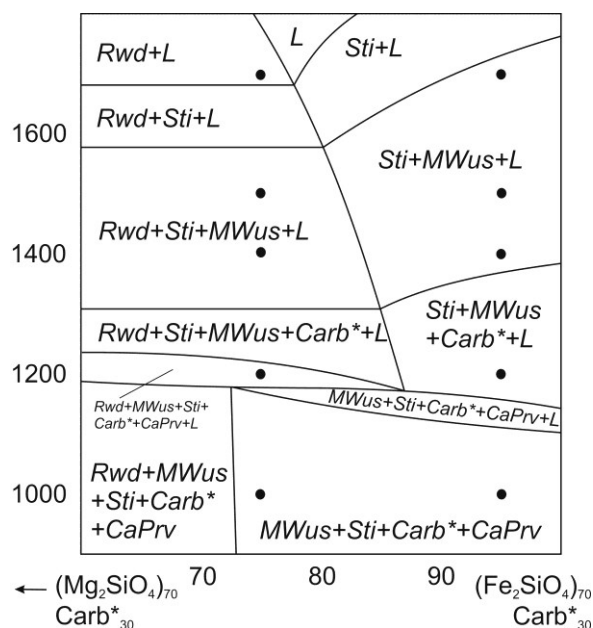


Fig. 1. Melting phase relations at polythermal section $(\text{Mg}_2\text{SiO}_4)_{70}\text{Carb}^*_{30} - (2\text{FeO}\cdot\text{SiO}_2)_{70}\text{Carb}^*_{30}$ at 20 GPa. Experimental conditions are marked by black circles. Symbols: *L* - melt; *Rwd* - ringwoodite; *MWus* - magnesiowustite; *CaPrv* - Ca-perovskite; *Sti* - stishovite; *Carb** - simplified simbol for carbonates (see text).

Ringwoodite crystals are observed in experiments with I starting composition at conditions of a partial melting. The starting compositions enriched in iron component influences mg# of ringwoodite (0.39 – 0.66). Stishovite is revealed in experimental samples in association with magnesiowustite. Ca-perovskite forms in result of a reaction of Ca-carbonate with silicate component of the system at temperatures of 1200 and 1000°C. On the experimental plane, the problem of ultrabasic to basic evolution of mantle and diamond forming melts acquired an actual value when its investigations in physico-chemical experiments with multicomponent multiphase deep substance of reproduced at boundary conditions composition became possible. So, at conditions of the lower mantle ultrabasic to basic evolution of mantle and diamond forming melts is controlled by peritectic reaction “brigemanite+melt = magnesiowustite + stishovite (Litvin, Spivak, 2017), that provides a continuously ultrabasic to basic evolution of melts at fractional crystallization regime.

The experimental researches reveal melting phase relations along polythermal section $(\text{Mg}_2\text{SiO}_4)_{70}\text{Carb}^*_{30} - (\text{Fe}_2\text{SiO}_4)_{70}\text{Carb}^*_{30}$ (fig. 1) of diamond forming system at 20 GPa, as well as peritectic reaction of ringwoodite with carbonate-containing melt, that basic association of stishovite, magnesiowustite, and carbonates forms in results of. In this case the peritectic reaction (*P*) is represented as $L + \text{ringwoodite } Rwd + \text{magnesiowustite } MWus + \text{stishovite } Sti + \text{Ca-perovskite } CaPrv + \text{carbonate minerals } Carb^*$.

The base peritectic reaction for derivate mantle system $\text{Mg}_2\text{SiO}_4 - \text{Fe}_2\text{SiO}_4$ would be look like: $L + Rwd = Sti + MWus$ with a loss of ringwoodite (“stishovite paradox” effect). There are liquidus *Rwd*, *Sti*, and subsolidus phases, as well as subsolidus associations $Rwd + MWus + Carb^* + CaPrv$, $MWus + Sti + Carb^* + CaPrv$ demonstrate ultrabasic to basic conversion of phase relations on figure 1, metasomatic interaction of Ca-carbonate component of the researched system and silicate ones with CaSiO_3 formation is also noted. Generally, received experimental results are in agreement with natural data for primary inclusions in diamonds of the transition zone.

The work is supported by grants of RFBR 16-05-00850 and MD-3464.2017.5, as well as program of the RAS I.II.08.

References:

Akaogi M. Phase transformations of minerals in the transition zone and upper part of the lower mantle / Advances in High-Pressure Mineralogy [Ohtani E., ed.]: Geol. Soc. Amer. Spec. Pap. – 2007. – 421. – P. 1-13.
 Frost D.J., Poe B.T., Tronnes R.G., Libscke C., Duba F., Rubie D.C. A new large-volume multianvil system // Phys. Earth Planet. Inter. – 2004. – 143. – P. 507-514.
 Ito E., Takahashi E. Postspinel transformations in the system $\text{Mg}_2\text{SiO}_4\text{-Fe}_2\text{SiO}_4$ and some geophysical implications // Journal of Geophysical Research. – 1989. – 94 (B8). – P. 10637– 10646.
 Kaminsky F. Mineralogy of the lower mantle: a review of ‘super-deep’ mineral inclusions in diamond // Earth Sci. Rev. – 2012. – 110. – P. 127-147.
 Anna Spivak and Yuriy Litvin. Evolution of Magmatic and Diamond-Forming Systems of the Earth's Lower Mantle. –Springer, 2018. – 95p.
 Litvin Yu.A., Spivak A.V., Simonova D.A., Dubrovskiy L.S. The stishovite paradox in the evolution of lower mantle magmas and diamond-forming melts (experiments at 24 and 26 GPa) // Doclady Earth Sciences . – 2017. – 473(2). – P. 444-448.

Spivak A.V.¹, Zakharchenko E.S.¹, Limanov E.V.¹, Bulatov K.M.², Bykov A.A.³, Ismailova L.S.⁴, Zinin P.V.², Safonov O.G.¹, Litvin Yu.A.¹ Investigation at 25 - 45 GPa of solid solutions of the lowermantle ferrobridgmanite $(\text{Mg,Fe})\text{SiO}_3$ in a diamond anvil cell with laser heating UDC 552.113, 552.18

¹Institute of experimental mineralogy of the Russian Academy of Sciences (IEM RAS), (spivak@iem.ac.ru)

²Scientific and Technological Center of Unique Instrumentation of the Russian Academy of Sciences (STC UI RAS),

³National Research University "Moscow Power Engineering Institute",

⁴Autonomic noncommercial organization of high education «The Skolkovo Institute of Science and Technology»

Abstract. We report Raman spectroscopic and microprobe studies of solid solutions of $\text{MgSiO}_3\text{-FeSiO}_3$ system obtained

in DAC with laser heating at 25–40 GPa. The studies are aimed on determining the solubility limit of iron component of FeSiO_3 in ferrobridgmanite, when a peritectic reaction must be initiated.

Keywords: Bridgmanite, ferrobridgmanite, lower mantle, ultrabasic-basic evolution, peritectic reaction, physical and chemical experiment, high pressures, diamond anvil cell, laser heating

Bridgmanite $(\text{Mg,Fe})\text{SiO}_3$ with a structure of perovskite (Tschauner, et al 2014) is justified as one among the main lower mantle minerals at depths over 660 km (>24 GPa) (Ringwood, 1975). It also occurs in paragenetic inclusions in lower mantle diamonds (Kaminsky, 2017). At processes of magmatic evolution of the lower mantle substance ferrobridgmanite decomposes in peritectic reaction with a melt and magnesiowustite and stishovite form (“stishovite paradox” effect) (Litvin et al., 2016). Based on earlier experimental data, ferrobridgmanite may include upto 5-10 mol % of FeSiO_3 - component into its composition at PT conditions of the upper part of the lower mantle (Wood and Rubie, 1996; Katsura and Ito, 1996). Preliminary experimental and model data showed a potential dependence of solubility of iron component on pressure (Irfune, 2007; Tange, 2009). Crystal chemistry and stability of ferrobridgmanite at high pressures and temperatures have a crucial meaning for understanding of structure, dynamic, and magmatism evolution of our planet. Conditions of stability and reactive interaction of minerals with melts of the lower mantle are important for understanding the processes of diamond formation at these depths. Investigation of the main mineral components of the lower mantle became possible at using of high-pressure diamond anvil cells and laser heating with using of Raman- and X-ray-spectroscopy, herewith studies of the lower mantle ferrobridgmanite became most relevant. The goal of the work is targeted study

Experimental researches of a solubility of iron component FeSiO_3 in ferrobridgmanite solid solution $(\text{Mg,Fe})\text{SiO}_3$ were carried out at pressure of 25–45 GPa, that corresponds to conditions of bridgmanite stability. The experiments were done using diamond anvil cell – DAC with laser heating (LH-DAC) 1700–2000 °C at IEM RAS and STC UI RAS. Starting material were homogenized gel mixtures of Mg_2SiO_4 , Fe_2SiO_4 with 70/30, 80/20 and 90/10 wt% proportions. Experimental conditions and results are shown in table 1. A starting sample is placed into a hole of diameter of 100–120 μm in rhenium gasket between NaCl layers. The Re-gasket is clamped by diamond anvils with working surfaces 300–250 μm . The sample is heated by focused continuous laser radiation with a wavelength of 1.064 μm (Nd: YAG laser) of power from 10 to 100 W, radiation is introduced through anvil areas, the laser beam diameter on the surface of the sample can be focused in the range from 5 to 100 μm . Laser heating is based on the principle of absorption of infrared laser light in a sample after light passes through one of the diamonds in a diamond anvil.

The installation of the LH-DAC (Fig. 1) consists of: (1) a high pressure cell attachment system with the ability to remotely move the sample along the three coordinate axes xyz ; (2) the optical system to obtain a sample image in the DAC; (3) the laser radiation control system for heating the sample. A fiber continuous laser with a wavelength of 1.064 μm (Nd: YAG fiber laser from IPG Photonics) is used for provide heating of the sample. The radiation from laser is reflected from the mirrors M1, M2, M3 (mirrors on reflection in the range 1047 - 1064 nm, 45 °). Mirrors are used for spatially align the IR laser radiation. The large-scale imaging system is based on

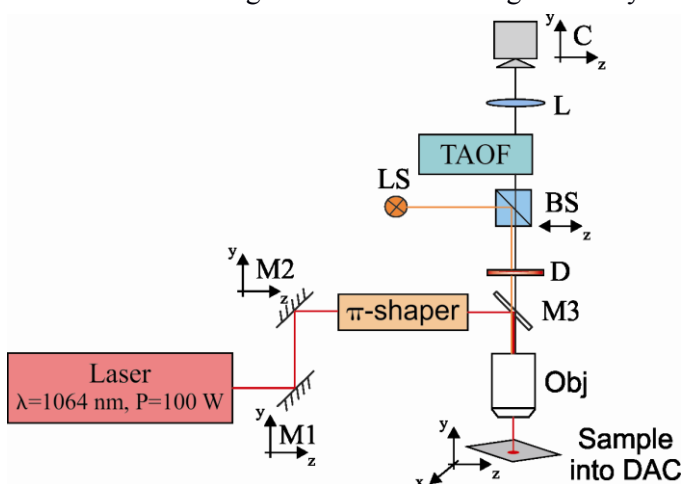


Fig. 1. Apparatus LH-DAC

of ultimate composition of limited solid solution of ferrobridgmanite.

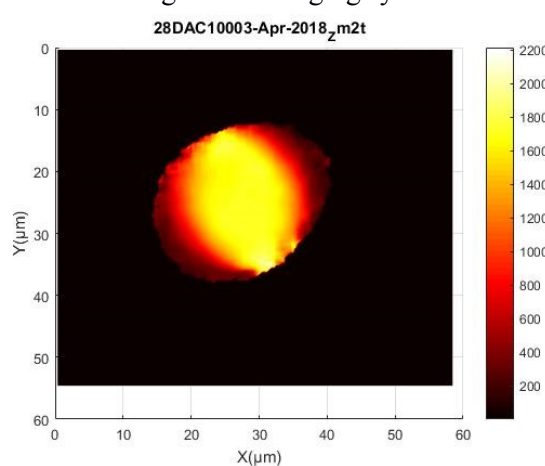


Fig. 2. An image of temperature distribution within a sample volume at laser heating

the Obj lens (10x, M, Plan Apo, L, NA = 0.28, f = 20 mm, Mitutoyo infrared lens, USA) with continuous

Mineral equilibria at high PT-parameters

correction of long working distance and narrow-band light source LS (600-660 nm.). To precisely control the shape and size of the laser spot, a pi-shaper is used, located between the mirrors M2 and M3. The radiation from the sample is directed through the optical path through the mirror M3. The image acquisition and processing system consists of: a tunable dual acousto-optical filter (TAOF), which allows multispectral imaging of the sample in the range from 590 nm to 1000 nm with a bandwidth of 2 nm; C camera (Allied Vision Mako G-030B), this camera can work at a speed of 300 frames per second with a resolution of 644 (H) × 484 (V) pixels; long focal lens L (f = 500 mm), used to focus radiation from the sample to the camera detector. Just before the acousto-optic filter, a dichroic mirror D (1047 - 1064 nm) is provided, which does not pass the laser spectrum. Accuracy of temperature estimation at the method is about ± 50°C. Heating duration was about 5 min. There was carried out a local heating of parts of a sample with diameter ~ 50 µm, untouched areas were convenient for comparison of changed parts with initial ones. Pressure in sample is determined by luminescent line shift of ruby, for this ruby grain with size of ~5 µm is placed inside the sample. Experimental samples were investigated by the scanning electron microscope CamScanM2300 (VEGA TS 5130MM) with spectral analyzer Link INCA at the Institute of Experimental Mineralogy RAS.

Raman-spectra of the experimental samples were measured in geometry of backscattering using the apparatus consisting of spectrograph Acton SpectraPro-2500i with detector cooling up to -70 °C CCD Pixis2K and the microscope Olympus with continuous solid-state monomeric laser with radiation wave length 532 nm and diode pumping at IEM RAS.

By preliminary experimental data, solid solution (MgSiO₃ • FeSiO₃)_{ss} is limited by ~20 wt% of iron component at pressures 28-40 GPa. A dependence of solubility of iron component on pressure is confirmed. Solubility limit of iron component FeSiO₃ in ferrobridgmanite concern to ferrobridgmanite composition in peritectic association in system MgO-FeO-SiO₂ ferrobridgmanite + stishovite + magnesiowustite + melt, that is justified at pressures 24-26 GPa (Litvin et al., 2016). The physico-chemical mechanism controls subsolidus associations

Table 1. Experimental conditions and results of researches of the lower mantle ferrobridgmanite solid solutions (Mg,Fe)SiO₃

| № sample | P, GPa | T, °C | Starting composition | phase association* |
|----------|--------|-------|--|--------------------|
| M7F3-1 | 40 | 2000 | (Mg ₂ SiO ₄) ₇₀ (Fe ₂ SiO ₄) ₃₀ | FBrd+Sti+MWus |
| M7F3-2 | 32 | 1800 | (Mg ₂ SiO ₄) ₇₀ (Fe ₂ SiO ₄) ₃₀ | FBrd+Sti+MWus |
| M7F3-3 | 45 | 1800 | (Mg ₂ SiO ₄) ₇₀ (Fe ₂ SiO ₄) ₃₀ | FBrd+Sti+MWus |
| M7F3-4 | 28 | 1900 | (Mg ₂ SiO ₄) ₇₀ (Fe ₂ SiO ₄) ₃₀ | FBrd+Sti+MWus |
| M8F2-1 | 37 | 1700 | (Mg ₂ SiO ₄) ₈₀ (Fe ₂ SiO ₄) ₂₀ | FBrd |
| M8F2-2 | 30 | 2000 | (Mg ₂ SiO ₄) ₈₀ (Fe ₂ SiO ₄) ₂₀ | FBrd+Sti+MWus |
| M8F2-3 | 29 | 2000 | (Mg ₂ SiO ₄) ₈₀ (Fe ₂ SiO ₄) ₂₀ | FBrd+Sti+MWus |
| M9F1-1 | 35 | 1800 | (Mg ₂ SiO ₄) ₉₀ (Fe ₂ SiO ₄) ₁₀ | FBrd |
| M9F1-2 | 29 | 1800 | (Mg ₂ SiO ₄) ₉₀ (Fe ₂ SiO ₄) ₁₀ | FBrd |

*experimental results by Raman-spectroscopy and electron microscope analyses

of system MgSiO₃ – FeSiO₃, especially boundaries between subsolidus phase fields ferrobridgmanite/ferrobridgmanite + stishovite + magnesiowustite/stishovite + magnesiowustite. There is a boundary line (plotted by dashed line) between two phase fields ferrobridgmanite / ferrobridgmanite + stishovite + magnesiowustite on fig. 3, it is a solubility curve of FeSiO₃ component in ferrobridgmanite.

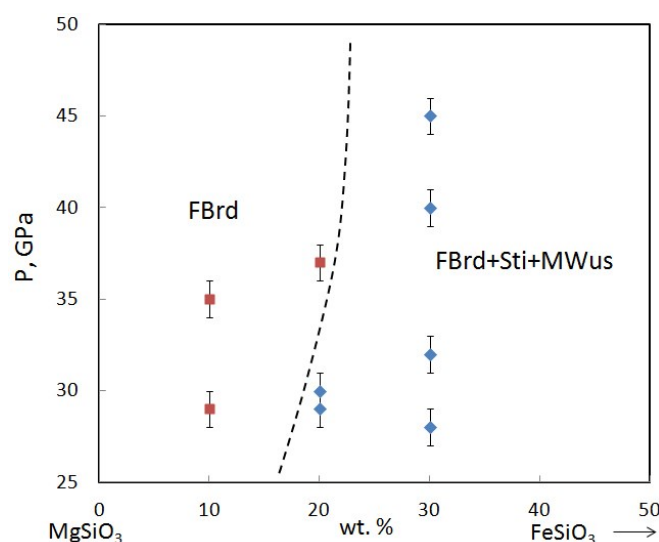


Fig. 3. Subsolidus scheme-diagram MgSiO₃ – FeSiO₃ with inserted preliminary boundary (dashed line) of a curve of a solubility of iron component FeSiO₃ in ferrobridgmanite

The work is supported by RFBR grant #16-05-00850 and MD-3464.2017.5, as well as the RAS program I.II.08.

References:

- Irifune T., Tsuchiya T. (2007) Phase transitions and mineralogy of the lower mantle D. Price (Ed.), Treatise on Geophysics. 2. 33–62.
- Kaminsky FV (2017) The Earth's Lower Mantle. Composition and Structure. Springer. 331 p.
- Katsura T., E. Ito (1996) Determination of Fe-Mg partitioning between perovskite and magnesiowu. stite, Geophys. Res. Lett., 23, 2005 - 2008
- Litvin YA, Spivak AV, Dubrovinsky L.S (2016) Magmatic evolution of the material of the Earth's lower mantle: stishovite paradox and origin of superdeep diamonds (experiments at 24-26 GPa). Geochem Internat 54(11):938-947
- Machikhin, A.S., Zinin P.V., Shurygin A.V. (2015) Acousto-optic Imaging System for In-situ Measurement of the High Temperature Distribution in Micron-size Specimens. Physics Procedia, 70, p. 733.
- Prakapenka V.B., Kubo A., Kuznetsov A., Laskin A., Shkurikhin O., et al. (2008) Advanced flat top laser heating system for high pressure research at GSECARS: application to the melting behavior of germanium. High Pres. Res., 28(3), p. 225.
- Ringwood, A.E. (1975). Composition and Petrology of the Earth's Mantle. New York - Toronto, McGraw-Hill. 618 p.
- Tange Y., Takahashi E., Nishihara Y, Funakoshi K, Sata N. (2009) Phase relations in the system MgO–FeO–SiO₂ to 50 GPa and 2000°C: An application of experimental techniques using multianvil apparatus with sintered diamond anvils. J. Geophys. Res. 114, B02214
- Tschauner O., Ma C., Beckett J.R., Prescher C., Prakapenka V., Rossman G.R. (2014) Discovery of bridgmanite, the most abundant mineral in Earth, in a shocked meteorite. Science. 346. 6213. 1100-1102.
- Wood, B. J., and D. C. Rubie (1996), The effect of alumina on phase transformations at the 660-kilometer discontinuity from Fe-Mg partitioning experiments, Science, 273, 1522 – 1524